INVESTIGATION OF MEDULLOBLASTOMA METABOLISM BY TISSUE-SPECIFIC GENOME-SCALE BRAIN METABOLIC MODEL AND IDENTIFICATION OF THERAPEUTIC TARGETS

by

İlkay İrem Özbek

B.S., Chemical Engineering, Kocaeli University, 2018

Submitted to the Institute for Graduate Studies in
Science and Engineering in partial fulfillment of
the requirements for the degree of
Master of Science

Graduate Program in Chemical Engineering

Boğaziçi University

2022

ACKNOWLEDGEMENTS

First of all, I would like to express my deepest appreciation to my thesis supervisor Prof. Kutlu Ülgen for providing me the great opportunity to work on this intriguing subject. The completion of this study could not have been possible without her immense knowledge, untiring support, patience, and enthusiasm throughout this process. Besides my advisor, I would also like to acknowledge my sincere gratitude to my thesis committee members, Assoc. Prof. Nazar İleri Ercan and Assist. Prof. Gülçin Tuğcu for devoting their valuable time and their invaluable comments.

I would like to give my warmest thanks to Mustafa Sertbaş for his help and recommendations. My sincere thanks also go to Mehmet Yiğit Demirtaş for his help, friendship, encouragement, and invaluable advice. I am grateful to them for answering my thousands of questions without any hesitation. I am also grateful to Seymen İlke Kaykanat for her kindness, sharing, and support. Furthermore, I wish to express my thanks to Ulgen Lab Members for creating a positive and welcoming work environment.

I cannot express enough thanks to my beloved friend Gökçe Sevgen who always listened to me patiently and motivated me with long voice records when I felt down and stepped out of my comfort zone. She was always with me, even when there were thousands of kilometers between us. I would also like to express my sincere thanks to my dear friend Aydan İlkay Yucak for always being there for me whenever I needed her. Her unexpected and thoughtful messages and her sincere friendship had a significant impact on me getting through this process. I would also thank my friend Fatma Güler for her friendship and genuine help offers. I feel incredibly lucky to have friends like them.

Finally, I would like to extend my profound gratitude to my precious parents, Ayla Özbek and Muammer Özbek for their unconditional love and unbelievable support. Thank you for always supporting my decisions (even crazy ones) without any hesitation. And thank you for never saying no to my requests related to my education and making it possible for me to complete this study.

I am deeply grateful to my beloved brothers and also my best friends, Eyüp Erkan Özbek and Asım Enes Özbek who always encouraged me to find and pursue my passions in life and never underestimated me when I made bold decisions. Feeling their support during this process was priceless. I also offer my sincere thanks and deepest love to my niece Zeynep Duru Özbek and my nephew Eren Özbek who filled the home with joy and made me go back to my childhood. I would like to thank Elçin Özbek and Büşra Özbek for their friendship and support. I feel privileged and fortunate to be part of Özbek family. This thesis is dedicated to Özbek family members for their endless love and everlasting support.

ABSTRACT

INVESTIGATION OF MEDULLOBLASTOMA METABOLISM BY TISSUE-SPECIFIC GENOME-SCALE BRAIN METABOLIC MODEL AND IDENTIFICATION OF THERAPEUTIC TARGETS

Medulloblastoma (MB) is the most prevalent pediatric brain tumor arising in the cerebellum. Since conventional therapies decrease life quality and cause deleterious effects on children, computer models are urgently required to simulate cancer phenotypes and determine potential therapeutic targets with minimum side effects on healthy cells. In the present study, metabolic alterations specific to MB were reflected on the brain genome-scale metabolic model by employing transcriptome data. Moreover, the relation between metastasis and the Warburg effects and the pathways utilized by MB without carbon source were investigated. Flux sampling analysis was also performed to detect statistically different reactions in healthy and MB cases. Regulation, flux coupling, and essentiality analyses were conducted as well to find therapeutic targets for MB. Additionally, the antimetabolites which might lessen the use of substrates in cells by causing competitive inhibition were identified by using similarity scores and conducting FBA. To investigate sphingolipid metabolism in depth, 79 reactions were newly included in the MB model. Consequently, the MB model captured metabolic characteristics of MB successfully as confirmed by experimental studies. It was found that targeting proteins/enzymes related to fatty acid synthesis, mevalonate pathway in cholesterol synthesis and inhibition of cardiolipin production, and tumor-inducing sphingolipid metabolites might be beneficial therapeutic strategies for MB. Furthermore, the suppression of GABA catalyzing and succinate-producing enzymes simultaneously might be a potential solution for metastatic MB. Using oleic acid as an antimetabolite owing to its structural similarity to linoleate and its downregulation in MB might be also a promising approach for this life-threatening disease.

ÖZET

DOKUYA ÖZGÜ GENOM ÖLÇEKLİ BEYİN METABOLİK MODELİ İLE MEDULLOBLASTOM METABOLİZMASININ İNCELENMESİ VE TERAPÖTİK HEDEFLERİN BELİRLENMESİ

Medulloblastom (MB), beyincikte ortaya çıkan en yaygın pediatrik beyin tümörüdür. Geleneksel tedaviler yaşam kalitesini düşürdüğü ve çocuklar üzerinde zararlı etkilere neden olduğu için, kansere özgü özellikleri simüle etmek ve sağlıklı hücreler üzerinde minimum düzeyde yan etkisi olan potansiyel ilaç hedeflerini belirlemek için bilgisayar modellerine ihtiyaç duyulmaktadır. Bu çalışmada, MB'ye özgü metabolik değişiklikler, transkriptom verileri kullanılarak genom ölçekli metabolik beyin modeline yansıtılmıştır. Metastaz ile Warburg etkileri arasındaki ilişki ve MB'nin karbon kaynağı mevcut olmadığında kullandığı yolaklar araştırılmıştır. Sağlıklı ve MB durumlarındaki istatistiksel olarak farklı reaksiyonları tespit etmek üzere akı örnekleme analizi yapılmıştır. MB için ilaç hedeflerini tespit etmek amacıyla regülasyon, akı bağlantısı ve tek/çift gen ve reaksiyon silme analizleri yapılmıştır. Ek olarak, akı denge analizi uygulanarak ve benzerlik skorları kullanılarak, yarışmalı inhibisyona neden olarak hücrelerde substrat kullanımını azaltabilecek antimetabolitler belirlenmiştir. Sfingolipit metabolizmasını derinlemesine araştırmak için MB modeline 79 reaksiyon dahil edilmiştir. Sonuç olarak, burada oluşturulan MB modeli, deneysel çalışmalarla da doğrulandığı üzere MB'nin metabolik özelliklerini başarılı bir şekilde yakalamıştır. Yağ asidi sentezi, kolesterol sentezindeki mevalonat yolağı ile ilgili proteinlerin/enzimlerin hedef alınmasının ve kardiyolipin üretiminin ve tümör indükleyici sfingolipit metabolitlerinin inhibe edilmesinin MB için faydalı terapi stratejileri olabileceği bulunmuştur. Ayrıca, GABA'yı parçalayan ve süksinat üreten enzimlerin eş zamanlı olarak baskılanmasının, metastatik MB için potansiyel bir çözüm olabileceği tespit edilmiştir. Son olarak, linoleat'a yapısal benzerliği ve MB'deki aşağı regülasyonu nedeniyle bir antimetabolit olarak oleik asidin kullanılması da yaşamı tehdit eden bu hastalık için umut verici bir yaklaşım olarak sunulmuştur.

TABLE OF CONTENTS

ACKNOWLEDGEMENTS ii

ABSTRACT iv

ÖZET v

LIST OF FIGURES ix

LIST OF TABLES xiv

LIST OF SYMBOLS xvi

LIST OF ACRONYMS/ABBREVIATIONS xvii

1. INTRODUCTION 1

2. BACKROUND ASPECTS 4

2.1. Systems Biology 4

2.1. Constraint Based Modeling 4

2.2.1. Flux Balance Analysis 5

2.2.2. Minimization of Metabolic Adjustment 8

2.2. Genome Scale Metabolic Networking Models 10

2.3.1. Context Specific Models 10

2.3.2. Transcription Data 11

2.4. Metabolism 12

2.4.1. Brain Metabolism 12

2.4.1.1. Medulloblastoma. 13

2.5. Genome-Scale Modeling of Cancer and Brain Metabolism 15

3. METHODS 18

3.1. Model Development 18

3.1.1. Addition of New Reactions to iMS570g 19

3.1.1.1. Taurine Pathway 19

3.1.1.2. Sphingolipid Metabolism. 24
3.1.2. Biomass Reaction Based on The Cerebellum 25
3.1.3. Determination of Constraints 34
3.1.4. Obtaining Medulloblastoma-Specific Genome Scale Models 37
3.1.4.1. Threshold Selection. 38
3.2. Analyses 42
3.2.1. Flux Balance Analyses 43
3.2.2. Sampling Approach 45
3.2.3. Regulation 46
3.2.4. Flux Coupling 48
3.2.5. Essentiality Anayses 48
3.2.6. Investigation of Threpautic Targets for Medulloblastoma 49
3.2.6.1. Determination of Common Essential Genes for Three Parameters. 49
3.2.6.2. Identification of Potential Metabolite-Antimetabolite Pairs. 51
4. RESULTS AND DISCUSSION 57
4.1. Validation of MB Model Results with Experimental Results 57
4.2. Energy Production without Carbon Source 66
4.3. The Relation Between Metastasis and The Warburg Effect 68
4.4. Sampling 71
4.5. Regulation 80
4.6. Flux Coupling Analysis 88
4.7. Essentiality Analyses 92
4.8. Therapeutic Targets for Medulloblastoma 103
4.8.1. Common Essential Genes for Three Critical Parameters 103
4.8.2. Potential Metabolite-Antimetabolite Pairs 117
4.8.3. Investigation of Sphingolipid Metabolism 135
4.8.3.1. Detection of Antimetabolites in Sphingolipid (SL) Metabolism. .. 140

4.8.3.2. Gene Deletion Analyses in Sphingolipid Metabolism. 145
5. CONCLUSION AND RECOMMENDATIONS 149
REFERENCES 155
APPENDIX A: THE LIST OF REACTIONS 189
APPENDIX B: INTEGRATION OF GIMME 190
APPENDIX C: THE LIST OF METABOLITE ANTIMETABOLITE PAIRS 191
APPENDIX D: THE LIST OF P VALUES 192
APPENDIX E: THE LIST OF COMMON ESSENTIAL GENES 193

LIST OF FIGURES

Figure 2.1.	Sample system A has 4 internal and 3 external reactions……	5
Figure 2.2.	Subgroups of Medulloblastoma WNT (Cross in Purple), SHH (Triangle in Red), Group 3 (Square in Green), Group 4 (Oval in Orange)……..	14
Figure 3.1.	Flow chart of works done in this study……	18
Figure 3.2.	The distribution of Z when μc ≠ μh at 5% significance level…….....	47
Figure 3.3.	Flow chart of investigation of therapeutic targets for MB.....	50
Figure 3.4.	Addition of SMILE of lactate in chemical structure search engine….....	53
Figure 3.5.	Setting search options…….	54
Figure 4.1.	Main reactions carried out in glycolysis, PPP, TCA cycle, and other pathways……..	58
Figure 4.2.	Pyruvate and lactate production rates of astrocyte (R10 and R11) and neuron (R55 and R56) for MB and healthy models ……..…	59
Figure 4.3.	Total ATP flux rates produced in glycolysis (R7+R10+R52+R55) and OXPHOS (R45+R88) for MB and healthy models……..	61
Figure 4.4.	The glucose uptake (R593 and R594), oxygen uptake rates (R595 and R596), 6-phosphogluconate (R17 and R61), and R5P production (R21 and R65) rates in PPP of astrocyte and neuron, respectively for MB and healthy models……..	62

Figure 4.5. Alterations of total hydrogen peroxide (H_2O_2) (R421+R431) and 6-phosphogluconate productions with respect to total oxygen uptake (R595+R596) for the MB model……. 64

Figure 4.6. Citrate (R25 and R69) and acetyl-CoA (R72) production rates in astrocyte and neuron for MB and healthy models……..….. 65

Figure 4.7. Alterations in total energy production rate with respect to glucose and glutamine uptake restrictions……... 67

Figure 4.8. Alterations in energy production distribution with respect to glucose and glutamine uptake restrictions…….… 68

Figure 4.9. The comparison of genes expression levels between non-metastatic and metastatic samples (M0 and M4)…… 69

Figure 4.10. The comparison of ATPG/ATPOP and LacR/OCR between non-metastatic (M0) and metastatic samples (M2 and M4)……..... 70

Figure 4.11. The percentages of significant reactions in neuron for each subsystem.. 73

Figure 4.12. The percentages of significant reactions in astrocyte for each subsystem……... 74

Figure 4.13. Lactate production (R11) in glycolysis for astrocyte. Flux sampling results for MB are shown in red while the results for healthy are shown in blue……. 75

Figure 4.14. Lactate production (R56) in glycolysis for neuron. Flux sampling results for MB are shown in red while the results for healthy are shown in blue……. 76

Figure 4.15. ATP production (R45) in OXPHOS for astrocyte. Flux sampling results for MB are shown in red while the results for healthy are shown in blue..... 76

Figure 4.16. ATP production (R88) in OXPHOS for neuron. Flux sampling results for MB are shown in red while the results for healthy are shown in blue..... 77

Figure 4.17. 6-phosphogluconate production (R17) in pentose phosphate pathway for astrocyte. Flux sampling results for MB are shown in red..... 77

Figure 4.18. 6-phosphogluconate production (R61) in the Pentose phosphate pathway for neuron. Flux sampling results for MB are shown in red..... 78

Figure 4.19. Citrate production (R25) in the TCA cycle for astrocyte. Flux sampling results for MB are shown in red while the results for healthy shown in blue..... 79

Figure 4.20. Citrate production (R69) in the TCA cycle for neuron. Flux sampling results for MB are shown in red while the results for healthy are shown in blue..... 79

Figure 4.21. The number of the reactions regulated metabolically (M), transcriptionally (T), and post-transcriptionally (PT) in both neuron and astrocyte for each pathway..... 81

Figure 4.22. The genes whose associated reactions are significantly different in MB compared to the reactions in the healthy model based on pathways..... 86

Figure 4.23. The distribution of reactions directionally coupled to growth based on the pathway..... 90

Figure 4.24. The distribution of common essential genes estimated in single-gene deletion and reaction deletion analyses based on associated pathways…. 98

Figure 4.25. The interrelationship of the genes found in double gene deletion analysis……. 100

Figure 4.26. The number of gene combinations obtained in double gene deletion analysis and their related pathways…….. 101

Figure 4.27. The relation between GABA shunt, TCA cycle and electron transfer chain……. 102

Figure 4.28. The number of essential genes obtained for each of the three cases…….. 104

Figure 4.29. The Number of Drugs/Compounds based on their status…….. 109

Figure 4.30. The distribution of substrates detected in FBA analysis according to their related pathways……... 118

Figure 4.31. Metabolite and antimetabolite pair with 0.90 similarity score. Number 1 and number 2 represent linoleate and oleic acid, respectively…… 131

Figure 4.32. Metabolite and antimetabolite pair with 0.83 similarity score. Number 1 and number 2 represent arachidonate and oleic acid, respectively……. 132

Figure 4.33. Metabolite and antimetabolite pair with 0.95 similarity score. Number 1 and number 2 represent arachidonate and icosapent, respectively……. 133

Figure 4.34. Metabolite and antimetabolite pair with 0.88 similarity score. Number 1 and number 2 represent linoleate and icosapent, respectively…….. 133

Figure 4.35. Metabolite and antimetabolite pair with 0.97 similarity score. Number 1 and number 2 represent linoleate and gamolenic acid, respectively….. 134

Figure 4.36. Metabolite and antimetabolite pair with 0.95 similarity score. Number 1 and number 2 represent arachidonate and gamolenic acid, respectively…….. 135

Figure 4.37. Metabolite and antimetabolite pair with 0.95 similarity score. Number 1 and number 2 represent R-mevalonate and meglutol, respectively….. 135

Figure 4.38. Sphingolipid Metabolism……. 137

Figure 4.39. Sphinganine and phytosphingosine with 0.825 similarity score. Number 1, number 2 and number 3 represent Sphinganine, Sphingosine and Phytosphingosine, respectively…… 143

Figure 4.40. The biomass reaction rate without and with drug effect in MB-GR4 model……... 147

LIST OF TABLES

Table 3.1. The number of reactions and genes in pathways of the expanded model.. 20

Table 3.2. Calculation of amino acid composition…… 26

Table 3.3. Calculation of gangliosides composition……..…… 27

Table 3.4. Calculation of cerebrosides composition……..…… 29

Table 3.5. Calculation of lipid composition……..…… 30

Table 3.6. Composition of lipid and protein in gray and white matter and distribution of gray and white matter in cerebellum…… 31

Table 3.7. Calculation of lipid and protein composition in cerebellum……. 33

Table 3.8. Updated and newly added biomass reactions……... 33

Table 3.9. Upper bounds and lower bounds of all the constraints used in MB models ……...……. 36

Table 3.10. GSE datasets used in this study……. 37

Table 3.11. The compounds similar to lactate……. 55

Table 3.12. Reactions related to glucose-6-phosphate……..…….. 56

Table 4.1. The comparison of MB-specific models results with healthy model and experimental results…….. 60

Table 4.2. Essential genes in MB model and their associated pathways…… 92

Table 4.3. Genes detected in both analyses and their associated pathways…… 93

Table 4.4. Eight potential therapeutic genes for medulloblastoma……... 106

Table 4.5. Drugs/ Compounds for HMGCR…….. 111

Table 4.6. Drugs/ Compounds for MVK and MVD…….. 113

Table 4.7. Drugs/ Compounds for FDFT1…… 115

Table 4.8. Drugs/ Compounds for FASN…….. 116

Table 4.9. Drugs/ Compounds for SQLE…….. 117

Table 4.10. The substrates whose enzymes could be used as drug targets……... 120

Table 4.11. The substrates whose enzymes could be used as drug targets in sphingomyelin metabolism and glycosphingolipid biosynthesis-ganglio series……. 141

LIST OF SYMBOLS

D	Euclidean distance
H_2O_2	Hydrogen peroxide
I	Unit matrix
L	Vector
M0	Non metastatic condition
M	Metabolically regulated reaction
P	Matrix
PT	Post-transcriptionally regulated reaction
Q	False discovery rate
S	Stoichiometric coefficient matrix
T	Transcriptionally regulated reaction
Var	Variance
V	Flux vectors for each reaction
v	Flux vector for perturbed condition
w	Flux vector for unperturbed condition
ZG	Z score for gene expressions
ZF	Z score for flux rates
α	Significance level
μ	Mean

LIST OF ACRONYMS/ABBREVIATIONS

A/P	Absent and Present Data
ACC	Acetyl-Coa Carboxylase
ACC1	Acetyl-Coa Carboxylase 1
ACL	ATP Citrate Lyase
AD	Alzheimer's Disease
ADK	Adenosine Kinase
ADP	Adenosine Diphosphate
ALDH5A1	Aldehyde Dehydrogenase 5 Family Member A1
AMD1	Adenosylmethionine Decarboxylase 1
ASNS	Asparagine Synthetase
ATP	Adenosine Triphosphate
ATPG	ATP Generated in Glycolysis
ATPOP	The Energy Produced in OXPHOS
BBB	Blood-Brain Barrier
BH	Benjamini-Hochberg Correction
CBM	Constraint-Based Model
CDP	Cytidine Diphosphate
COBRA	Constraint-Based Reconstruction and Analysis
DNA	Deoxyribonucleic Acid
EA	Ellagic Acid
ECs	Endothelial Cells
EP	Ependymoma
ER	Endoplasmic Reticulum
ETFDH	Electron Transfer Flavoprotein Dehydrogenase
FAD	Flavin Adenine Dinucleotide
FADH2	Reduced Flavin Adenine Dinucleotide
FAs	Fatty Acid Synthesis
FASN	Fatty Acid Synthase
FBA	Flux Balance Analysis

FCA	Flux Coupling Analysis
FDA	Food and Drug Administration
FH	Fumarate Hydratase
G6PDH	Glucose-6-Phosphate Dehydrogenase
GABA	α-Aminobutyric Acid
GAD1	Glutamate Decarboxylase 1
Gb4	Globotetraosylceramide
GBM	Glioblastoma
GcMAF	Gc Protein-Derived Macrophage Activating Factor
GDW	Gram Dry Weight
GEO	Gene Expression Omnibus
GIMME	Gene Inactivity Moderated by Metabolism and Expression
GLA	Gamolenic Acid
GLS1	Glutaminase
GLUT1	Glucose Transporter 1
GPCRs	G-Coupled Protein Receptors
GPD1	Glycerol-3-Phosphate Dehydrogenase 1
GPD2	Glycerol-3-Phosphate Dehydrogenase 2
GPI	Glucose-6-Phosphate Isomerase
GSL	Glycosphingolipids
GSMM/GEM	Genome-Scale Metabolic Model
HIF-alpha	Hypoxia-Inducible Factor 1-Alpha
HK2	Hexokinase 2
HMG-CoA	3-Hydroxy-3-Methylglutaryl Coa
HMGCR	3-Hydroxy-3-Methylglutaryl-Coa Reductase
KIC	A-Ketoisocapriate
KIV	A-Ketoisovalerate
KMV	A-Keto-B-Methylvalerate
LacR	Lactate Production
LAT1	L-Type Amino Acid Transporter 1
LB	Lower Bound
LBDD	Ligand-Based Drug Design

LDHA	Lactate Dehydrogenase
LP	Linear Programming
MAOA	Monoamine Oxidase A
MAPK	Mitogen-Activated Protein Kinase
MB	Medulloblastoma
MOMA	Minimization of Metabolic Adjustment
MVA	Mevalonate
NADH	Nicotinamide Adenine Dinucleotide
NADPH	Nicotinamide Adenine Dinucleotide Phosphate
NB	Neuroblastoma
NCBI	National Center for Biotechnology Information
OCR	Oxygen Uptake
OTX2	Orthodenticle Homeobox 2
OXPHOS	Oxidative Phosphorylation and Atpase Pathway
PEP	Phosphoenolpyruvate
PFK-1	Phosphofructokinase
PGM	Phosphoglucomutase
PKM2	Pyruvate Kinase M2 Subtype
PNP	Purine Nucleoside Phosphorylase
PPP	Pentose Phosphate Pathway
QDPR	Quinoid Dihydropteridine Reductase
R5P	Ribose-5 Phosphate
RDMSD	Ratio of The Difference Between Flux Means of Both Conditions to The Sum of The Standard Deviations of Both Conditions
RNA	Ribonucleic Acid
ROS	Reactive Oxygen Species
RPE	Ribulose-5-Phosphate-3-Epimerase
S1P	Sphingosine-1-Phosphate
SBDD	Structure-Based Drug Design
SDH	Succinate Dehydrogenase
SHH	Sonic Hedgehog
SMILES	Simplified Molecular Input Line Entry System

SMOX	Spermine Oxidase
SMS	Spermine Synthase
SPHK1	Sphingosine Kinase
SRM	Spermidine Synthase
SUCLA2	Succinate-Coa Ligase ADP-Forming Subunit Beta
SUCLG1	Succinate-Coa Ligase GDP/ADP-Forming Subunit Alpha
TALDO1	Transaldolase 1
TCA	Tricarboxylic Acid Cycle
TIGAR	Tp53-Induced Glycolysis and Apoptosis Regulator
TPI	Triosephosphate Isomerase
TPI1	Triosephosphate Isomerase 1
Ub	Upper Bound
WNT	Wingless-Related Integration Site

1. INTRODUCTION

Brain cancer is a serious disease that influences both children and adults (Chakraborty *et al*., 2018)**.** In children, after leukemia, primary brain tumor is the second prominent pediatric cancer. Among pediatric brain tumors, medulloblastoma (MB) is the most prevalent kind with an annual rate of ~5 cases per 1 million population. (Girardi *et al*., 2019; Northcott *et al*., 2019). In 2014, the malignant medulloblastoma was reported as the most prevalent brain tumor type appearing in children by World cancer report (Stewart and Wild, 2014).

The treatment for MB is surgery followed by radiation and chemotherapy to remove any remaining tumor and decrease the risk of metastasis (Kumar *et al*., 2017). However, radiation therapy is generally not applied to children younger than three since radiation can be detrimental for the developing brain, thus this can jeopardize patient survival (Kumar *et al*, 2017). Moreover, many patients face treatment-related neurological sequelae after these therapies (Hovestadt *et al*., 2019). The most prominent side effect is a decline in intelligence (Riggs *et al*., 2014). The patients also had issues such as poor memory and difficulty focusing after receiving chemotherapy and spinal irradiation (Palmer *et al*., 2013). Therefore, there is a dire need for innovative and effective strategies which have minimum toxic effects on healthy cells and alleviate patients' therapy-related burdens.

Genome-scale metabolic modeling has been an effective tool to study cancer metabolism within the past two decades (Özcan and Çakır, 2016). The opportunity to get information about the transcriptomic activities and analyze the intricate metabolism of brain tumors makes genome-scale models attractive.

Herein, the genome-scale brain metabolic model iMS570, developed by Sertbaş et al and then customized to iMS570g model to reflect glioblastoma metabolism by Özcan and Çakir, was expanded and changed to capture the metabolic variations that occur in medulloblastoma and thus named MB model.

There are two main goals of the present study. Firstly, to obtain a brain metabolic model that imitates the metabolic and transcriptomic changes in brain metabolism caused by medulloblastoma and make accurate predictions about this disease in question. Secondly, to propose effective and non-hazardous approaches/ compounds that can pass through the blood-brain barrier, and that will act on the therapeutic targets uncovered by this model. The genome-scale model and transcriptomic data are the two major tools required to achieve these two goals.

The next chapter covers background information about these tools. In addition, Flux balance analysis and minimization of metabolic adjustment methods employed in this study are explained comprehensively. The information about metabolic activities of medulloblastoma and a brief explanation about earlier studies that have investigated cancer using genome-scale modeling approach are included.

The third chapter answers questions such as how the biomass reaction was made specific to the cerebellum, which reactions were added to the model and for what purpose, how the constraints required for the analysis were determined, and how the transcription data were integrated into the model. The aims of flux balance, flux sampling, regulation, flux coupling, essentiality analyses, and how they were performed are also given in this methods chapter. Lastly, investigation of therapeutic targets for medulloblastoma and analyses done particularly for this part of the study are presented.

The fourth chapter contains the results of flux balance analysis of the MB model and a comparison of these findings with the literature and healthy brain model results. Then comes the part that examines wherefrom the cell meets its energy requirement without a carbon source. Next, the question of whether there is a relation between metastasis and the Warburg effect is discussed. Furthermore, flux sampling results, flux sampling histograms of the key reactions, and statistically most different reactions in the MB model compared to ones in the healthy model are detailed. Regulation, flux coupling, and essentiality analyses results are also discussed extensively with the purpose of uncovering potential drug targets. Afterward, the two parts of the investigation process of therapeutic targets in medulloblastoma are explained in detail.

The first part includes the common genes that are essential for lactate and energy production alongside growth and therapeutic suggestions based on these results. The second part includes the results of the flux balance analyses where drug effects were simulated for each metabolite in the model to identify the antimetabolites which might reduce the use of substrates in cells. Potential antimetabolite-metabolite pairs using similarity scores and FBA results are also presented. Lastly, the results of essentiality and flux balance analyses specifically performed for the sphingolipid pathway and therapeutic targets that were found based on these findings are covered.

The main conclusions and recommendations for further studies are summarized in the "Conclusion and Recommendations" chapter.

2. BACKROUND ASPECTS

2.1. Systems Biology

Systems biology is an important field of science that links constituents of biological systems (cells, tissues, and organs) and controls these biological systems by taking advantage of computational and experimental methods (Tavassoly *et al*., 2018). Systems biology methods allow researchers to study behaviors and interactions of biological components (Tavassoly *et al*., 2018). It is also possible to investigate alterations that occurred in biological entities entailed by chemical, biological, and genetic perturbations (Ideker *et al*., 2001).

A systems biology approach requires 4 main steps (Palsson, 2015). Firstly, necessary components for biological processes are determined and compiled. Then, relations of these components are investigated to develop genome-scale networks. Developed networks are adapted to mathematical format to be investigated. Afterward, computational models are constructed to predict hypothetical biological information to be verified experimentally.

2.1. Constraint Based Modeling

The constraint-based modeling is the most frequently used approach that allows reconstructing of genome-scale in silico models which observe properties of organisms under different conditions (Haggart *et al*., 2011), (Sun *et al*., 2009). Constraint-based model (CBM) development process over the last decades can be explained in four stages (Bordbar *et al*., 2014). At first, CBMs have been utilized to detect pathway yields.

Experimental fluxes have been demonstrated to agree with the results obtained with objective functions such as minimum generation of reactive oxygen species (ROS) and maximum biomass in hybridoma cells and *Escherichia coli*, respectively. The similarity between CBM and experimental results has encouraged researchers to benefit from in silico models to predict characteristics from a reconstructed metabolic network.

Afterward, whole-genome sequencing has enabled the construction of CBM at the genome-scale and made the reactions in CBM connect to the genes. Gene-reaction relation has also made it possible to obtain the outcomes of gene silencing method providing detection of drug targets. After omics data became more accessible, researchers started to integrate these data sets into CBM. Then omics data were utilized by restricting certain metabolic reactions to enhance the context specificity of CBM (Bordbar *et al*., 2014). Finally, all these efforts culminated in Genome-scale metabolic models (GSMMs) that allow determining the properties of metabolism in biological systems (Bordbar *et al*., 2014).

2.2.1. Flux Balance Analysis

Flux Balance Analysis **(**FBA) is the most used constraint-based modeling method that computes the flows of metabolites in a biochemical network, thus ensures prediction of the experimental flux rate of metabolites or growth rate in a biological system (Orth *et al*., 2010). In a certain condition, FBA presumes that the biological system will achieve a steady-state where given constraints are met (Kauffman *et al*., 2003).

FBA has three major steps: (i) definition of components found in the model, (ii) addition of constraints, and (iii) optimization of the system. In the first step, all reactions and metabolites in the metabolic model should be defined.

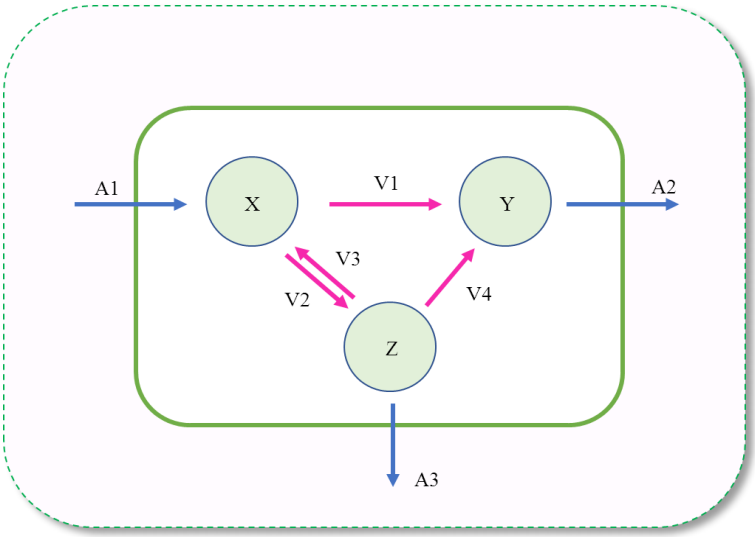

Figure 2.1. Sample system A has 4 internal and 3 external reactions.

As given in Figure 2.1 sample system A has 3 metabolites (X, Y, and Z) related to 3 external (A1, A2, and A3) and 4 internal (V1, V2, V3, and V4) reactions.

There are three types of constraints used in CBMs (Reed, 2017). The first constraint is the mass-balance constraint where flux rates of metabolites are computed based on the steady-state condition. Once all components in the model are defined as explained in the first step, metabolic reactions in the model are required to be expressed mathematically. Mass balance equations for each component are expressed in differential forms (Kauffman *et al*, 2003). The mass balance equations for sample system A are shown as

$$\begin{aligned} \frac{dX}{dt} &= -v1 + v2 - v3 + A1 \\ \frac{dY}{dt} &= v1 + v4 - A2 \\ \frac{dZ}{dt} &= -v2 + v3 - v4 - A3. \end{aligned} \tag{2.1}$$

Subsequently, the differential equations are written in a matrix notation (Kauffman *et al*, 2003) as shown in

$$\begin{bmatrix} -1 & 1 & -1 & 0 & 1 & 0 & 0 \\ 1 & 0 & 0 & 1 & 0 & -1 & 0 \\ 0 & -1 & 1 & -1 & 0 & 0 & -1 \end{bmatrix} * \begin{bmatrix} v_1 \\ v_2 \\ v_3 \\ v_4 \\ A_1 \\ A_2 \\ A_3 \end{bmatrix} = \begin{bmatrix} \frac{dX}{dt} \\ \frac{dY}{dt} \\ \frac{dZ}{dt} \end{bmatrix}. \tag{2.2}$$

Since the system is assumed to be carried out in the steady-state condition, the changes in flux rates over time were reduced to zero as given in

$$\begin{bmatrix} -1 & 1 & -1 & 0 & 1 & 0 & 0 \\ 1 & 0 & 0 & 1 & 0 & -1 & 0 \\ 0 & -1 & 1 & -1 & 0 & 0 & -1 \end{bmatrix} * \begin{bmatrix} v_1 \\ v_2 \\ v_3 \\ v_4 \\ A_1 \\ A_2 \\ A_3 \end{bmatrix} = \begin{bmatrix} 0 \\ 0 \\ 0 \end{bmatrix}. \quad (2.3)$$

The first matrix in Equation (2.3) is a stoichiometric matrix (S) which includes stoichiometric coefficients of each differential reaction. The second matrix (V) includes flux vectors of each reaction in sample system A. Thus, Equation (2.3) can be expressed as *S x V* = 0.

In the stoichiometric matrix, while each column represents reactions found in the metabolic model, each row represents metabolites in the model. Since there are 3 metabolites and 7 reactions in sample system A, the dimension of the stoichiometric matrix is (3 x 7). While negative numbers show the metabolites consumed, positive numbers indicate the metabolites generated in sample system A. Zero indicates the metabolites that do not have a relation with the corresponding reactions.

The second constraint used in FBA is related to the reversibility of the reactions found in the metabolic model (Reed, 2017). Acceptable maximum and minimum values for reversible reactions are +∞ and -∞, respectively. This range for irreversible reactions on the other hand is between 0 and +∞.

The third constraint used in FBA is usually an experimentally measured or known flux value. Based on the flux value measured, upper and lower bounds can be defined as constraints (Reed, 2017).

In the last step of FBA, optimization is employed to detect the optimum value of a determined objective function with the specified constraints in order to find a biologically logical result. In unconstrained solution space, many flux profiles for the metabolic network can be obtained. When mass balance and other constraints are included, solution space for flux profile decreases. However, more than one flux profile results are obtained within the solution space since a metabolic network includes more reactions than metabolites. (Orth *et al*., 2010). Therefore, optimization is utilized to predict a single and optimum flux distribution solution without extra constraints. Optimization is based on linear programming (LP) technique which computes minimum or maximum value of a certain variable (Bordbar *et al*., 2014), (Oath *et al*., 2010). That is why an objective function is required to specify how much each reaction contributes to desired objective (Oath *et al*., 2010). Maximization of growth is a prevalent objective function in microorganisms owing to their tendency to increase their biomass (Chen *et al*., 2019), (Haggart *et al*., 2011). Maximal production of a biologically important metabolite and maximal and minimal production of energy, maximization and minimization of nutrient uptake rate, are other objective functions used in biological entities (Haggart *et al*, 2011).

2.2.2. Minimization of Metabolic Adjustment

Minimization of Metabolic Adjustment (MOMA) is another constraint-based method developed by assuming that perturbated biological systems cannot adapt their metabolisms quickly to reach the optimum biomass solution as their normal counterparts do (Haggart *et al.,* 2011). Therefore, MOMA does not search for the optimum solution unlike FBA, instead aims for a suboptimal biomass flux profile solution that is closest to an unperturbed condition (Raman and Chandra, 2009). In other words, it works by considering the unperturbed condition in addition to the perturbated condition. It was indicated that MOMA gives more accurate and realistic results in perturbated biological systems compared to FBA (Segre *et al*., 2002).

MOMA is also employed with FBA to improve the flux distribution results (Haggart *et al*., 2011). Dual objective function was used in the studies where human brain metabolism was investigated because it allows minimum enzyme use to reach the first objective determined for FBA (Çakır *et al*., 2007), (Özcan and Çakır, 2016), (Sertbaş *et al*., 2014). The mathematical expression of MOMA is given as

$$D\ (w, v) = \sqrt{\sum_{i=1}^{N}(wi - vi)^2}\ . \tag{2.4}$$

W and v represent flux vectors of the unperturbed (wild type for microorganisms) and perturbated conditions, respectively. D represents the Euclidean distance between w and v. The expansion of Equation (2.4) is given as

$$D\ (w, v) = \sqrt{\sum_{i=1}^{N}(wi^2 - 2wivi + vi^2)}\ . \tag{2.5}$$

Since flux distribution in the unperturbed condition is known, wi^2 term is accepted as a constant and omitted from Equation (2.5). Hence minimization of Euclidean distance is equivalent to the minimization of the sum of $-2wivi$ and vi^2 terms as given in

$$Min(-2wivi + vi^2). \tag{2.6}$$

FBA employs linear programming technique, whereas MOMA uses quadratic programming principle due to quadratic terms in Equation (2.6) (Raman and Chandra, 2009). Quadratic programming solvers solve this expression based on

$$f\ (x) = L.x + \frac{1}{2}x^{T}.P.x \tag{2.7}$$

where x values are found by minimizing the f (x) function. L and P signify a vector and a matrix, respectively, and x^{T} means transpose of *x*.

When -2*wi*, *xi*, and 2*I* where I represents unit matrix, are placed into Equation (2.7), Equation (2.6) is expressed as given in

$$\text{Min}(-2wixi + xi^2). \quad (2.8)$$

Conclusively, MOMA finds flux profile of perturbed condition that satisfies Equation (2.8).

2.2. Genome Scale Metabolic Networking Models

The development of genome-scale metabolic models is a promising field of system biology supported by constraint-based modeling methods (Haggart *et al*., 2011). Genome-scale metabolic models (GSMM), composed of the gene, metabolite, and reaction interactions, allow us to determine the features of metabolism like growth rate, gene essentiality and robustness with the addition of few constraints (Duarte *et al*., 2007), (Puchałka *et al*., 2008).

The first genome-scale metabolic model was constructed for *Haemophilus influenzae* in 1995. This GSMM included 488 reactions, 343 metabolites, and 296 genes (Fleischmann *et al*., 1995). In 2007, the first human-specific genome-scale metabolic network (Recon1) including 2766 metabolites, 1496 genes, and 3744 reactions was developed (Duarte *et al*., 2007). Afterward, different human models have been constructed by various research groups (Agren *et al*., 2012), (Brunk *et al*., 2018), (Ma *et al*., 2007), (Mardinoglu *et al*., 2014), (Thiele *et al*., 2013). Over time the number of metabolites, reactions, and genes forming of GSMMs, has enhanced remarkably.

2.3.1. Context Specific Models

Human genome-scale metabolic models contain all reactions realized in the human metabolism. Therefore, the reconstruction of a tissue-specific model is crucial to investigate a particular tissue.

To this end, several algorithms (such as iMAT, INIT, and GIMME) have been created in order to obtain a tissue-specific model by employing omics data (Becker and Palsson, 2008), (Shlomi *et al*., 2008), (Agren *et al*., 2012). These methods are categorized into two groups based on the approach they use. The first group employs context-specific omics data without processing to enhance the predictability of flux profiles. The most known examples of the first group are MADE (Jensen and Papin, 2011), TEAM (Collins *et al*., 2012), E-Flux (Colijn *et al*., 2009), tFBA (van Berlo *et al*., 2011), PROM (Chandrasekaran and Price, 2010). The second group generates context-specific models after processing the omics data. Examples of the second group are GIMME (Becker and Palsson, 2008), iMAT (Shlomi *et al*., 2008), INIT (Agren *et al*., 2012), AdaM (Töpfer *et al*., 2012), mCADRE (Wang *et al*., 2012). It has been determined that the two groups do not have an obvious advantage over each other (Machado and Herrgård, 2014).

2.3.2. Transcription Data

The genetic material of a biological entity is stored in the Deoxyribonucleic Acid (DNA) and expressed with transcription (Lowe *et al*., 2017). Transcription is realized by which the information in a segment of DNA is replicated into an RNA molecule (Mercadante and Mohiuddin, 2020).

Transcriptomics technologies that determine the expressions of genes in a microchip are employed to analyze an organism's transcriptome (Lowe *et al*., 2017). The experimental findings obtained using Transcriptomics technology are shared by the Gene Expression Omnibus database (Edgar, 2002). GEO database contains four types of data which are GEO Platform (GPL), GEO Series (GSE), GEO Sample (GSM), and curated GEO DataSet (GDS). A Platform record (GPLxxx) involves a brief explanation of probe ID's corresponding to related gene names.

A Series record (GSExxx) has a group of samples associated with each other and it explains the important points of the study alongside outcomes and analyses. A Sample record (GSMxxx) includes the information about the results of samples utilized in the experiment.

In addition to this information, this data contains information about what changes the sample has undergone and what substances are derived from it. Curated Dataset (GDSxxx) is a curated compilation of GEO Samples.

2.4. Metabolism

Metabolism is a series of reactions carried out in organisms to sustain living conditions (Baart and Martens, 2012). Enzymes are essential in biochemical processes because they execute chemical reactions. The link between enzyme and reaction can be employed to reconstruct a network of reactions and thus create a model that reflects the metabolism. Metabolism is composed of catabolic and anabolic processes.

Catabolic reactions generate the energy required by the organism breaking down large substances. On the other hand, anabolic reactions synthesize large substances by consuming the energy produced by catabolic reactions (Bronk, 1999).

2.4.1. Brain Metabolism

The brain is the most intricate organ in the human body, and it has seven main sections: the medulla, the pons, the midbrain, the spinal cord, the cerebellum the diencephalon, and the cerebral hemispheres.

The forebrain is composed of cerebral hemispheres and the diencephalon which enfold the lateral and 3rd ventricles. The pons, midbrain, and medulla together form the brainstem and they enclose the midbrain and 4th ventricle (Purves, 2004). The brainstem that links the cerebrum with the spinal cord, is a channel for the central nervous system, that either transmit sensory input from the spinal cord to the forebrain or transmits motor commands from the forebrain to the motor neurons in the spinal cord (Singh, 2014), (Purves, 2004). The brainstem has several nuclei that play a role in many significant functions like the regulation of respiration, heart rate, and blood pressure (Purves, 2004).

The cerebellum that extends through the dorsal aspect of the brainstem, is crucial for motor control, coordination and movement (Purves, 2004). It also plays a role in the regulation of language and attention (Wolf *et al*., 2009), (Schmahmann and Caplan, 2006).

Glucose is the major source of energy and very substantial for the regular functions of the brain. It is known that in a fast person, the brain spends about 60% of glucose. (Wasserman, 2009). In addition, cerebral metabolism requires one-five of the body's oxygen.

Neurons that receive and send impulses are major cells in the central nervous system. Other significant cells for the central nervous system are glial cells that are responsible for providing support for neurons and regulating metabolic processes.

Astrocyte is a kind of glial cell and procures substrates and eliminates unused substances from the brain (Bronk, 1999). There are complex metabolic relations between neurons and astrocytes with significant reactions.

The transition of toxic substances to the brain is hindered by the blood-brain barrier (BBB). The BBB controls the entry of molecules and ions between the brain and blood. Endothelial cells (ECs) composing the walls of the blood vessels, regulate the blood-brain barrier (Daneman and Prat, 2015). BBB ensures the important substances like amino acids water, and glucose, cross with selective transport and passive diffusion. On the contrary, the movement of long-chain fatty acids and protein are restricted by the barrier (Bronk, 1999).

2.4.1.1. Medulloblastoma.

MB is an embryonal tumor arising in the cerebellum in early life and considered to occur from the neuronal progenitor or stem cells. (Northcott *et al*., 2019). MB has been grouped into four molecular subtypes as Sonic Hedgehog (SHH), WNT, Group 3, and Group 4 with peculiar molecular and clinical traits (Wang *et al*., 2018).

SHH occurs in cerebellum while WNT and Group 4 occur in dorsal brain stem and brain stem, respectively.

Group 3 MB which arises in fourth ventricle, is the most aggressive subgroup of MB (Northcott *et al*., 2019). A high rate of metastasis is frequently encountered at GR3 diagnosis and that is a strong indication that the outcome will be poor (Northcott *et al*., 2019). Especially patients with MYC gene over-expressed are in the highest risk group (Northcott *et al*., 2019). Group 3 MB patients make up approximately 25% of all MB patients (Northcott *et al*., 2019).

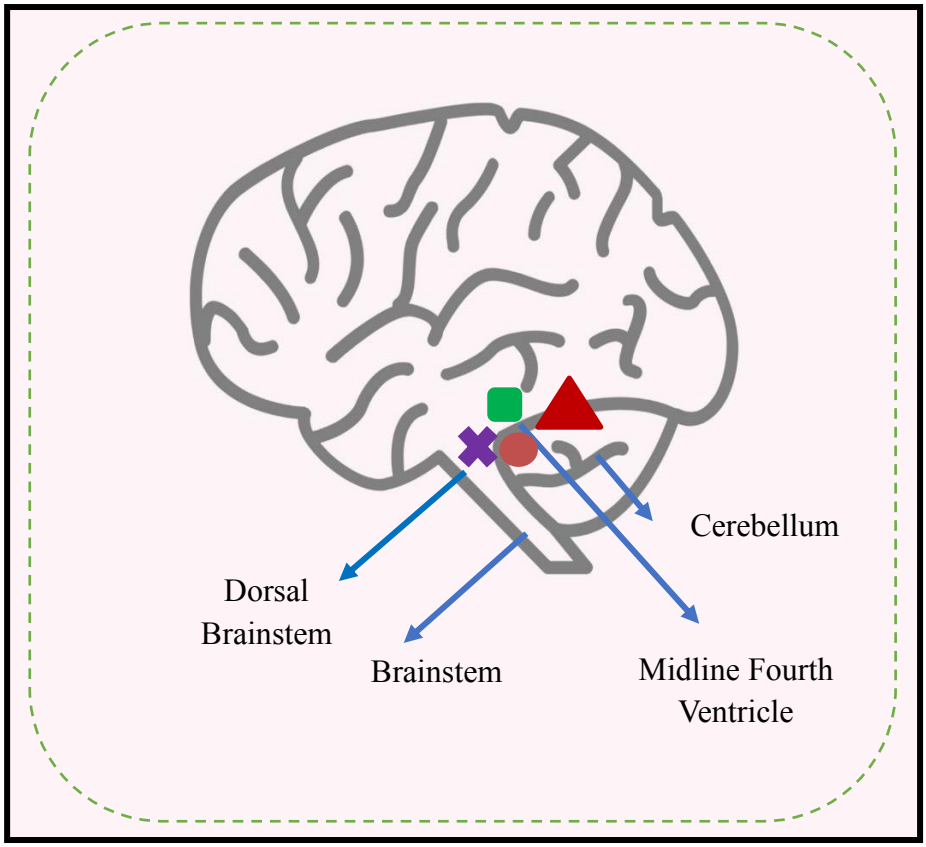

Figure 2.2. Subgroups of Medulloblastoma WNT (Cross in Purple), SHH (Triangle in Red), Group 3 (Square in Green), Group 4 (Oval in Orange).

GR4, other aggressive subtype of MB, is the most prevalent subtype consisting of approximately 35–40% of patients and nearly 1 of 3 patients with GR4 are metastatic (Northcott *et al*., 2019). On the contrary, WNT type of MB which is composed of approximately 10% of all diagnoses, is rarely metastatic, and young individuals generally show a good prognosis (Northcott *et al*., 2019). The risk criteria of the SHH group changes concerning age, metastatic level, genotype, and histology (Northcott *et al*., 2019).

For example, SHH with Tp53 mutation is categorized as one of the most malignant types (Northcott *et al*., 2019). The regions where MB subtypes occur are given in Figure 2.2.

High production of glycine, lipid and taurine are characteristics of MB (Bennett *et al*., 2018), (Davies *et al*., 2008), (Hekmatyar *et al*., 2010). Another distinctive feature of MB is the Warburg effect whose typical properties are abnormal glucose use and overproduction of lactate even in the presence of oxygen (Tech and Gershon, 2015), (Warburg, 1925). As a result of the Warburg Effect, low activity in citric acid cycle (TCA cycle) and oxidative phosphorylation pathways was observed in MB (Tech *et al*., 2015).

Moreover, lipid synthesis is triggered to increase tumor growth. On the other hand, protein production is decreased to restrain energy consumption (Tech *et al*., 2015). It was also detected that the expression of amino acid transporter SLC1A5 which allows uptake of glutamine into cells was enhanced in MB (Munford, 2019).

Furthermore, experimental results on cancer and MB showed that PPP activity is increased relative to normal cell (Bensaad *et al*., 2006), (Niklison-Chirou *et al*., 2017).

2.5. Genome-Scale Modeling of Cancer and Brain Metabolism

Lately, omics data have been used to be integrated with a human GSMM in order to study cancer. Alongside the investigation of metabolic changes related to different cancer types, it was aimed to identify drug targets and biomarkers (Yizhak *et al*., 2015).

In 2011, Folger et al created the first genome scale metabolic model for cancer (Folger *et al*., 2011). They also used omics data to examine cancer-related metabolic alterations. Their findings were consistent with the main metabolic changes observed in various cancer types. Additionally, they identified essential genes for tumor growth (Yizhak *et al*., 2015).

Many studies investigated common changes seen in different cancers such as higher biomass production, proliferation, and the Warburg effect (Folger *et al*., 2011), (Resendis-Antonio *et al*., 2010), (Shlomi *et al*., 2011), (Vazquez, 2011).

In a study conducted by Yizhak et al. a GSMM of NCI-60 cell lines was developed to find a correlation between metastasis and the Warburg effect (Yizhak *et al*., 2014). Lewis et al. reconstructed a brain-specific genome-scale metabolic model (iNL403) by utilizing brain proteome databases (Lewis *et al*., 2010). They validated the model by comparing its flux rates with the experimental results. iNL403 model is employed to study Alzheimer's Disease (AD) and determine genes that cause neuron-related effects.

In the following years, iMS570, which is also a brain-specific genome-scale metabolic model (Sertbaş *et al*., 2014), was developed expanding the model created earlier by the same group (Çakır *et al*., 2007). The scope of the study was to examine transcriptional changes associated with six prevalent neurodegenerative diseases: Parkinson's disease (PD), Alzheimer's disease (AD), Huntington's disease (HD), and schizophrenia (SCH), multiple sclerosis (MS), and amyotrophic lateral sclerosis (ALS). The model was verified by comparing the flux profile with the experimental findings.

Subsequently, Özcan and Çakır reconstructed iMS570g by expanding iMS570 to study one of the most malignant brain tumors, glioblastoma (Özcan and Çakir, 2016). Their results were in agreement with both in-vitro and in-vivo works.

Then, Martin-Jimenez et al. created a genome-scale astrocyte-specific metabolic model called MODEL 1608180000 in 2017 (Martín-Jiménez *et al*., 2017).

RasÏkevičius et al. demonstrated that how GSMMs can be employed for drug design and compared molecular structures of human metabolites and drugs/compounds found in the DrugBank database (Raškevičius *et al*., 2018), (Wishart, 2006). They determined that the compounds whose similarity scores are higher than 0.9 with a human metabolite are more probable to interact with the enzymes metabolizing that metabolite than other compounds.

In another study, Larsson et al. used GSMMs to investigate the transcriptomic data of glioblastoma (GBM) patients and they determined therapeutic targets (Larsson *et al*., 2020).

Recently, Paul et al. studied the gene silencing methods to be utilized as the detecting of drug targets using GSMMs of NCI60 cell lines developed by Yizhak et al (Paul *et al*., 2021), (Yizhak *et al*., 2014).

3. METHODS

In this study, the first genome-scale brain metabolic model iMS570g was customized to the MB model to capture metabolic changes caused by medulloblastoma. Then several analyses including flux balance, flux sampling, flux coupling, and essentiality analyses were performed. Afterward, therapeutic targets for MB were investigated in depth. The summary of these works is shown in Figure 3.1.

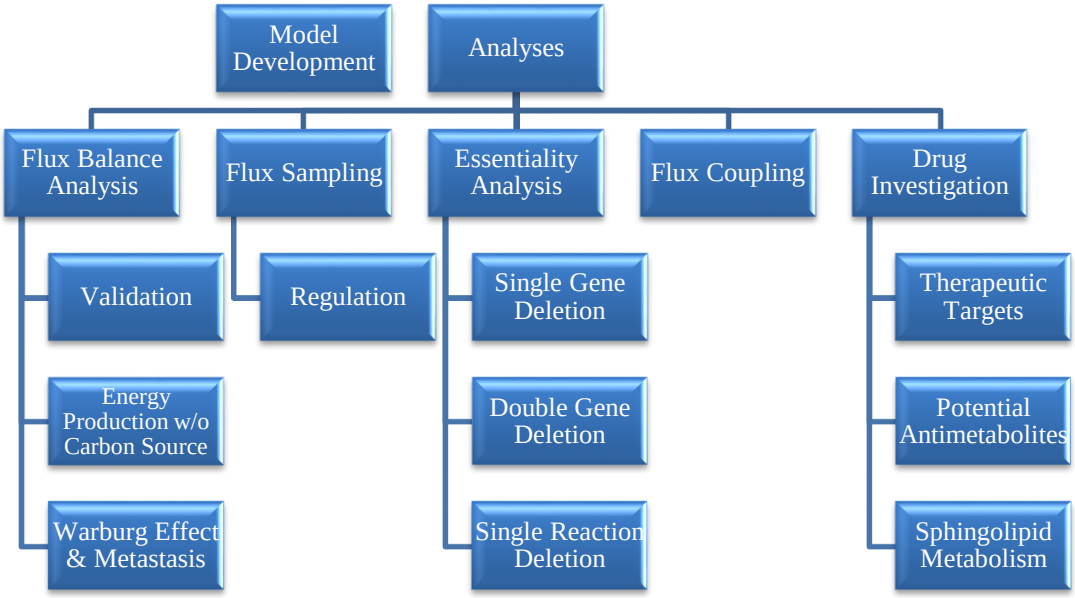

Figure 3.1. Flow chart of works done in this study.

3.1. Model Development

The genome-scale brain metabolic model iMS570 (Sertbaş *et al*., 2014), was expanded to reflect the metabolic alterations that occur in glioblastoma and named iMS570g by Özcan and Çakir (Özcan and Çakir, 2016). The objective of the present study is to investigate metabolic changes realized in MB by further expanding iMS570g and consequently suggest putative therapeutic approaches.

The genome-scale brain metabolic model iMS570 (Sertbaş *et al*., 2014) created by Sertbas et al., has 630 metabolic reactions realized between astrocyte and neuron regulated by 570 genes. iMS570g has 659 metabolic reactions controlled by 572 genes (Özcan and Çakir, 2016). iMS570g covers the main pathways like glycolysis, pentose phosphate pathway, TCA cycle, oxidative phosphorylation, cholesterol synthesis, fatty acid synthesis and amino acid uptake and synthesis pathways. Since tumor cells proliferate unlike normal brain cells, growth reactions based on white matter where glioblastoma is observed, were defined by Özcan and Çakır. Additionally, four reactions indicating the glutaminolysis pathway and glutamine uptake were added to iMS570g in order to include the tumor-induced alterations in glutamine metabolism.

In this work, the composition of the growth reactions based on the white matter defined by Özcan and Çakir was recalculated based on the brain cerebellum where MB frequently forms (Özcan and Çakir, 2016), (Northcott *et al*., 2019). Taurine and glycosphingolipid production pathways were added into iMS570g model. Furthermore, sphingomyelin pathway included by Sertbaş et al. was expanded. The expanded model has 753 metabolic reactions controlled by 601 genes (See Table 3.1).

3.1.1. Addition of New Reactions to iMS570g

3.1.1.1. Taurine Pathway.

Taurine is known as semi-essential amino acid and is found amply in the leukocytes, heart, skeletal muscle, retina, and brain (Schuller-Levis and Park, 2003). Taurine, which is produced from cysteine, plays a key role in the functions related to development in the brain (Ripps and Shen, 2012). Taurine deprivation leads to issues such as renal dysfunction, cardiomyopathy, and developmental anomalies.

As a result of extended research, it was concluded that high level taurine is the characteristic feature of medulloblastoma (Bennett *et al*., 2018), (Davies *et al*., 2008), (Hekmatyar *et al*., 2010). Therefore, 15 Taurine Synthesis reactions were added to the model. These reactions are given in Appendix A.

Table 3.1. The number of reactions and genes in pathways of the expanded model.

Pathway	Number of Reactions	Number of Genes
Glycolysis	31	38
Pentose Phosphate Pathway	16	9
TCA Cycle	31	30
Oxidative Phosphorylation and ATPase	10	92
Glutamate - Glutamine Cycle	11	6
GABA Cycle	6	4
Aspartate Metabolism	3	3
Asparagine Metabolism	1	1
Histamine Metabolism	2	2
Alanine Metabolism	3	2
Glycine-Serine Metabolism	9	9
Leucine Metabolism	9	8
Leucine Metabolism; Ketone Body Metabolism	2	5
Valine Metabolism	10	14

Table 3.1. The number of reactions and genes in pathways of the expanded model. (cont.)

Pathway	Number of Reactions	Number of Genes
Valine Metabolism; Isoleucine Metabolism	3	4
Isoleucine Metabolism	9	16
Lysine Metabolism	10	4
Lysine Metabolism; Ketone Body Metabolism	1	4
Phenylalanine-Tyrosine Metabolism	9	8
Tryptophan Metabolism	4	5
Acetylcholine Metabolism	1	1
Proline metabolism	2	5
Methionine Metabolism	15	13
Threonine Metabolism	6	1
Cholesterol Synthesis	51	23
Fatty Acid Synthesis	92	37
Glycerol-3-phosphate Shuttle	3	2

Table 3.1. The number of reactions and genes in pathways of the expanded model. (cont.)

Pathway	Number of Reactions	Number of Genes
Phosphatidylethanolamine Metabolism	10	8
Phosphatidylethanolamine Metabolism; Phosphatidylcholine Metabolism	2	1
Phosphatidylcholine Metabolism	6	6
Cardiolipin Metabolism	6	2
Sphingomyelin Metabolism	22	17
CDP-Diacylglycerol Biosynthesis	4	17
Inositol Metabolism	26	53
Inositol Metabolism; CDP-Diacylglycerol Biosynthesis	2	2
Lipid Synthesis	2	
Reactive Oxygen Species Pathway	18	16

Table 3.1. The number of reactions and genes in pathways of the expanded model. (cont.)

Pathway	Number of Reactions	Number of Genes
Glycogen Degradation Metabolism	2	6
Ketone Body Metabolism	7	3
Arginine Metabolism	16	13
Polyamine Metabolism	13	16
Creatine Metabolism	6	7
Heme Metabolism	20	13
Purine Nucleoside Metabolism	36	70
Pyrimidine Nucleoside Metabolism	36	10
Taurine Synthesis	11	3
Glycosphingolipid Metabolism	62	16
Exchange	96	

3.1.1.2. Sphingolipid Metabolism.

Since one of the aims of this work is to investigate sphingolipid pathway in detail, the sphingomyelin metabolism pathway included by Sertbaş et al. was expanded and the glycosphingolipid pathway which is the subsequent pathway of sphingomyelin metabolism was added into MB model (Sertbaş *et al*., 2014). 79 reactions including sphingosine-1-phosphate (S1P), phosphoryl-ethanolamine, ceramide derivatives production reactions employed in sphingolipid and glycosphingolipid metabolism pathways were added to the MB model. Additionally, galactose uptake reactions were included since galactose is used in the generation of galactosylceramide (Kanehisa *et al*., 2021), (Roser *et al*., 2009). These reactions are given in Appendix A.

Sphingolipids are divided into two classes according to their head groups as glycosphingolipids and phosphosphingolipids (Ternes *et al*., 2011). The most known phosphosphingolipid is sphingomyelin which forms with the combination of phosphocholine and ceramide (Quinville *et al*., 2021). Sphingomyelins whose structures are cylindrical and have phosphate groups are known to be the main constituents of myelin (Quinville *et al*., 2021). Ceramide 1-phosphate produced by ceramide kinase from ceramide is also phosphosphingolipid (Kanehisa *et al*., 2021).

Glycosphingolipids are grouped into two categories as acidic and neutral glycosphingolipids (Quinville *et al*., 2021). Neutral glycosphingolipids are divided into three groups: glucosylceramide, lactosylceramide, and galactosylceramide (Quinville *et al*., 2021). Cerebrosides (glucosylceramide and galactosylceramide) are made up of monosaccharides and ceramide (Quinville *et al*., 2021). Acidic glycosphingolipids are grouped into four classes; gangliosides, phosphoglycosphingolipids, glucuronoglycosphingolipids, and sulfatoglycoshpingolipids (Quinville *et al*., 2021).

Sphingolipids are knowns to participate in cell membranes as structural elements (Ogretmen, 2018). Sphingolipids also play important roles in many cellular processes like proliferation, growth, migration, and metastasis by controlling signaling functions in the cancer cell (Oskouian and Saba, 2010).

Ceramide and sphingosine-1-phosphate (S1P) are especially significant sphingolipid metabolites responsible for regulating cell apoptosis and survival, respectively (Ogretmen, 2018). In other words, while ceramide is a tumor inhibitor lipid, sphingosine-1-phosphate is a tumor promoting lipid (Ogretmen, 2018).

3.1.2. Biomass Reaction Based on The Cerebellum

Protein, lipid reactions and the biomass reaction including protein, lipid, RNA, and ATP were calculated (Chavko *et al*., 1993), (Ellis *et al*., 2005), (Scandroglio *et al*., 2008), (Sultan, 2002), (Brady *et al*., 2012). Firstly, the composition of amino acids (alanine, methionine, valine, leucine, isoleucine glutamine, glutamate, gamma-aminobutyric acid (GABA), glycine, serine, threonine, phenylalanine, tyrosine, aspartate, asparagine, lysine, arginine, ornithine, histidine, and taurine) was calculated using amino acid contents in the human cerebellum (given in moles of compounds found in gram fresh tissue) for the protein reaction (Banay-Schwartz *et al*., 1993). For example, alanine content was found as 4.9 μmol/g fresh tissue.

It is known that 1-gram fresh brain tissue is equivalent to 0.25 gram dry weight (gDW) (Andersen, 1997). Therefore, alanine content was calculated as given in

$$\frac{4.9\ \mu mol}{g\ fresh\ tissue} * \frac{1\ g\ fresh\ tissue}{0.25\ gram\ dry\ weight} * \frac{1\ mmol}{1000\ \mu mol} = \frac{0.0196\ mmol}{gram\ dry\ weight}. \quad (3.1)$$

Like alanine, all compound contents were converted to mmol/gram dry weight (gDW). The results are given in the second column of Table 3.2. In order to find the mol fractions, each amino acid content in mmol/gram dry weight was divided to the total amino acid content which is 0.420 mmol/gDW. These fractions were used as stoichiometric coefficients for protein reaction composed of amino acids. Then, multiplying molecular weights of all amino acids (Özcan and Çakır, 2016) with molar fractions calculated, the molar weight of protein was detected as 0.13 g/mol to be used in the main biomass reaction.

Table 3.2. Calculation of amino acid composition.

Compound	Compound Content in Fresh Tissue (μmol/g fresh tissue) (Banay-Schwartz *et al*., 1993)	Compound Content in Cerebellum (mmol/ gDW)	Mol Fraction (mmol Compound /mmol protein)	Molecular Weight (g/mol)	Compound Content in 1 mol of Protein (g amino acid/1 mol protein)
Alanine	4.90	0.020	0.047	89.094	4.16
Methionine	0.57	0.002	0.005	149.214	0.81
Valine	1.72	0.007	0.016	117.148	1.92
Leucine	2.42	0.010	0.023	131.175	3.02
Isoleucine	0.82	0.003	0.008	131.175	1.02
Glutamine	19.84	0.079	0.189	146.146	27.63
Glutamate	28.34	0.113	0.270	147.130	39.73
GABA	6.94	0.028	0.066	103.120	6.82
Glycine	11.74	0.047	0.112	75.067	8.40
Serine	4.63	0.019	0.044	105.093	4.64
Threonine	3.84	0.015	0.037	119.120	4.36
Phenylalanine	0.85	0.003	0.008	165.192	1.34
Tyrosine	2.41	0.010	0.023	181.191	4.16
Aspartate	3.74	0.015	0.036	133.103	4.74
Asparagine	1.01	0.004	0.010	132.119	1.27
Lysine	0.98	0.004	0.009	146.190	1.36
Arginine	1.80	0.007	0.017	174.200	2.99
Ornithine	0.60	0.002	0.006	132.160	0.75

Table 3.2. Calculation of amino acid composition. (cont).

Compound	Compound Content in Fresh Tissue (µmol/g fresh tissue) (Banay-Schwartz *et al*., 1993)	Compound Content in Cerebellum (mmol/ gDW)	Mol Fraction (mmol Compound /mmol protein)	Molecular Weight (g/mol)	Compound Content in 1 mol of Protein (g amino acid/1 mol protein)
Histidine	0.72	0.003	0.007	155.157	1.06
Taurine	7.08	0.028	0.067	125.150	8.44
Total	104.95	0.420	1		0.13

Additionally, cerebrosides and gangliosides reactions were created for the main lipid reaction (Norton *et al*., 1975), (Scandroglio *et al*., 2008). The distribution of gangliosides (GM3, GM2, GM1a, GD3, GD1a, GT1a, GD1b, GT1b, and GQ1b) was calculated using ganglioside contents in the whole brain (given in moles of compounds found in gram fresh tissue) (Scandroglio *et al*., 2008).

Table 3.3. Calculation of gangliosides composition.

Compound	Compound Content in Fresh Tissue (nmol/mg fresh tissue) (Scandroglio *et al*., 2008)	Compound Content in Brain (mmol/ gDW)	Mol Fraction (mmol Compound /mmol Gang.)	Molecular Weight (g/mol)	Compound Content in 1 mol (g Compound /1 mol Gang.)
GM3	0.010	0.00004	0.0145	1269	18.40
GM2	0.006	0.00002	0.0087	1385	12.04

Table 3.3. Calculation of gangliosides composition. (cont.)

Compound	Compound Content in Fresh Tissue (nmol/mg fresh tissue) (Scandroglio *et al*., 2008)	Compound Content in Brain (mmol/ gDW)	Mol Fraction (mmol Compound /mmol Gang.)	Molecular Weight (g/mol)	Compound Content in 1 mol (g Compound /1 mol Gang.)
GM1/GM1a	0.119	0.00050	0.1725	1547	267
GD3	0.032	0.00013	0.0464	1517	70
GD1/ GD1a	0.172	0.00070	0.2500	1910	476
GT1a	0.041	0.00020	0.0600	1989	119
GD1b	0.081	0.00032	0.1174	1854	218
GT1b	0.199	0.00080	0.2884	2130	614
GQ1b	0.030	0.00012	0.0435	2505	109
Total	0.690	0.00300	1		1903

Mol fractions of gangliosides were obtained as determined for alanine in Equation (3.1). Afterward, using mol fractions calculated and molecular weights of all gangliosides (Kim *et al*., 2021) the molecular weight of all ganglioside (Gang.) compounds was detected to be used in the main lipid reaction (See Table 3.3). Then, glucosylceramide and galactosylceramide compositions were determined using their contents detected in the whole brain (given in molarity per gram dry tissue) (See Table 3.4) (Norton *et al*., 1975).

Table 3.4. Calculation of cerebrosides composition.

Compound	Compound Content in Brain (M/gDW) (Norton *et al*., 1975)	Molar fraction (M component/ M Cerebrosides)
Glucosylceramide	0.000007	0.388
Galactosylceramide	0.000011	0.611
Total	0.000018	1

Molar fractions of phosphatidyl ethanolamine, phosphatidyl choline, phosphatidyl serine, sphingomyelin, phosphatidyl inositol, cholesterol, and cerebrosides were determined by using their molar weights and contents (given in mg compound found in gram fresh tissue) in the cerebellum for the lipid reaction (Chavko *et al*., 1993). For instance, cholesterol was calculated as 12.84 mg/g in cerebellum (Chavko *et al*., 1993). Cholesterol content in gDW was determined as

$$\frac{12.84\ mg}{g\ fresh\ tissue} * \frac{1\ g\ fresh\ tissue}{0.25\ gram\ dry\ weight} * \frac{1\ g}{1000\ mg} = \frac{0.05\ g}{gram\ dry\ weight}, \quad (3.2)$$

and the result was divided to cholesterol molecular weight to find the amount of mole found in gram dry weight as given in

$$\frac{0.05\ g}{gram\ dry\ weight} * \frac{mol}{386.65\ g} * \frac{1000\ mmol}{1\ mol} = \frac{0.133\ mmol}{gram\ dry\ weight}. \quad (3.3)$$

All compounds except cardiolipin and gangliosides were calculated as shown in Equation (3.2) and Equation (3.3).

Table 3.5. Calculation of lipid composition.

Compound	Compound Content in Fresh Tissue (mg/g fresh tissue) (Chavko *et al.*, 1993)	Compound Content in Cerebellum (mmol/gDW)	Mol Fraction (mol Compound /mol Lipid)	Molecular Weight (g/mol)	Compound Content in 1 mol (g Compound /1 mol Lipid)
Cholesterol	12.84	0.133	0.356	387	138
Phosphatidyl-ethanolamine	13.96	0.076	0.204	734	150
Phosphatidyl-choline	17.34	0.091	0.245	758	186
Phosphatidyl-serine	4.26	0.022	0.058	788	46
Sphingomyelin	2.40	0.013	0.035	741	26
Phosphatidyl-inositol	1.14	0.005	0.014	887	12
Cardiolipin		0.002	0.006	1466	8
Cerebrosides	8.16	0.022	0.058	1510	88
Gangliosides		0.009	0.025	1903	47
Total		0.373	1		700

Then, the ratio of sphingomyelin to gangliosides contents in the whole brain and sphingomyelin content in the cerebellum were used to determine ganglioside content in the cerebellum (Scandroglio *et al.*, 2008), (Chavko *et al.*, 1993).

After finding the proportion of sphingomyelin to gangliosides contents in the whole brain as given in

$$\frac{Sphingomyelin\ content\ in\ brain}{Gangliosides\ content\ in\ brain} = \frac{1.03\,\frac{nmol}{mg\ fresh\ tissue}}{0.73\,\frac{nmol}{mg\ fresh\ tissue}} = 1.411, \qquad (3.4)$$

sphingomyelin content in cerebellum was divided to this result in order to detect gangliosides contents in cerebellum as shown in

$$\frac{0.013\,\frac{mmol}{gram\ dry\ weight}}{1.411} = 0.0092\ \frac{mmol}{gram\ dry\ weight}. \qquad (3.5)$$

Likewise, the ratio of moles of sphingomyelin to that of cardiolipin in the whole brain was used to find the cardiolipin content in the cerebellum (Chavko *et al*., 1993), (Ellis *et al*., 2005). The results for lipid reaction are included in Table 3.5.

Table 3.6. Composition of lipid and protein in gray and white matter and distribution of gray and white matter in cerebellum.

Compound	Compound Content in Gray Matter (g/gDW)	Compound Content in White Matter (g/gDW)	Gray Matter in Cerebellum	White Matter in Cerebellum
Protein	0.55	0.40	74%	26%
Lipid	0.33	0.55		

The central nervous system consists of white matter and gray matter (Mercadante and Tadi, 2021). The cerebellum is composed of an external layer of folded gray matter named the cerebellar cortex which covers white matter named the tree of life which also encloses cerebellar nuclei (Jimsheleishvili and Dididze, 2021). It is known that cerebellar nuclei also consist of gray matter (Mercadante and Tadi, 2021).

Therefore, the main biomass reaction was updated based on the total amounts of protein and lipid found in gray and white matter (Brady *et al*., 2012). While the white matter volume is 24% of the total amount of gray and white matter in *Alouatta palliata*, a type of monkey, this value was found as 17% for *Applodontia rufa*, a type of rodent (Bush and Allman, 2003). The human neocortex is made up of approximately 42% white matter, whereas this rate is 26% for the human cerebellum (Sultan, 2002). Since Brady et al. published the composition of lipid and protein in both gray and white matter, the calculation of the composition of these compounds in the whole cerebellum became possible (Sultan, 2002), (Bush and Allman 2003), (Brady *et al*., 2012) (See Table 3.6).

For instance, protein content in cerebellum was calculated by multiplying percentages of gray matter and white matter in cerebellum with the contents of protein found in white matter and gray matter as shown in

$$Protein\ content\ in\ white\ matter = 0.4\ \frac{g}{gDW} * \frac{26}{100} = 0.1\ \frac{g}{gDW} \qquad (3.6)$$

$$Protein\ content\ in\ gray\ matter = 0.55\ \frac{g}{gDW} * \frac{74}{100} = 0.4\ \frac{g}{gDW}. \qquad (3.7)$$

The sum of these results was divided to protein molecular weight to detect the amount of protein in mmol/gDW as given in

$$\frac{0.5\ g}{gram\ dry\ weight} * \frac{mmol}{0.1286\ g} = \frac{3.97\ mmol}{gram\ dry\ weight}\ . \qquad (3.8)$$

The results obtained for protein and lipid are given in Table 3.7. The results obtained, 3.97 mmol/gDW and 0.55 mmol/gDW for protein and lipid, respectively, were used for main biomass reaction. RNA and ATP compositions calculated by Özcan et al for GBM model were included to biomass reaction in MB model (Özcan and Çakır, 2016).

Table 3.7. Calculation of lipid and protein composition in cerebellum.

Compound	Compound Content in Cerebellum (mmol/gDW)	Molecular Weight (g/mmol)	Total Compound Content in Cerebellum (g/gDW)
Protein	3.97	0.1286	0.5
Lipid	0.55	0.6966	0.4

Newly added ganglioside and cerebrosides reactions for the neuron and recalculated lipid, protein and main biomass reactions for the whole system are given in Table 3.8.

Table 3.8. Updated and newly added biomass reactions.

	Reaction
Gangliosides reaction	0.0145 GM3_N + 0.0087 GM2_N + 0.1724 GM1_N + 0.046 GD3_N + 0.25 GD1a_N + 0.06 GT1a_N + 0.1174 GD1b_N + 0.28 GT1b_N + 0.043 GQ1b_N -> gangliosides_N
Cerebrosides reaction	0.4 Glucosylceramide_N + 0.6 Galactosylceramide_N -> cerebrosides_N

Table 3.8. Updated and newly added biomass reactions. (cont.)

	Reaction
Protein reaction	0.047 Alanine + 0.005 Methionine + 0.016 Valine + 0.023 Leucine + 0.008 Isoleucine + 0.189 Glutamine + 0.270 Glutamate + 0.066 GABA + 0.112 Glycine + 0.044 Serine + 0.037 Threonine + 0.008 Phenylalanine + 0.023 Tyrosine + 0.036 Aspartate + 0.010 Asparagine + 0.009 Lysine + 0.017 Arginine + 0.006 Ornithine + 0.007 Histidine + 0.067 Taurine -> Protein
Lipid reaction	0.356 Cholesterol + 0.204 Phosphoryl_ethanolamine + 0.245 Phosphatidyl_choline + 0.058 Phosphatidyl_serine + 0.0347 sphingomyelin + 0.0137 phosphatidyl_inositol + 0.0056 cardiolipin + 0.058 cerebrosides + 0.0246 gangliosides -> Lipid
Biomass Reaction	3.97 Protein + 0.55 Lipid + 0.11 RNA + 24 ATP -> Biomass + 24 ADP

3.1.3. Determination of Constraints

In an experimental study conducted by Dranoff et al, glioblastoma (GBM) and medulloblastoma (MB) cell lines, U-251 and TE-671 which were kept in a concentration of 5 ml of glutamine for 10 days, showed similar proliferation trend (Dranoff *et al.*, 1985). It was determined that on the 6th day the viable cell counts for U-251 and TE-671, were 25.73 x 10^5 and 29.77 x 10^5, respectively.

Therefore, it is pertinent to think that the two cells may have used similar amounts of glutamine. It was concluded that experimental glutamine uptake for GBM, 0.080 mmol/gDW/h employed for iMS570g could be used for MB model.

In another study executed by Gershon et al, it was observed that the amount of glucose consumed in the SHH cell culture was approximately 3-11 times that of glutamine used by cells (Gershon *et al*., 2013). Based on this information, it was deduced that experimental glutamine uptake for GBM, 0.080 mmol/gDW/h and glucose uptake 0.852 mmol/gDW/h which is approximately 11 times of the amount of glutamine uptake, utilized in iMS570g could be also used in this study.

Various oxygen uptake rates were tested to obtain optimum flux distribution. The test where oxygen uptake was set as 1/6 of MB glucose uptake gave better results. Lower than this value depleted the amount of glucose-6-phosphate entering pentose phosphate pathway (PPP). However, experimental findings on cancer and MB indicate that PPP activity should be higher compared to normal cell (Moreno-Sánchez *et al*., 2009), (Niklison-Chirou *et al*., 2017). Since cancer cells are rapidly proliferating, they need to increase nucleotide generation. Through PPP, cancer cells obtain large amounts of ribose-5 phosphate which is a precursor for nucleotide and NADPH productions (Villa *et al*., 2019). On the other hand, higher oxygen uptakes led to an increase in oxidative phosphorylation which is inconsistent with the Warburg effect known to be observed in MB (Tech *et al*., 2015). Therefore, oxygen uptake was fixed as 0.142 mmol/gDW/h which is 1/6 of determined glucose uptake.

Upper bound of leucine uptake was constrained to 0.034 mmol/gDW/h since Gershon et al found that glucose consumed by SHH cells is 25 time higher than leucine consumed (Gershon *et al*., 2013).

The ratio of maximum tryptophan uptake in MB to normal cerebellum was found as 3.5-3.7 using a mouse model for SHH subgroup of MB (Xin *et al*., 2020). In another study conducted by Dunkl et al, the ratio of maximum tyrosine uptake in MB to normal cerebellum was detected as 2.8 (Dunkl *et al*., 2015). Tryptophan and tyrosine uptakes in healthy brain were determined as 0.002 mmol/gDW/h and 0.001 mmol/gDW/h by Sertbaş et al. (Sertbaş *et al*., 2014).

Using both information, upper bounds of tryptophan tyrosine uptakes were calculated as 0.0074 mmol/gDW/h and 0.0028 mmol/gDW/h. Upper bound of methionine was restricted to 0.008 which was used for GBM in iMS570g (Özcan and Çakır, 2016).

Ketone metabolism and glycogen uptake were fixed to zero because these pathways are used when the activity of glucose metabolism is not sufficient for the cell and glucose avidity is one of the main characteristic of MB as observed in many primary brain tumor metabolism (Çakır *et al*., 2007), (Gururangan *et al*., 2004), (Venneti and Thompson, 2017).

Table 3.9. Upper bounds and lower bounds of all the constraints used in MB models.

Reaction	Lower bound	Upper bound
-> Glucose_A	0.02556	0.02556
-> Glucose_N	0.82644	0.82644
-> O2_A	0.00426	0.00426
-> O2_N	0.13774	0.13774
-> Glutamine_N	0.0776	0.0776
-> Glutamine_A	0.0024	0.0024
-> Leucine_A	0	0.0340
-> Tyrosine_N	0	0.0028
-> Tryptophan_N	0	0.0074
-> Methionine	0	0.0080
-> Glycogen	0	0
-> BHB	0	0
-> Acetoacetate	0	0
<-> NH3_A	-1000	1000

Upper bounds and lower bounds of all the constraints used in MB models are shown in Table 3.9. These uptake values were shared between neuron and astrocyte as 97% and 3% respectively, due to the distribution of these cells in the cerebellum (von Bartheld *et al*., 2016).

3.1.4. Obtaining Medulloblastoma-Specific Genome Scale Models

To acquire Medulloblastoma-specific genome scale models, GSE datasets were integrated to MB model by implementing Gene Inactivity Moderated by Metabolism and Expression (GIMME) algorithm (Becker and Palsson, 2008).

Herein three GSE datasets were used from two different platforms, which are GPL570 and GPL96 (Affymetrix Human Genome U133 Plus 2.0 Array and Affymetrix Human Genome U133A Array) (See Table 3.10). The Samples in GSE62600 (Hooper *et al*., 2014) and GSE37418 (Robinson *et al*., 2012) from GPL96 and GPL570 platforms, respectively, have been classified with respect to MB subtypes.

Table 3.10. GSE datasets used in this study.

GSE Dataset	GPL Platform	Content	Reference
GSE62600	GPL96	28 MB samples including 4 different subgroups and normal neural tissue samples	(Hooper *et al*., 2014)
GSE37418	GPL570	76 pediatric MB samples including 4 different subgroups	(Robinson *et al*., 2012)
GSE10327	GPL570	Non-metastatic, and metastatic MB tissue samples from grade 1 to grade 4	(Kool *et al*., 2008)

GSE10327 from GPL570 platform including non-metastatic, and metastatic MB samples, was utilized to find whether there is a correlation between metastasis and the Warburg effect in MB as found in breast cancer cell lines (Yizhak *et al*., 2014).

In GSE62600, gene expression profiles of different MB subtypes and normal neural tissue samples were compared (Hooper *et al*., 2014).

In GSE37418, 76 pediatric MB samples including 4 different subgroups were analyzed in order to determine mutations that cause MB types (Robinson *et al*., 2012). Both datasets were integrated into the computational model to reflect alterations occurring in MB subtypes and compare them with each other. As it was stated earlier, MB has been categorized into four main subtypes as WNT, Sonic Hedgehog (SHH), Group 3, and Group 4 (Wang *et al*., 2018). Since GR3 is known to be the most aggressive type of MB, the genes controlling lactate production in GR3 have significantly higher expression values compared to other subgroups in both datasets (Northcott *et al*., 2019), (Hooper *et al*., 2014), (Robinson *et al*., 2012).

To create context-specific MB reconstructions, these three-transcription data were integrated by using GIMME algorithm which requires binarized GSE data and a metabolic network (Becker and Palsson, 2008). GIMME algorithm eliminates the reactions whose gene expression values fall below a predetermined threshold. In this study, gene expression values were binarized using a determined threshold to identify up-regulated and down-regulated genes.

3.1.4.1. Threshold Selection.

The threshold for the MB model was considered to be lower than the expression value of Hexokinase 2 (HK2), Pyruvate kinase M2 subtype (PKM2), Fatty Acid Synthase (FASN), Acetyl-CoA Carboxylase 1 (ACC1), Glutaminase (GLS1) genes which are known to be over-expressed in MB (Bhatia *et al*., 2012), (Gershon *et al*., 2013), (Marie and Shinjo, 2011), (Tech *et al*., 2015), (Tech and Gershon, 2015), (Venneti and Thompson, 2017), (Munford, 2019).

HK2, PKM2, FASN, ACC1, GLS1 genes are responsible for controlling glucose-6-phosphate, pyruvate, fatty acid, malonyl-CoA, glutamate productions, respectively (Sertbaş *et al*., 2014).

At first, to find the optimal range for the threshold, random values like 150%, 100%, 75%, 50%, 33%, of the mean of transcriptome data of three datasets were used. For GSE37418, the thresholds which are higher than 75% of the mean of transcriptome data of MB were eliminated because these values were higher than the FASN expression value.

It was detected that the thresholds lower than 50% of the mean of transcriptome data were too low, consequently, no reactions were removed by GIMME. Therefore, the range between 75% and 50% of means of transcriptome data were considered optimum and various thresholds between these values were tested on the MB model to find the ideal results. Since expression levels of genes in this dataset were too close to each other, slight changes in thresholds affected the flux distribution and the number of removed reactions significantly. For example, with 72% of means of GSE37418 transcriptome data, 4 reactions were extracted by GIMME, while 7 reactions were removed with 72.3% of means of transcriptome data. To capture MB-specific flux values, the highest threshold possible was chosen. Eventually, 72.3% of the means of GSE37418 transcriptome data was considered as the optimum threshold for the MB model. That threshold was slightly lower than the FASN expression level and high enough to change the model so that it resembles MB metabolism.

Afterward, the thresholds for SHH, WNT, GR3, and GR4 subgroups were calculated. Since the gene expression levels of the more aggressive subtypes are higher, the threshold values were increased accordingly.

TP53 gene which activates glycolysis by upregulating HK2 and phosphoglucomutase (PGM) is a mutated gene in WNT and the highest risk group of SHH (Marie and Shinjo, 2011), (Northcott *et al*., 2019).

Elevated MYC expression level, which is a typical hallmark of GR3, induces glycolysis activity by upregulating HK2, PKM2, phosphofructokinase (PFK1), lactate dehydrogenase (LDHA), and glucose transporter 1 (GLUT1) (Northcott *et al*., 2019), (Marie and Shinjo, 2011). Therefore, the thresholds which exceed the expression levels of these glycolytic genes specific to WNT, SHH, and GR3 were eliminated.

For GR4, the thresholds higher than 76.34% of means of GR4 gene expressions exceed the expression levels of the FASN gene. Furthermore, the glutamate decarboxylase 1 (GAD1) gene which is responsible for GABA production using glutamate is known to be downregulated in MB (Munford, 2019). Hence GAD1 gene expression level became the lower limit for choosing thresholds. Based on the bounds determined, maximum thresholds for all groups were determined as 72.5%, 74.7 %, 90.24%, and 76.34% of means of WNT, SHH, GR3, and GR4 gene expressions, respectively.

For all subgroups, as threshold values increases, the flux distribution became more like MB metabolism. It was observed that as the threshold became lower than 76.34% of means of gene expressions, flux values on PPP decreased in GR4. Additionally, lower thresholds than the determined value for GR3 led to an increase in the activation of oxidative phosphorylation and ATPase pathway (OXPHOS) which is supposed to have low flux values due to the Warburg effect. While 7 reactions were removed by GIMME from the MB model 7, 9, 13, and 8 reactions were extracted from WNT, SHH, GR3, and GR4 models respectively for GSE37418.

For GSE62600, higher thresholds than 50% of the mean of transcriptome data of MB were eliminated since these values were higher than the GLS expression value. Unlike GSE37418, the expression values in GSE62600 were too high and far from each other. Therefore, slight changes in the threshold value did not affect the system tremendously. The expression values of the specified genes (HK2, PKM2, FASN, ACC1, and GLS1) were accepted as the limit like in GSE37418. As a result of testing all threshold values, 30% of the mean of transcriptome data of MB was selected. 38 reactions were removed by GIMME from the MB model for GSE62600.

For GSE10327, the means of expression values of each non-metastatic and metastatic groups were calculated. According to Chang's classification, in the M0 stage, there is no sign of metastasis (Chang *et al*., 1969). In the M1 stage, there are microscopic cancer cells in cerebrospinal fluid. In the M2 stage, metastasis is detected in cerebral subarachnoid space or cerebellar or in the third or lateral ventricle. In the M3 stage, metastasis is observed in spinal subarachnoid space. And lastly, in the M4 stage, metastasis occurs outside the central nervous system.

To find whether there is a relation between metastasis and the Warburg effect in MB, the expression values of M0, M2, and M4 stages were used. The ratio of ATP generated in glycolysis over the energy produced in OXPHOS (ATPG/ATPOP), was found to be higher in metastatic breast cancer cell lines compared to non-metastatic samples (Yizhak *et al*., 2014).

Moreover, the ratio of lactate production over oxygen uptake (LacR/OCR) was also detected to be higher in metastatic breast cancer cell lines relative to non-metastatic ones (Yizhak *et al*., 2014). This metabolic difference detected in non-metastatic and metastatic samples indicate that the Warburg effect intensifies as the metastasis increases.

Finding proper thresholds played a critical role to reflect these changes to the MB model. Values higher and lower than 45% of the mean of transcriptome data led to an increase in LacR/OCR for non-metastatic (M0) condition. As a result, inconsistent with experimental findings, LacR/OCR became much higher than both LacR/OCR values found for M2 and M4 metastatic samples. Therefore, 45% of the mean of transcriptome data was chosen for the non-metastatic (M0) condition.

Higher thresholds than 55% of the means of transcriptome data for the M4 sample caused an increase in OXPHOS which is inconsistent with the literature. Lower thresholds resulted in a lower LacR/OCR value than the one found for the non-metastatic (M0) sample which is also inconsistent with the literature. Therefore, 50% and 55% of the means were taken as thresholds for M2 and M4 metastatic conditions, respectively.

While 31 reactions were extracted by GIMME from non-metastatic (M0) and metastatic (M2) MB models, 26 reactions were removed from the metastatic (M4) MB model.

After determining the appropriate thresholds for nine MB-specific metabolic models, they were used to detect upregulated and downregulated genes. Genes with an expression value below the threshold were defined as Absent (A) and genes with an expression value above the threshold were defined as present (P). Absent and present (A/P) data which indicates inactive and active genes and the list of Entrez Gene ID's which are identifiers for the genes in the NCBI Entrez database, corresponding to (A/P) data were used as inputs for GIMME. Alongside binarized gene expression data, GIMME uses the genome-scale metabolic network to generate a context-specific reconstruction. Therefore, GIMME should be run with the constraints which show important characteristics of MB. The implementation of the GIMME algorithm in the COBRA Toolbox is explained in detail in Appendix B.

3.2. Analyses

After the integration of MB transcriptome data from Gene Omnibus Database with the model, the MB-specific metabolic alterations were examined, and the drug targets were determined in a context-specific manner. MB transcriptome data was also used to detect whether there is a correlation between metastasis and the Warburg effect in MB as found in breast cancer cell lines (Yizhak *et al.*, 2014).

FBA combined with MOMA was employed to predict the behavior of MB under different conditions. In addition, flux sampling was performed to observe all feasible flux solutions of the reactions. The results obtained from the flux sampling approach were used to calculate statistical p values to identify MB reactions that differ significantly from the ones in the healthy model. Subsequently, various analyses like the regulation analysis and Flux coupling analysis (FCA) were performed to decipher therapeutic targets in MB.

Single-double gene and reaction deletion analysis for growth were conducted to find essential genes and reactions in MB.

Moreover, to detect potential drug targets, the essential genes necessary for all three important parameters for the survival of cancer cells were obtained. It was aimed to identify genes that have an impact on cell energy production and lactate production as well as growth rate.

Another prediction was on the compounds that could be used as antimetabolites targeting metabolic enzymes and to observe the impact of these compounds on both MB and healthy cells. The compounds similar to 315 metabolites present in the brain model were searched one by one from DrugBank Database (Wishart, 2006) by using SMILES (Simplified Molecular Input Line Entry System) of the metabolites and similarity score.

Lastly, after the addition of sphingolipid and glycosphingolipid pathways, essentiality analyses and FBA analyses were repeated to investigate potential therapeutic targets in these pathways as well.

3.2.1. Flux Balance Analyses

The results obtained with GUROBI and CPLEX ILOG optimizers were almost the same whereas the ones obtained with GLPK were remarkably different and not plausible compared to others. Hence all analyses were performed using CPLEX ILOG optimization algorithms provided by IBM's Academic Initiative Program on COBRA toolbox under MATLAB 2017b.

Firstly, flux balance analyses were carried out. After the addition of taurine, sphingolipid reactions, and growth reactions to the iMS570 brain model, the constraints for glycogen, ketone, ammonia, glucose, oxygen, glutamine, tyrosine uptakes were defined as mentioned earlier.

Then objective function was set as maximization of biomass reaction. In all analyses, two flux balance analyses were carried out, before and after the integration of transcription data by GIMME. If the model does not obtain the desired results, GIMME adds back the reactions extracted. After the first FBA, an updated gene rules list including Entrez ID's of all genes corresponding to reactions in the model was uploaded.

This is a critical step because GIMME removes the reactions and the genes controlling these reactions based on the gene rules list after determining upregulated and downregulated genes in AP and EID lists. Subsequently, AP and EID lists created based on the thresholds determined for nine MB-specific metabolic models were uploaded to be used by GIMME.

After the implementation of transcription data based on the specified constraints, additional constraints for tryptophan, methionine, and leucine uptakes were defined. These constraints were defined after the integration of GIMME because defining all constraints before GIMME caused a 65% decrease in the first reaction of PPP and a 74% increase in ATP production in OXPHOS. Ammonia and tyrosine uptake constraints were defined before GIMME because when their constraints were defined after integration of GIMME, FBA solution space reduced, and no solution was obtained as a result of FBA analysis.

After MB-specific models were created by GIMME, the second FBA was performed. Subsequently, the minimization of metabolic adjustment method which aims to find closer results to healthy state rather than finding optimum result was executed to improve the flux results obtained with FBA (Haggart *et al*., 2011), (Özcan and Çakir, 2016). While objective function for FBA was maximization of growth reaction, the objective function for MOMA was minimization of distance between healthy condition and perturbated condition. In other words, it is aimed to minimize the Euclidean distance between these two conditions to obtain results closer to healthy condition.

Flux balance analysis combined with MOMA was performed in various analyses to predict metabolic alterations that occurred in MB. Furthermore, it was aimed to compare the results with the computational healthy model and experimental results obtained for MB. In addition to two analyses carried out for the MB-specific model where the mean of all gene expression levels was used for two GSE data, 4 analyses were performed for subtypes of MB which are WNT, SHH, GR3, GR4.

Additionally, glucose uptake constraint was restricted to zero to detect whether the system produces ATP without a carbon source. In another analysis, glutamine uptake was also restricted to zero to observe energy production without two important carbon sources.

The relation between metastasis and the Warburg effect was also investigated by using the FBA approach.

3.2.2. Sampling Approach

10000 results which satisfy the constraints in solutions space were obtained by using gpSampler function for each reaction. The plots were created for each reaction to show all feasible solutions.

Exchange reactions required for growth reaction were removed from the MB model because the healthy model does not have them. The reactions removed by GIMME from MB model were also erased manually from the healthy model. The number of common reactions found in both models became 594.

In order to determine whether there is statistically important difference between flux sampling results in MB and healthy models, 2-sample t-test with unequal variances was applied to both models. After obtaining p values, Benjamini-Hochberg correction (BH) was used to reduce false discovery rate. As a first step of BH, all p values are sequenced in smallest to largest. Each p-value was given a value in order of smallness and 1 was assigned to the smallest p value. The numbers given to other p-values were increased as p values get higher. Then all numbers assigned to p values were multiplied with false discovery rate (Q) which was determined as 0.01. The results obtained were divided to the number of tests which is 10000. The highest p value smaller than BH correction result was accepted as a critical value and 79 p values higher than this value, were eliminated. In order to reduce the number of p values, the difference between flux sampling mean of the reactions in both conditions were calculated and then the results were divided to sum of the standard deviations of the reactions in both conditions. 94 results lower than 0.5 were removed. The reactions, which have lowest p values, in other words, the ones statistically different, were listed.

3.2.3. Regulation

DNA microarrays give information that can be used to compare mRNA expression levels under different conditions. Transcriptionally important points can be determined with these data. However, metabolic fluxes are controlled by the interaction of gene expression, metabolite levels, and enzyme kinetics. DNA microarrays do not give information about the relation between metabolic flux and gene expression. Bordel et al., developed a method which combines flux data with gene expression data by converting flux and DNA microarray data into statistical scores (Bordel *et al*., 2010). This method allows us to detect whether reactions are metabolically or transcriptionally or post-transcriptionally regulated. The results obtained with this method can be used to study the metabolic diseases in humans.

As a first step of regulation, sampling algorithm was used to obtain a set of flux distributions satisfying the constraints in solutions space for each reaction. The means and standard deviations of the reactions present in both models were calculated using the results obtained from the sampling algorithm.

In order to determine the significance of change between MB and healthy conditions, Z-scores were calculated by dividing the difference of the means between two conditions to the square root of sum of the two variances (Bordel *et al*., 2010). This equation where μm, μh, Var(m) and Var(h) represent flux sampling means and variances of each reaction for MB and healthy conditions respectively, is shown as

$$Z = \frac{\mu m - \mu h}{\sqrt{Var(m) + Var(h)}}. \tag{3.9}$$

After the calculation of Z scores for metabolic fluxes, Z scores for expression data were determined following same steps. Z scores are named as ZF and ZG for Z scores of fluxes and gene expression data, respectively. In order to eliminate statistically less important reactions, which have Z scores close to 0, Z critical value is required.

When the difference of the means between both cases (μm-μh) were compared, it was observed that there were values both greater and less than 0.

That is why, two tailed Z test was chosen where a difference is hypothesized ($\mu c \neq \mu h$) (Montgomery and Runger, 2003). Z critical value was calculated at 5% significance level. Low significance level was chosen deliberately in order to differentiate the reactions which have highest and lowest significance scores.

$Z_{\alpha/2}$ critical value is $Z_{0.025}$ for two tailed Z test at 5% significance level. $Z_{\alpha/2}$ critical value was calculated by subtracting 0.025 from 1 and then determining corresponding value to this result in Z distribution table.

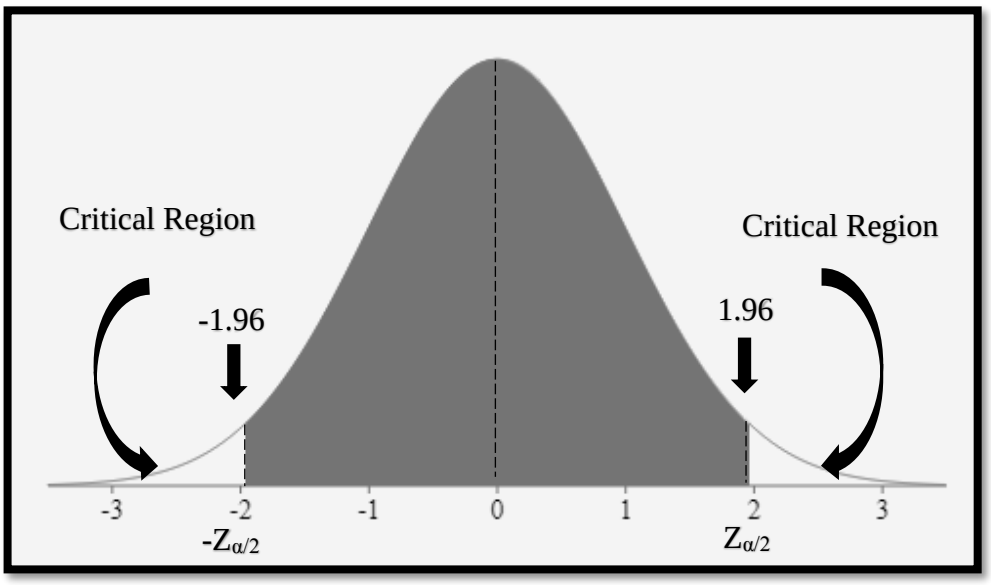

Figure 3.2. The distribution of Z when $\mu c \neq \mu h$ at 5% significance level.

The reactions whose flux values and/or expression levels higher/lower than 1.96 and -1.96 which are critical values, were classified based on whether they are metabolically or transcriptionally or post-transcriptionally regulated. On the other hand, the reactions whose ZF and ZG scores found in dark areas on the bell curve were removed (See Figure 3.2). In other words, the ones which have a significance score close to 0 were eliminated since they do not show important difference between two cases.

The reactions where there is an alteration in its flux but not an alteration in its gene expression are called metabolically regulated reactions.

The reactions, where there is an alteration in its gene expression but not an alteration in its flux, are called post-transcriptionally regulated reactions. Lastly, the ones whose flux and gene expression vary as well, are named as transcriptionally regulated (Bordel *et al*., 2010).

Some reactions have more than one controlling gene, consequently they have more than one ZG score. ZG scores of these reactions were calculated by summing up all ZG values found for each gene controlling these reactions. The reactions whose genes having ZG scores lower/higher than 1.96/-1.96 were not taken into account.

3.2.4. Flux Coupling

Flux coupling analysis is used to detect the reactions that are fully coupled, partially coupled, or directionally coupled to growth reaction (Burgard and Maranas, 2003). When the two fluxes control the activity of each other, these fluxes are named as partially coupled. When two fluxes control and fix the activity of each other, these fluxes are called fully coupled. When the flux of a reaction controls the activity of other flux however not reciprocally, these fluxes are named as directionally coupled.

Flux coupling analysis was carried out with the F2C2 function to find reactions directly related to biomass reaction. Thus, it was determined which reactions should be interfered with in order to inhibit growth in MB.

3.2.5. Essentiality Anayses

In essentiality analysis, all genes or reactions are removed one by one from the model and if the deletion of genes or reactions causes a determined reaction to decrease less than the specified lower bound of that reaction, then they are assumed to be essential. In several studies, essentiality analyses were used to detect a therapeutic target (Folger *et al*., 2011), (Larsson *et al*., 2020), (Paul *et al*., 2021).

In the present study, single, double gene deletion and reaction deletion analyses were also conducted in order to detect essential genes and reactions.

In this part of the study, the genes or reactions whose removal reduces the flux rate of growth reaction under 10^{-6} mmol/gDW*hour were assumed to be essential for the MB model.

Unlike single deletion analysis, in double gene analysis, gene pairs are removed one at the time from the MB model, and the flux rate of a specified reaction is detected after each removal. If the flux rate of the determined reaction falls below a certain value because of double gene deletion, these gene combinations are accepted as essential for the system. In double gene analysis, the gene pairs whose removal decreases the flux rate of biomass reaction under 10^{-6} mmol/gDW*hour were assumed to be essential for the MB model. For double gene deletion analysis, the single genes already found as essential were removed from the analysis, and the remaining genes were searched in pairs for essentiality.

3.2.6. Investigation of Threpautic Targets for Medulloblastoma

In the first part, the essential genes for the MB model were detected. They were analyzed based on their effects on the healthy and MB models. All drugs/compounds related to essential genes were investigated in DrugBank Database and then therapeutically potential ones were detected.

In the second part, the compounds similar to all metabolites in the brain model were detected by using DrugBank Database (Wishart, 2006). Then, the metabolic reactions related to these metabolites were determined. Drug effect was simulated in both healthy and MB models by inhibiting these reactions. The metabolites whose reaction inhibitions do not affect/ slightly affect the healthy model and decrease cancer growth reactions significantly (Biomass reactions) were detected. The appropriate drug/compound candidates were identified. The flow chart of both works is shown in Figure 3.3.

3.2.6.1. Determination of Common Essential Genes for Three Parameters.

It was aimed to identify genes that have an impact on cell energy production and lactate production as well as growth rate.

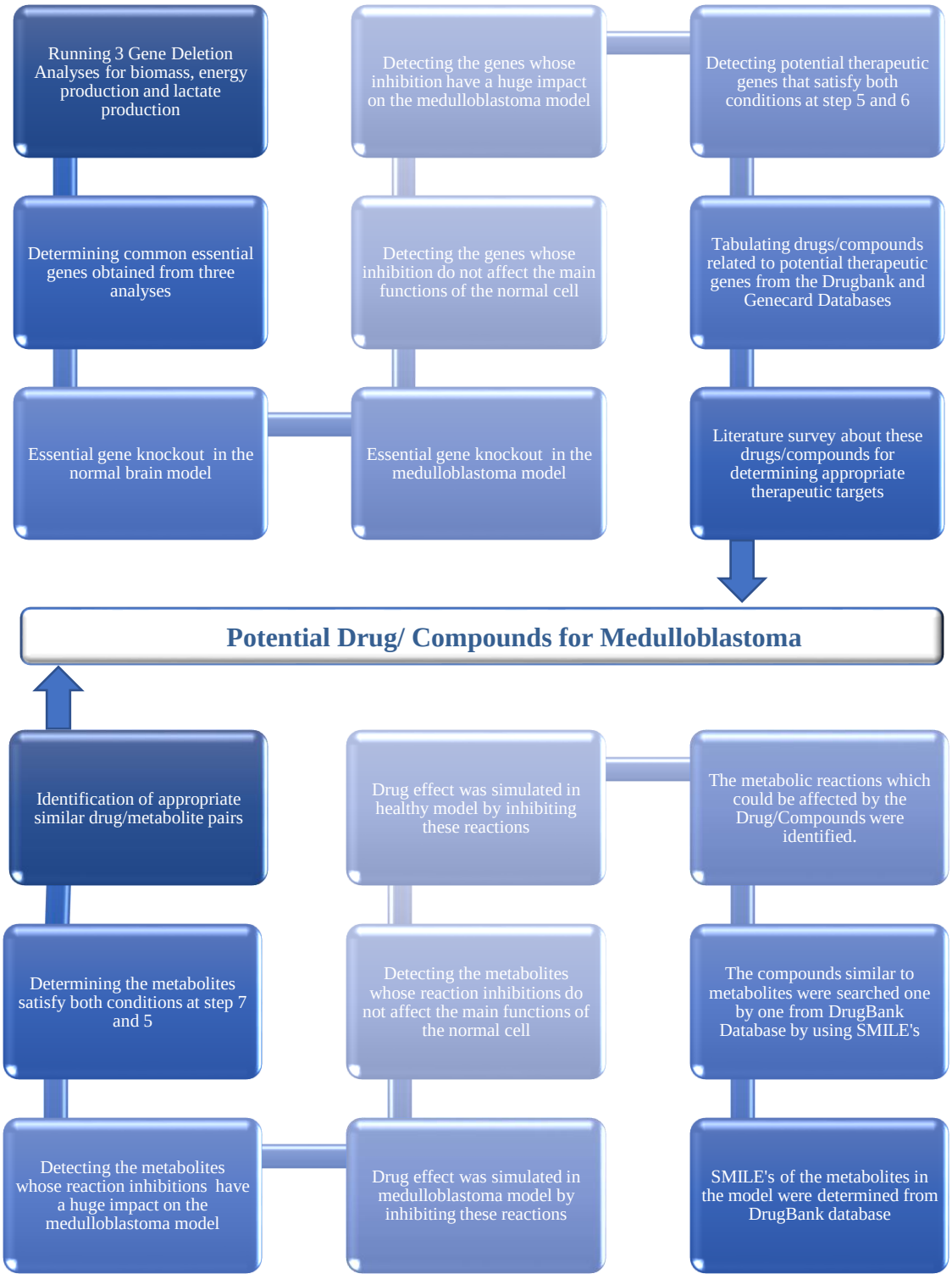

Figure 3.3. Flow chart of investigation of therapeutic targets for MB.

Therefore, in addition to gene deletion analysis for biomass reaction, the same analysis was executed by maximizing ATP production and lactate production one at a time. For both analyses, the upper bound of biomass reaction was constrained to biomass flux obtained in the MB model (0.000116 mmol/gDW*hour) while the lower bound was restricted to 50% of it (0.000058 mmol/gDW*hour). With this, it was ensured that the biomass value does not fall below a certain value while determining the genes that are essential for lactate production and energy production.

As a result, the essential genes necessary for all three important parameters for the survival of cancer cells were obtained. It is expected that targeting the genes that are certainly necessary for all these three parameters would increase the impact of the treatment. 32 essential genes found in three analyses were analyzed in detail.

To identify potential therapeutic targets, among 32 common the essential genes whose inhibition do not affect healthy brain cells were determined. Therefore, the constraints of reactions controlled by essential genes were restricted to zero one by one in the healthy model. Subsequently, results were compared with normal healthy cell and the ones which fail to fulfill vital tasks were left out. For instance, the genes whose inhibitions affect the main pathways like glycolysis, PPP tremendously were eliminated, Afterward, the same gene inhibition procedure was applied for the MB model. The ones whose inhibition influences the MB model significantly were detected.

3.2.6.2. Identification of Potential Metabolite-Antimetabolite Pairs.

Drug design is a process where new medicines are designed relied on the data of a metabolic target (Zhou and Zhong, 2017). Drug discovery is a long, difficult, and expensive process in spite of recent developments in biotechnology.

Computer-aided drug design is an indispensable alternative that accelerates this process. Computer-aided drug design is divided into two groups, ligand-based drug design (LBDD) and structure-based drug design (SBDD) (Yu and MacKerell, 2017). LBDD is used when the structure of target cannot be identified by modeling methods (Huang *et al.*, 2010).

Statistical methods are used to associate ligand activity with structural data. In SBDD, it is important to have a target structure before studying the link between receptor and ligand (Huang *et al.,* 2010). The target molecule for SBDD should be related to the disease and it should have a binding site so that the designated substance competes with the natural metabolite for the target to lose its effect (Anderson, 2003). Enzymes, hormone receptors, G-coupled protein receptors (GPCRs), transporters, nucleic acid, and ion channels are the main drug targets (Robertson, 2007). Enzymes are known as potential drug targets because they have ligand-binding pockets which is ideal for drug development (Anderson, 2003). Furthermore, knowing the ligands of enzymes and the substrates with which they interact makes enzymes promising drug targets. It is assumed that compounds similar to natural metabolites will bind to the enzyme by causing competitive inhibition of that enzyme (Raškevičius *et al.,* 2018).

Drug repurposing is a promising approach where novel uses of approved drugs/compounds are investigated for another use other than its intended purpose (Pushpakom *et al.,* 2018). This approach has an edge over designing a new drug for a certain indication. Since the repurposed drug has already been detected to be harmless in humans, the probability of being unsuccessful is lower. Additionally, the drug designing process may be decreased as various assessments have already been performed. Furthermore, less expenditure is required than is necessary to develop a new drug.

Antimetabolites are chemically similar substances to natural metabolites, which are part of cellular metabolism (Peters, 2014). Antimetabolites which are often used for cancer and viral diseases, inhibit the use of metabolites (Peters, 2014), (Smith, 1997). Raškevičius et al. compared molecular structures of human metabolites and drugs found in the DrugBank database (Raškevičius *et al.,* 2018), (Wishart, 2006). They found that the drug agents whose Tanimoto scores are more than 0.9 with a human metabolite are almost 30 times more possible to interact with the enzymes metabolizing that metabolite than other ligands. Considering these results obtained in this study, here, it was aimed to predict the compounds targeting metabolic enzymes and their impact on both medulloblastoma and healthy cells.

In this work, all the compounds similar to 315 metabolites present in the medulloblastoma brain model were determined using the DrugBank database (Wishart, 2006). Firstly, SMILES (Simplified Molecular Input Line Entry System) of the metabolites were determined from the DrugBank database and then tabulated to be used in search of similar compounds (Wishart, 2006). Afterward, the compounds whose chemical structures are similar to these metabolites were searched one by one from the Chemical Structure Search engine found in the DrugBank Database by using SMILES of these metabolites (Wishart, 2006). For example, to find similar compounds to lactate, the chemical structure of lactate was drawn by importing SMILE of that metabolite (See Figures 3.4).

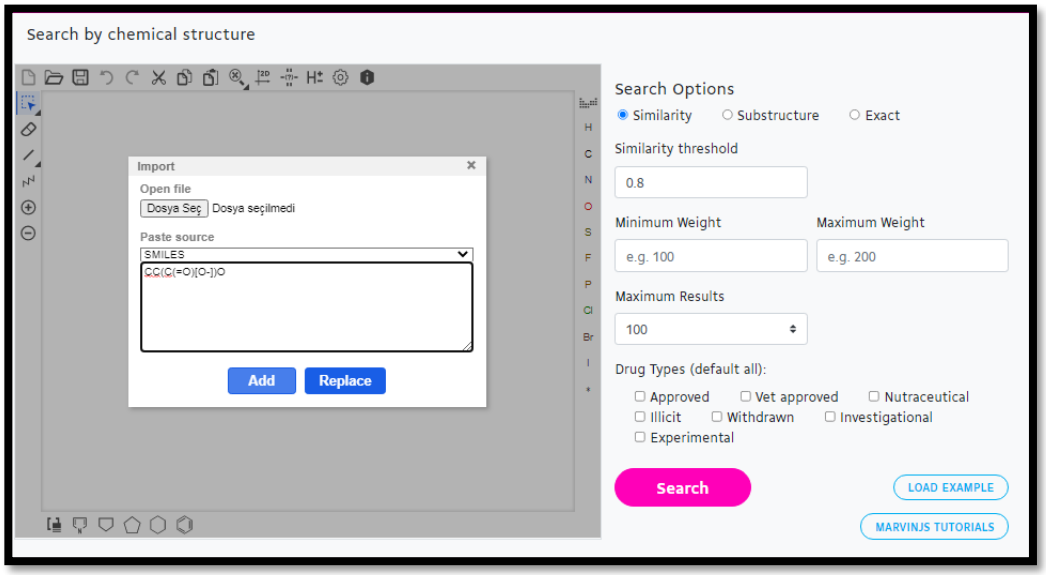

Figure 3.4. Addition of SMILE of lactate in chemical structure search engine (Wishart, 2006).

Search options were set for similarity and the similarity threshold was specified as 0.8 (See Figure 3.5). As a result, 7 compounds similar to lactate were detected (See Table 3.11). In the first column of Table 3.11, there are similarity scores, which show the similarity between the chemical structures of the compound and the metabolite. The second column of the table includes the DrugBank ID's of these compounds. Other columns contain name, SMILE, and status for these compounds. These steps done for lactate were repeated for all 315 metabolites (See Appendix C). Almost 1900 similar compound-metabolite pairs were detected and tabulated (See Appendix C).

Then all the metabolic genes/proteins that catalyze the reactions of the metabolites (anti-metabolites/substrates) and that could be targeted by the drug to create a drug effect on the model were determined. For example, it was considered that a compound similar to glucose-6-phosphate will target reactions R2, R17, R47, and R61 (See Table 3.12).

The constraints of reactions were set as 0.1 of their flux rates determined without the drug. The results were compared with normal healthy cell and the ones which fail to fulfill vital tasks in the presence of drug were left out.

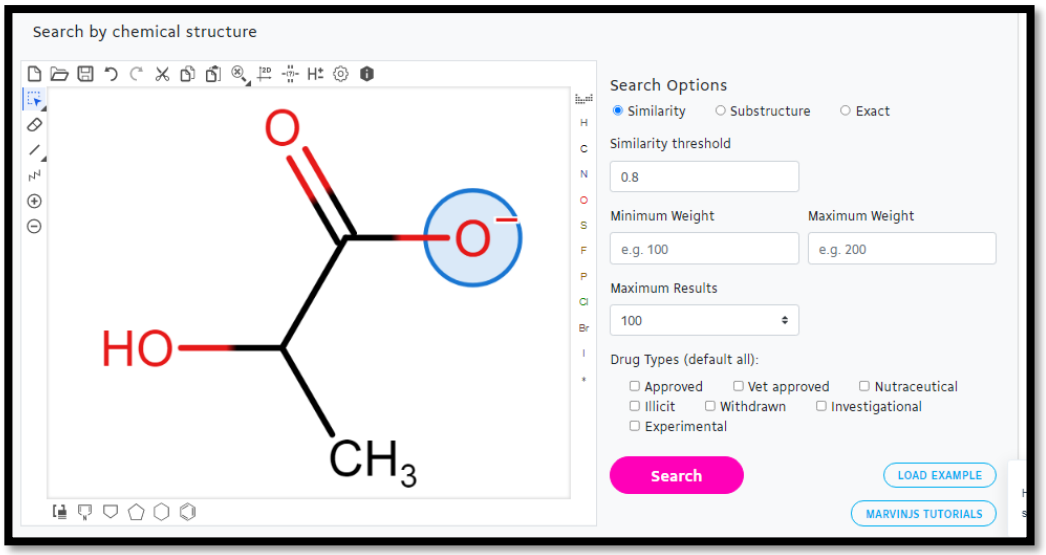

Figure 3.5. Setting search options (Wishart, 2006).

For example, after decreasing the constraints of reactions whose substrate are glucose-6-phosphate, (R2, R17, R47, and R61) solution space reduced with new constraints, and no solution was obtained as a result of FBA analysis. It is considered that their inhibition will damage healthy cells alongside cancer cells. As a result, drug effects were created in the healthy model by performing 315 flux balance analyses for each metabolite in the model.

Flux balance analyses in the presence of drug were carried out in the MB model as well. The same procedure used for the healthy model was repeated. The decrease in growth rates (Biomass) of all results realized in the medulloblastoma model with the drug was calculated as a percentage.

Table 3.11. The compounds similar to lactate (Wishart, 2006).

Similarity Score	Drug Bank ID	Compound Name	Status	Compound Smile
1	DB03066	D-Lactic acid	Experimental	[H][C@](C)(O)C(O)=O
1	DB14475	D-Lactic acid	Approved, Experimental	C[C@H](O)C(O)=O
0.95	DB06768	Ammonium lactate	Approved	[NH4+].CC(O)C([O-])=O
0.95	DB09483	Potassium lactate	Approved	[K+].CC(O)C([O-])=O
0.95	DB13231	Calcium lactate	Approved, Investigational, Vet approved	[Ca++].CC(O)C([O-])=O.CC(O)C([O-])=O
0.95	DB14515	Magnesium lactate	Nutraceutical	[Mg++].CC(O)C([O-])=O.CC(O)C([O-])=O
0.826	DB03680	Tartronate	Experimental	OC(C([O-])=O)C([O-])=O

The results in which the growth rate decreased by less than 40% in the medulloblastoma model were left out. The results where vital tasks were realized in the healthy model and the ones in which growth rate reduce more than 40% in the MB model were detected and evaluated.

Table 3.12. Reactions related to glucose-6-phosphate.

Pathway	Reactions Related to Metabolites	Reaction Name	Controlling Gene
Glycolysis	Glucose-6-phosphate_A <-> Fructose-6-phosphate_A	R2	GPI
Pentose Phosphate Pathway	Glucose-6-phosphate_A + NADP_A <-> 6-phosphoglucone_A + NADPH_A	R17	G6PD
Glycolysis	Glucose-6-phosphate_N <-> Fructose-6-phosphate_N	R47	GPI
Pentose Phosphate Pathway	Glucose-6-phosphate_N + NADP_N <-> 6-phosphoglucone_N + NADPH_N	R61	G6PD

4. RESULTS AND DISCUSSION

4.1. Validation of MB Model Results with Experimental Results

This section includes the comparison of healthy brain model and the experimental findings with the results obtained from MB-specific models. SHH, WNT, GR3, and GR4 MB specific models are going to be referred to as SHH-MB, WNT-MB, GR3-MB, and GR4-MB from now on. MB model where the mean of all expression values was used, is going to be referred to as MB.

As it was mentioned in the previous section, the glucose uptake rate for all nine MB-specific models is constrained to 0.852 mmol/gDW/h (3-11 fold of glutamine uptake as reported in Gershon et al., 2013) while this value was 0.08 mmol/gDW/h for the healthy model (Sertbaş *et al.,* 2014). The high difference between glucose uptake rates in healthy and MB models stems from the Warburg Effect whose typical characteristics are excessive glucose consumption and high lactate production (Warburg, 1925). Tumor cells tend to generate ATP via glycolysis rather than oxidative phosphorylation regardless of the availability of oxygen (Kim *et al*., 2012). In accordance with the Warburg effect, high lactate production, low TCA cycle, and OXPHOS activities were observed in all MB specific models.

Pyruvate kinase is a significant enzyme that carries out the conversion of phosphoenolpyruvate and ADP to pyruvate and ATP (Sertbaş *et al.,* 2014). PKM2, one of the isozymes of pyruvate kinase, is overexpressed in MBs and GBMs (Venneti and Thompson, 2017). Consistent with experimental results, high flux rates in pyruvate production reactions (R10 and R55) were observed in MB models (See Figure 4.1 and Figure 4.2). The ratio of pyruvate production to glucose uptake was calculated as 1.96 in MB models while it is only 1.2 for the healthy model.

Furthermore, ATP generation in glycolysis was significantly higher in MB models compared to the healthy model (See Figure 4.3).

ATP generation reactions in glycolysis (R7+R10+R52+R55) met 99% of the ATP needs of the system while OXPHOS reactions (R45+R88) which are the main ATP producer reactions of normal cells, only met 1% of the ATP needs of tumor cell. On the contrary, the healthy model produced only 11% of ATP in the glycolysis pathway.

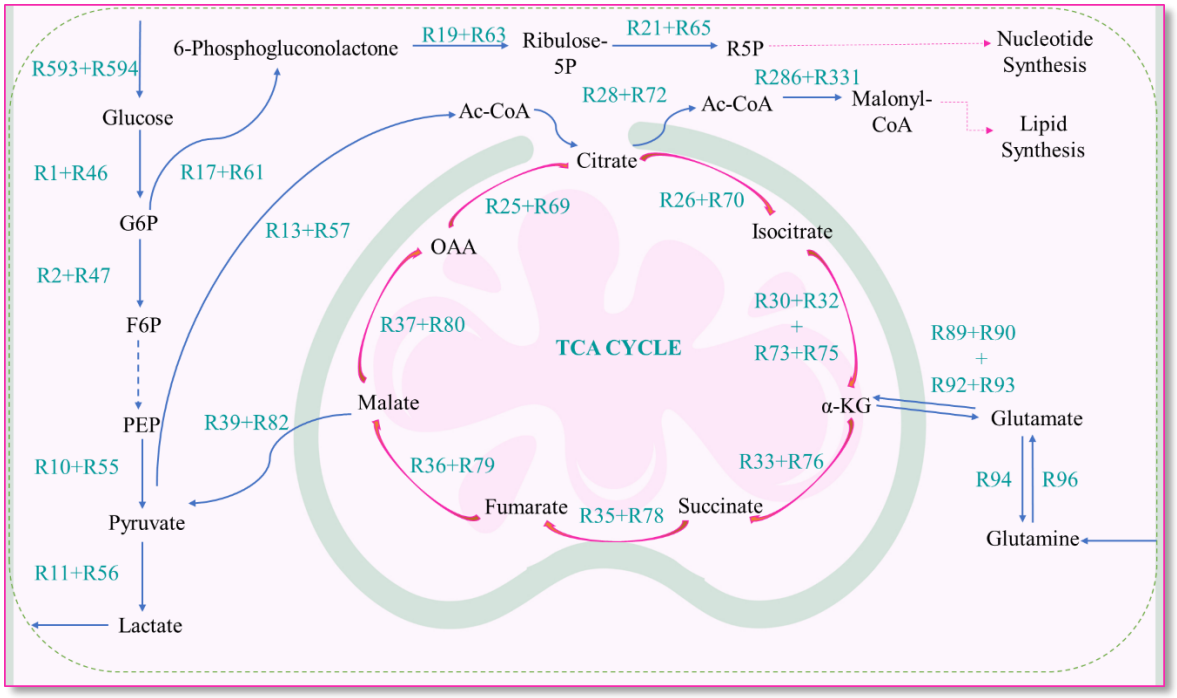

Figure 4.1 Main reactions carried out in glycolysis, PPP, TCA cycle, and other pathways.

High lactate synthesis is one of the prominent characteristics of MB (Valvona, 2016). Gershon et al, found that the cerebellar granule cell with Sonic Hedgehog (SHH) produces almost twice as much lactate as its glucose uptake (Gershon *et al.*, 2013). In agreement with experimental findings, the flux values of the lactate production reactions (R11 and R56) were found as approximately 1.67 mmol/gDW/h in MB computational models which is correlated with the stoichiometric coefficient of 1 molecule glucose producing 2 molecules of lactate (See Figure 4.2 and Table 4.1) (Gershon *et al.*, 2013), (Holthoff *et al.*, 1993).

On the other hand, the lactate production rate in the healthy model was detected to be eight times lower than its glucose uptake rate (See Table 4.1). These alterations observed in the glycolysis pathway of MB models are consistent with the Warburg Effect which is known as one of the important hallmarks of cancer metabolism.

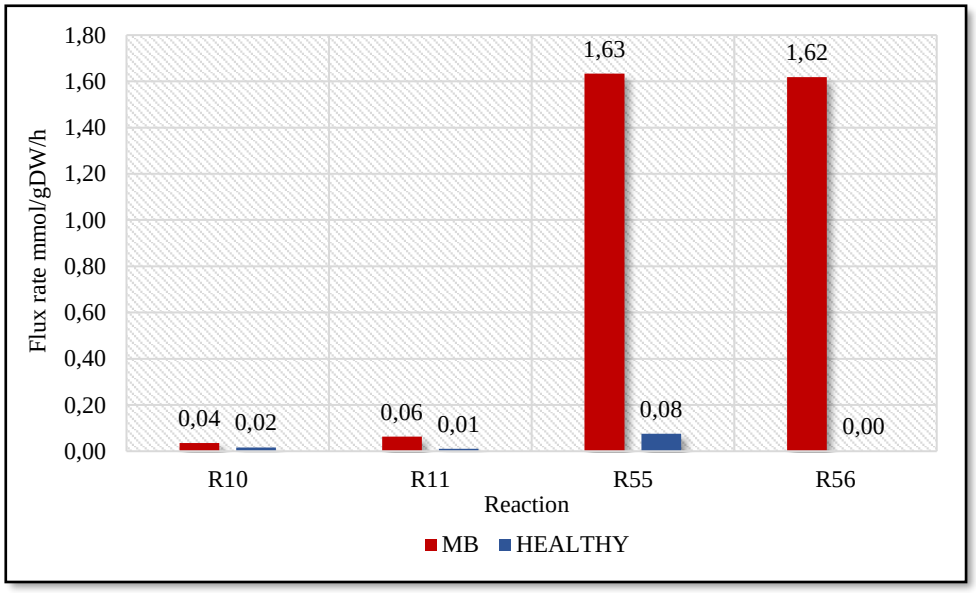

Figure 4.2. Pyruvate and lactate production rates of astrocyte (R10 and R11) and neuron (R55 and R56) for MB and healthy models.

It is known that cancer cells need ribose-5 phosphate to be used in the productions of nucleotides to support their uncontrollable proliferation. To meet their needs, cancer cells activate PPP where ribose-5 phosphate and NADPH are generated (Villa *et al.*, 2019). It is determined that phosphofructokinase (PFK-1) is 22–56 times more active in various human cancer cells than normal cells (Moreno-Sanchez *et al*., 2009). However, in brain cancers (gliomas, medulloblastoma, meningiomas, schwannomas), the activity of PFK-1 is the same or 1.3–2.5 times less active compared to normal brain (Moreno-Sanchez *et al*., 2009). The low activity of PFK-1 stems from the stimulation of the TIGAR gene (Tp53-induced glycolysis and apoptosis regulator) (Bensaad *et al.*, 2006). Consequently, the deactivation of PFK-1 causes glucose 6-phosphate to head to the pentose phosphate pathway (PPP) and activate this pathway. Additionally, the TAp73α gene was detected to be considerably upregulated in GR4 and GR3 subtypes of MB relative to normal brain (Niklison-Chirou *et al.*, 2017). TAp73α gene is known to be responsible for increasing serine production, PPP activity, and regulating glutaminolysis (Niklison-Chirou *et al.*, 2017). Based on these experimental findings on cancer and MB, the ratio of glucose-6-phosphate rate entering PPP to glucose uptake rate was aimed to keep at higher level in MB models than healthy models. As seen from Figure 4.4, the first reactions of PPP (R17 and R61) and R5P production reactions (R21 and R65) are more active in the MB model than the healthy model.

Table 4.1. The comparison of MB-specific models results with healthy model and experimental (exp.) results.

	MB-All	SHH	WNT	GR3	GR4	Healthy	Exp. Results for MB
Glucose uptake rate	0.852	0.852	0.852	0.852	0.852	0.080	
Lactate production rate	1.67	1.67	1.67	1.67	1.67	0.011	Twice of glucose uptake rate
PPP rate /glucose uptake	0.084	0.084	0.084	0.085	0.084	0.055	Higher than healthy brain
R5P production rate	0.024	0.024	0.024	0.024	0.024	0.001	Higher than healthy brain
(TCA) flux	0.043	0.043	0.043	0.043	0.043	0.120	Lower than healthy brain
Acetyl-CoA flux	0.043	0.043	0.043	0.043	0.043	0.003	Higher than healthy brain
Glutamate Production	0.074	0.074	0.074	0.074	0.073	0.056	Higher than healthy brain
Glutamate production /glutamine production	1.43	1.43	1.43	1.43	1.43	No Data	1.18 - 1.71

Table 4.1. The comparison of MB-specific models results with healthy model and experimental (exp.) results. (cont.)

	MB-All	SHH	WNT	GR3	GR4	Healthy	Exp. Results for MB
GABA Production	0.0004	0.0004	0.0004	0.0005	0.0004	0.0659	Lower than healthy brain

Other models of MB have also more active flux rates than the healthy model as seen in Table 4.1. While the 7.5% of total glucose is diverted to PPP in the MB model, this value is 5% for the healthy model. As mentioned earlier in the method section, defining a proper oxygen uptake constraint was a crucial step to keep higher flux rates in PPP in MB models. The test where oxygen uptake rate was restricted to 1/6 of MB glucose uptake gave plausible results as shown in Table 4.1 and Figure 4.4.

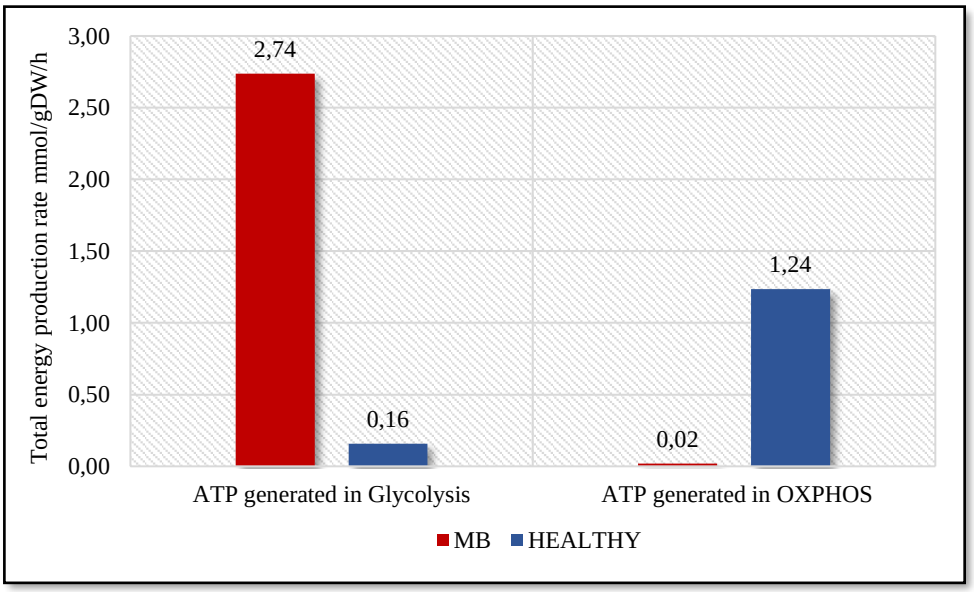

Figure 4.3. Total ATP flux rates produced in glycolysis (R7+R10+R52+R55) and OXPHOS (R45+R88) for MB and healthy models.

A higher oxygen uptake rate than this value led to significant increase in OXPHOS which is inconsistent with the Warburg effect. Lower oxygen uptake rates than this value resulted in a decrease in PPP activity, which is inconsistent with the literature. There could be two possible reasons that the oxygen uptake rate affects PPP tremendously. The first reason may be that when there is a limited amount of oxygen, cancer cell uses most of the glucose to obtain energy from glycolysis instead of spending it in PPP. Low-level oxygen restricts cancer cells to divert some of glucose-6-phosphate to PPP in order to produce sufficient energy in glycolysis. But when cancer cell takes up more oxygen, more energy is produced in OXPHOS, hence the energy production in glycolysis decreases, and some of glucose 6 phosphate molecules are directed to PPP.

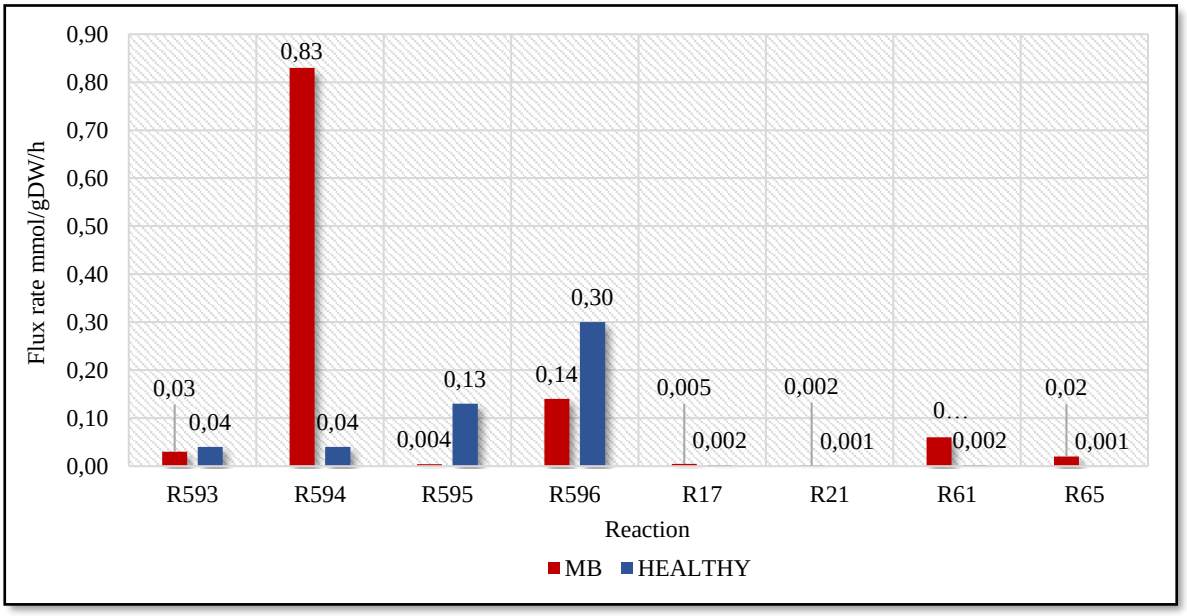

Figure 4.4. The glucose uptake (R593 and R594), oxygen uptake rates (R595 and R596), 6-phosphogluconate (R17 and R61), and R5P production (R21 and R65) rates in PPP of astrocyte and neuron, respectively for MB and healthy models.

Even though the activity of OXPHOS decreases in many cancer types, most cancers including MB utilize the respiratory chain for ATP generation (Moreno-Sánchez *et al.*, 2009), (Niklison-Chirou *et al.*, 2017), (Stincone *et al.*, 2015). That is why optimum oxygen uptake was chosen that would not conflict with the Warburg effect and would support the information about PPP activation.

The second reason may be that PPP is activated when cells are subjected to oxidative stress (Stincone *et al.,* 2015). PPP not only contributes to precursor synthesis for nucleotide production but also keeps cell reduction-oxidation (redox) in balance (Stincone *et al.,* 2015). The ratio of glucose-6-phosphate entering PPP to glucose uptake changes depending upon reactive oxygen species (ROS) generation. Hydrogen peroxide (H_2O_2) produced in the reactive oxidative pathway disrupts the ratio of nicotinamide adenine dinucleotide phosphate (NADH) to NADPH. Consequently, this disruption makes the glucose-6-phosphate dehydrogenase (G6PDH) enzyme which generates 6-phosphogluconate and NADPH, susceptible to oxidants. At first, glyceraldehyde 3-phosphate dehydrogenase (GAPDH) and pyruvate kinase (PK) are inhibited leading to a slowdown in glycolysis.

Subsequently, transcriptional regulators enhance the activity of PPP by inducing responsible enzymes that activate G6PDH (Stincone *et al.,* 2015). Then triosephosphate isomerase (TPI) is suppressed as the amount of phosphoenolpyruvate (PEP) increases, thus, the fluxes in PPP reactions enhance even more (Stincone *et al.,* 2015). It was observed that PK activity decreases in cancer cells to prevent oxidative damage (Stincone *et al.,* 2015). In agreement with the literature, in addition to PPP activity, the H_2O_2 production rate was detected to be elevated after increasing the oxygen uptake rate (See Figure 4.5). As seen in Figure 4.5, when the total oxygen uptake rate (R595+R596) was increased from 0.006 to 0.14 mmol/gDW/h, the total H_2O_2 production rate (R421+R431) was also enhanced from 5e-06 to 0.13 mmol/gDW/h. The flux of the first reaction in PPP was also increased significantly.

Consistent with the Warburg effect, TCA cycle activity is lower in MB models than in the healthy model (See Table 4.1). The first reaction of the TCA cycle, citrate synthase reaction (R69), in which acetyl-CoA and oxaloacetic acid (OAA) are converted to citrate in neuron, is active due to its use in the production of acetyl-CoA but it has still lower flux rate relative to one in the healthy model (See Table 4.1 and Figure 4.6). The same reaction carried out in astrocyte (R25) is relatively less active compared to one in neuron because astrocyte takes only 3% of all uptakes.

Acetyl-CoA produced in mitochondria is the source of most of the carbon found in fatty acids (Marie and Shinjo, 2011). Since acetyl-CoA cannot be transported from mitochondria, oxaloacetate and acetyl-CoA produce citrate which can be exported from the mitochondria. Then, citrate is converted back to acetyl-CoA by ATP citrate lyase (ACL). Subsequently, malonyl-CoA is produced from acetyl-CoA by acetyl-CoA carboxylase (ACC) and both are used for the fatty acid synthesis (Marie and Shinjo, 2011).

Bennet et al. determined that the high amount of lipid found in MB differentiates it from some other pediatric tumors (Bennett *et al*., 2018). Bhatia et al. also found that the SHH pathway, which leads to the SHH subtype of MB, activates necessary proteins for lipid synthesis (Bhatia *et al*., 2012). In the early years of life, the number of cerebellar granule cells is increased by sonic hedgehog (SHH) signaling.

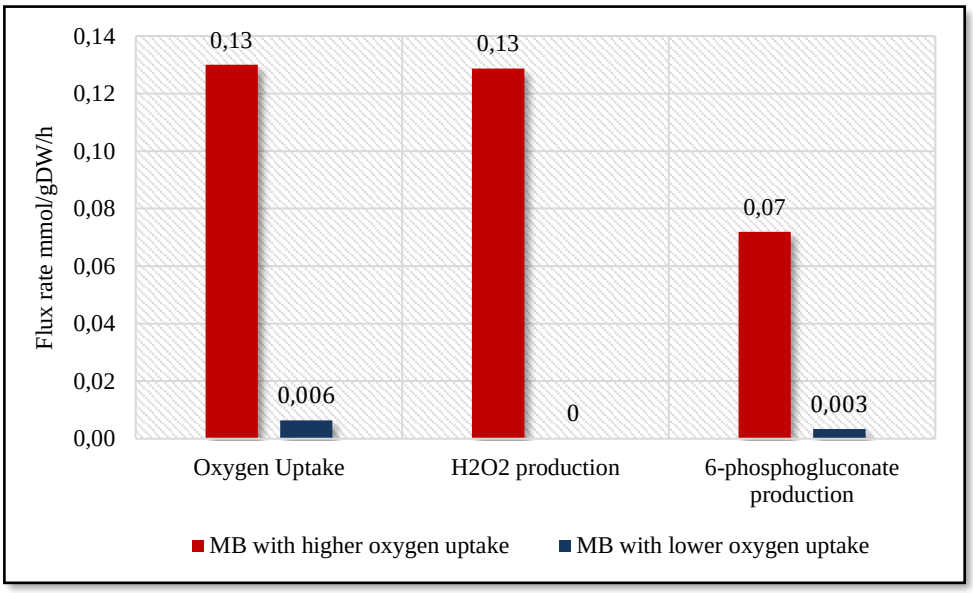

Figure 4.5. Alterations of total hydrogen peroxide (H_2O_2) (R421+R431) and 6-phosphogluconate productions with respect to total oxygen uptake (R595+R596) for the MB model.

When the cerebellum develops, sonic hedgehog (SHH) signaling ceases. However, when the SHH pathway is abnormally regulated, it may keep on stimulating proliferation, which makes this pathway prone to MB (Munford, 2019).

Moreover, the SHH pathway changes the metabolic properties of the cells by enhancing lipogenesis and glycolysis activity. In order to activate lipid production, SHH upregulates major lipid synthesis enzymes like FASN and ACC1 (Bhatia *et al*., 2012). Since acetyl-CoA production in the TCA cycle is a precursor reaction for lipid synthesis, their flux values are expected to be higher than the normal brain model. In agreement with the literature, the flux rate of this reaction (R72) in neuron was found to be higher than healthy brain model (See Table 4.1 and Figure 4.6). However, the flux rate for the same reaction (R28) in astrocyte was too close to zero in both MB and healthy models. Therefore, this reaction (R28) was not included in Figure 4.6 for both cases.

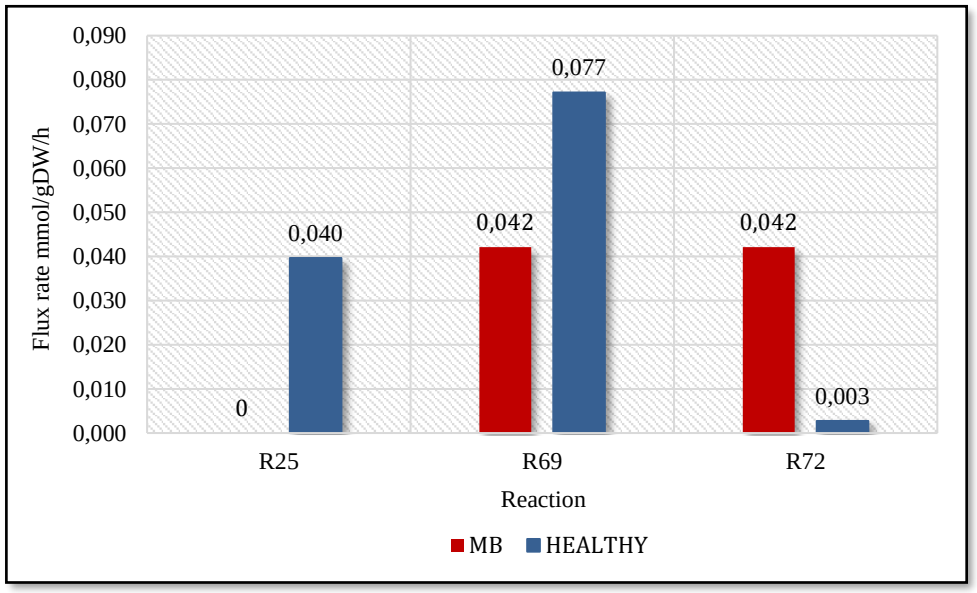

Figure 4.6. Citrate (R25 and R69) and acetyl-CoA (R72) production rates in astrocyte and neuron for MB and healthy models.

It was detected that in all MB subtypes, the expression levels of EAAT1 and EAAT2-4 proteins which control glutamate uptake were decreased (Munford, 2019). It was also found that the expression level of the SLC1A5 gene which controls glutamine uptake was considerably higher than normal cells (Munford, 2019). These results show that MB prefers de novo glutamate production over external glutamate uptake. The expression of the GLS1 gene which regulates glutamate and ammonia productions was determined to be higher in all MB subtypes relative to healthy cerebellum in the same study (Munford, 2019).

In agreement with the literature, the reaction where glutamine is converted to glutamate has higher flux values in all MB models compared to the healthy model (See Table 4.1). Additionally, in MB models, the ratio of glutamate over glutamine concentration was determined as 1.43 which is very similar to the results obtained experimentally (Davies *et al.*, 2008), (Kohe *et al.*, 2018), (Panigrahy *et al.*, 2006) (See Table 4.1).

GAD1, one of the genes regulating the GABA cycle, is also expressed lowly in MB relative to the healthy brain (Munford, 2019). Furthermore, the expression of SLC6A1 which plays an important role in GABA uptake was found to be lowly expressed in MB. All this information supports that MB prefers low concentrations of GABA and inhibits its production. Agreement with the literature, it was observed that all MB subtypes have lower GABA synthesis fluxes than the healthy model (See Table 4.1).

4.2. Energy Production without Carbon Source

The aim of this section is to determine from which pathway the MB cell meets its energy needs in the case of glucose and glutamine deficiency by employing Flux balance analysis. Firstly, the glucose uptake rate was constrained to zero so that the effects of glucose absence on energy generation in the brain can be observed. It was determined that the difference in total ATP production between the MB model with a carbon source and the one without a carbon source is distinctive (See Figure 4.7). In the absence of glucose, total energy production decreased by 83%. In the presence of glucose, the main ATP producer is the glycolysis pathway in the MB model due to the Warburg effect (See Figure 4.8).

However, when glucose uptake was restricted to zero, the OXPHOS met most of the energy needs of the system. This result is compatible with the opinion about the ketogenic diet targeting the glycolysis pathway by decreasing the required metabolites for this pathway (Tech and Gershon, 2015). Ketones that are produced in fatty acid degradation can be the main energy source with a diet that includes high-fat nutrients and restricts carbohydrates. This diet was applied to brain cancer patients in several studies. In the study reported by Seyfried et al. the size of astrocytoma decreased 80% in mice after ketogenic diet application (Seyfried *et al.*, 2003). The reason 6% of energy needs are met from the TCA cycle is that glutamine is one of the main carbon sources for this pathway (Özcan and Çakır, 2016).

In glucose absence, MB also uses glutamine to meet its energy and carbon needs. It was found that TCA cycle intermediates are enhanced in the absence of glucose suggesting that cells also meet their energy needs from TCA by using glutamine (Le *et al.*, 2012).

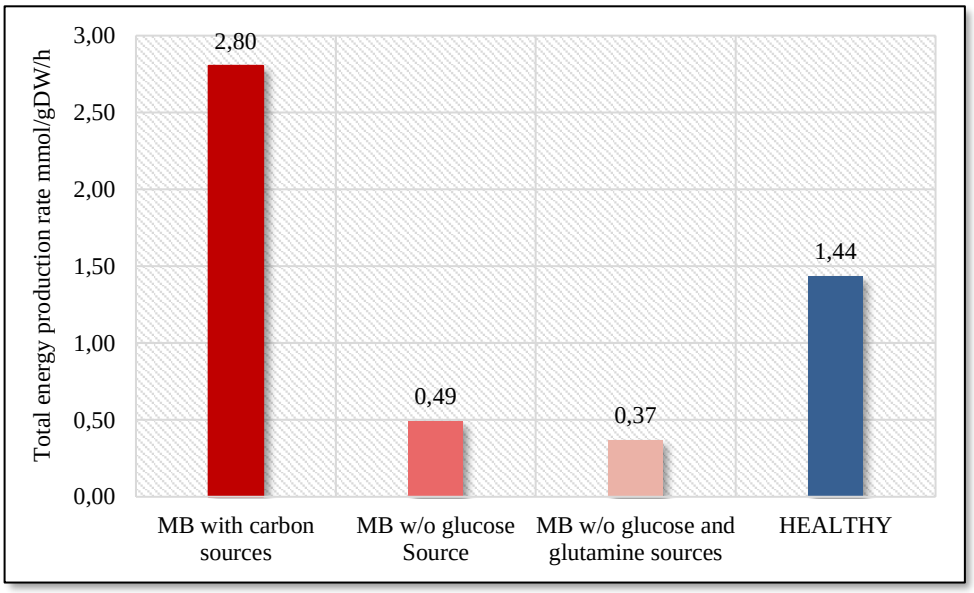

Figure 4.7. Alterations in total energy production rate with respect to glucose and glutamine uptake restrictions.

Afterward, the glutamine uptake rate was also constrained to zero in order to observe the impact of two simultaneous perturbations on the MB model. Without two main carbon sources, like before, MB obtained most of its energy needs from OXPHOS as shown in Figure 4.8. In the TCA cycle, ATP is generated as a result of succinate production from succinyl-CoA (Sertbaş *et al.*, 2014). Succinyl-CoA is produced from alpha-ketoglutarate which is also used in the glutamine-glutamate cycle. When glutamine uptake was restricted to zero alongside glycolysis, alpha-ketoglutarate was consumed to produce glutamate thus MB could obtain glutamine from glutamate. That is why, energy produced in TCA cycle decreased to 4% from 6%. However, in the absence of glutamine, the total energy production rate was reduced by only 25% than in the case where there was only glucose deficiency. In other words, glutamine absence did not influence the system as much as glucose deficiency.

Consequently, in both cases (Without glucose and without both glucose and glutamine), to meet its energy requirement MB turned to OXPHOS which was the only option for ATP production.

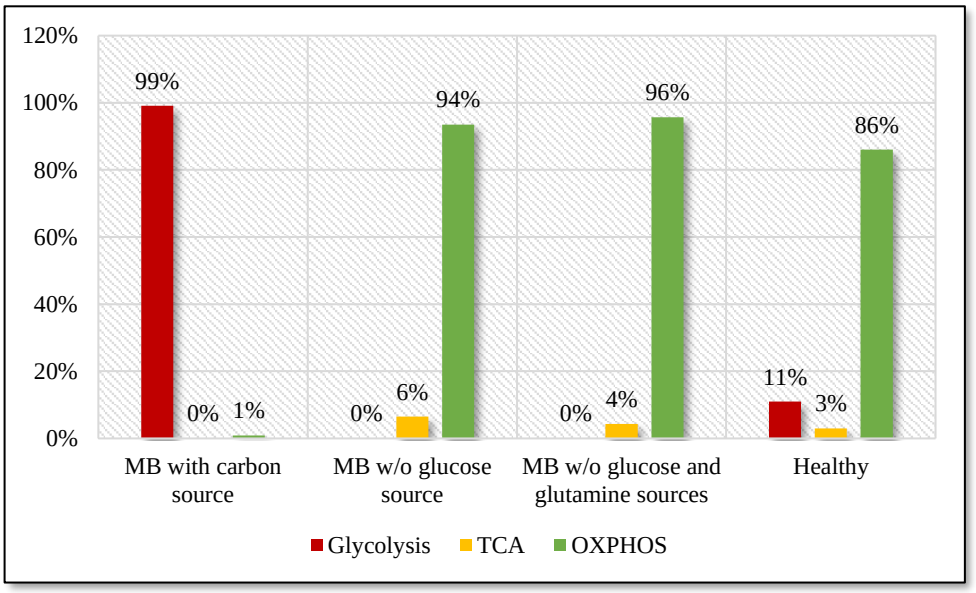

Figure 4.8. Alterations in energy production distribution with respect to glucose and glutamine uptake restrictions.

MB using aerobic glycolysis even in the presence of oxygen was observed to be almost completely dependent on OXPHOS in glucose deficiency. Furthermore, the decrease in total energy production observed in both cases suggests that the absence of glucose makes survival difficult for MB, as observed in the ketogenic diet results for astrocytoma (Seyfried *et al.*, 2003).

4.3. The Relation Between Metastasis and The Warburg Effect

The objective of this section is to find whether there are any changes in the Warburg effect as primary MB tumor spreads to other parts of the human body by using Flux balance analysis and gene expression data.

Once MB metabolic model was integrated with GSE10327 dataset which included expression data of 62 human medulloblastoma samples (Kool *et al.*, 2008), MB-M0, MB-M2, and MB-M4 models which reflect non-metastatic, grade 2 and grade 4 metastatic MB tumors were obtained.

Yizhak et al. detected that as migration enhances in NCI-60 cell lines, the ratio of ATP generated in glycolysis over the energy produced in OXPHOS increases. They silenced some of the active genes in glycolysis such as PGAM1, PGK2, GAPDH, and HK2 whose expression values were higher in metastatic samples and detected a decrease in glycolysis activity as metastasis decelerates. For instance, after HK2 was inhibited, they found that oxygen uptake elevated whereas the activity of glycolysis and lactate production reduced.

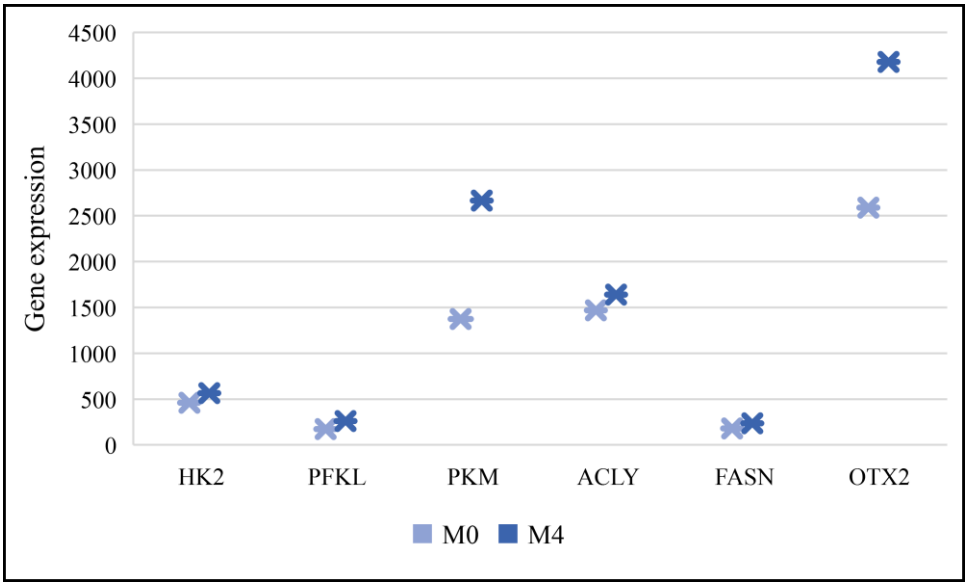

Figure 4.9. The comparison of genes expression levels between non-metastatic and metastatic samples (M0 and M4).

According to the experimental data reported by Kool et al (Kool *et al.*, 2008), HK2, PFKL, and PKM genes found in the glycolysis pathway have higher expression levels in grade 4 metastatic tumors (M4) compared to M0 (Figure 4.9). ATP citrate lyase (ACL) and fatty acid synthase (FASN) which are responsible for the production of acetyl-CoA and fatty acids (Marie and Shinjo, 2011) have also higher expression levels in metastatic tumor samples compared to non-metastatic (M0) samples.

Orthodenticle Homeobox 2 (OTX2) which has been shown as a potential oncogene in several cancers has also a higher expression level in metastatic tumor samples compared to M0 (See Figure 4.9) (Lu *et al.*, 2017). Previously, OTX2 was described as an oncogene in all types of MB. However, the aggressive role of OTX2 in GR4 and GR3 compared to WNT and SHH subgroups was emphasized in few studies (Wortham *et al.*, 2012). Additionally, it was indicated that OTX2 inhibition decreases the size of tumor (Panwalkar *et al.*, 2015).

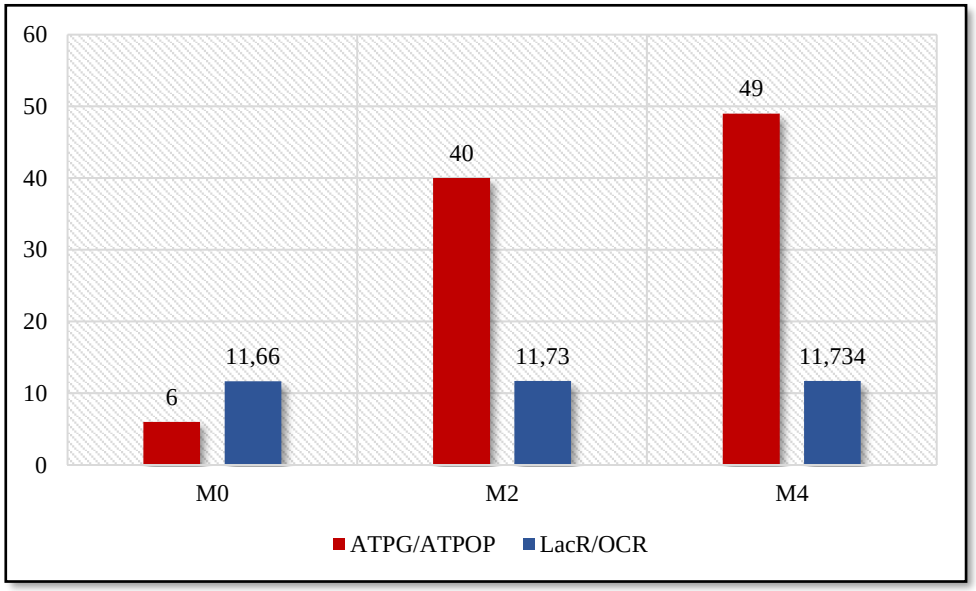

Figure 4.10. The comparison of ATPG/ATPOP and LacR/OCR between non-metastatic (M0) and metastatic samples (M2 and M4).

Since the expression levels of HK2, PFKL, and PKM genes functioning in glycolysis are higher in metastatic samples, the Warburg effect is expected to increase in metastatic cases of MB. Indeed, the ratio of ATP generated in glycolysis over ATP generated in OXPHOS (ATPG/ATPOP) was found to be almost 7 times higher in MB-M2 than ATPG/ATPOP detected in MB-M0 (See Figure 4.10). Although the difference in ATPG/ATPOP observed between MB-M0 and MB-M2 was not detected between MB-M2 and MB-M4, ATPG/ATPOP was distinctly higher in MB-M4 compared to one in MB-M2.

The ratio of lactate secretion to oxygen consumption rate (LacR/OCR) increased slightly as metastasis intensified suggesting that MB uses its energy to support metastasis rather than growth. Consistently, no important change was observed between growth reactions of MB-M0 and MB-M2 models.

Consequently, the alteration observed in ATPG/ATPOP indicates that the Warburg effect increases as the metastatic level in MB increases. Metastasis in MB can be alleviated by targeting the genes linked to the Warburg effect and reducing ATPG/ATPOP. Yizhak et al. also detected that the cells that have a higher Warburg effect, are more resilient and need a higher dose of drugs to inhibit their growth (Yizhak *et al*., 2014). With this finding, it can be concluded that a different approach is required for metastatic samples of MB to suppress them.

4.4. Sampling

In this section, it was aimed to obtain all possible flux values that can be obtained within the given constraints that each reaction can take and compare these ranges of values for the two cases. Additionally, it was aimed to detect whether there is a statistical difference between reaction flux rates of MB and healthy models. To find the flux range and the most probable flux values for each reaction, flux sampling analysis was performed by using gpSampler function of COBRA Toolbox, and 10000 results which satisfy the constraints in solutions space were obtained for each reaction.

Moreover, in order to determine whether there is statistically important difference between flux sampling results in medulloblastoma and healthy models, 2-sample t-test with unequal variances was applied to both models.

After obtaining p values, Benjamini-Hochberg correction was used to reduce false discovery rate. False discovery rate (Q) was determined as 0.01. The reactions were divided into two lists for neuron and astrocyte. Then the ratio of the difference between flux means of both conditions to the sum of the standard deviations of both conditions (RDMSD) was used to reveal the most important reactions for neuron and astrocyte.

Since only 3% of metabolites are taken up by astrocytes in the cerebellum, the difference in reactions between MB and healthy models for astrocyte is notably higher than the ones obtained for neuron. Therefore, lower p values were found for astrocyte.

To acquire the most significant reactions in both cells, 98 reactions whose RDMSD values are higher than 60 were assumed to be significantly different in astrocyte while 80 reactions whose RDMSD values are higher than 3 were assumed to be statistically different in neuron. Furthermore, 27 exchange reactions whose RDMSD values are higher than 60 were accepted as statistically important reactions. Consequently, 205 reactions out of 594 common reactions found in both models, were determined to be the statistically important reactions. All significant reactions detected are given in Appendix D with fold changes (the ratio of flux values in the MB model to flux values in the healthy model), p values, and RDMSD values. For both cells, the percentages of significant reactions for each subsystem were calculated as shown in Figure 4.11 and Figure 4.12.

In leucine metabolism, transport reaction of leucine from neuron to astrocyte, ketoisocaproic acid transport reaction from astrocyte to neuron, and leucine production from glutamate and ketoisocaproic acid were found to be significantly decreased in the MB model relative to the healthy model. Similar transport reactions required for isoleucine generation and the reaction in which isoleucine produced from glutamine were also detected to be lower than the fluxes of the normal brain. It is known that L-type amino acid transporter 1 (LAT1) which is responsible for transporting amino acids including leucine, valine, glutamine, and isoleucine are upregulated in MB (Cormerais *et al*., 2018), (Munford, 2019).

It was also found that several brain malignancies break down leucine, valine, and isoleucine to support their metabolism (Cormerais *et al*., 2018). In another work, the SHH subtype of MB consumed leucine and valine to be used for cancer metabolism rather than producing them (Gershon *et al*., 2013). Additionally, MB cells require glutamate tremendously to synthesize glutamine and support the TCA cycle because glutamate uptake was found to be downregulated in MB (Munford, 2019). Hence instead of consuming glutamate to generate leucine and isoleucine, MB may prefer to use them for glutamine production.

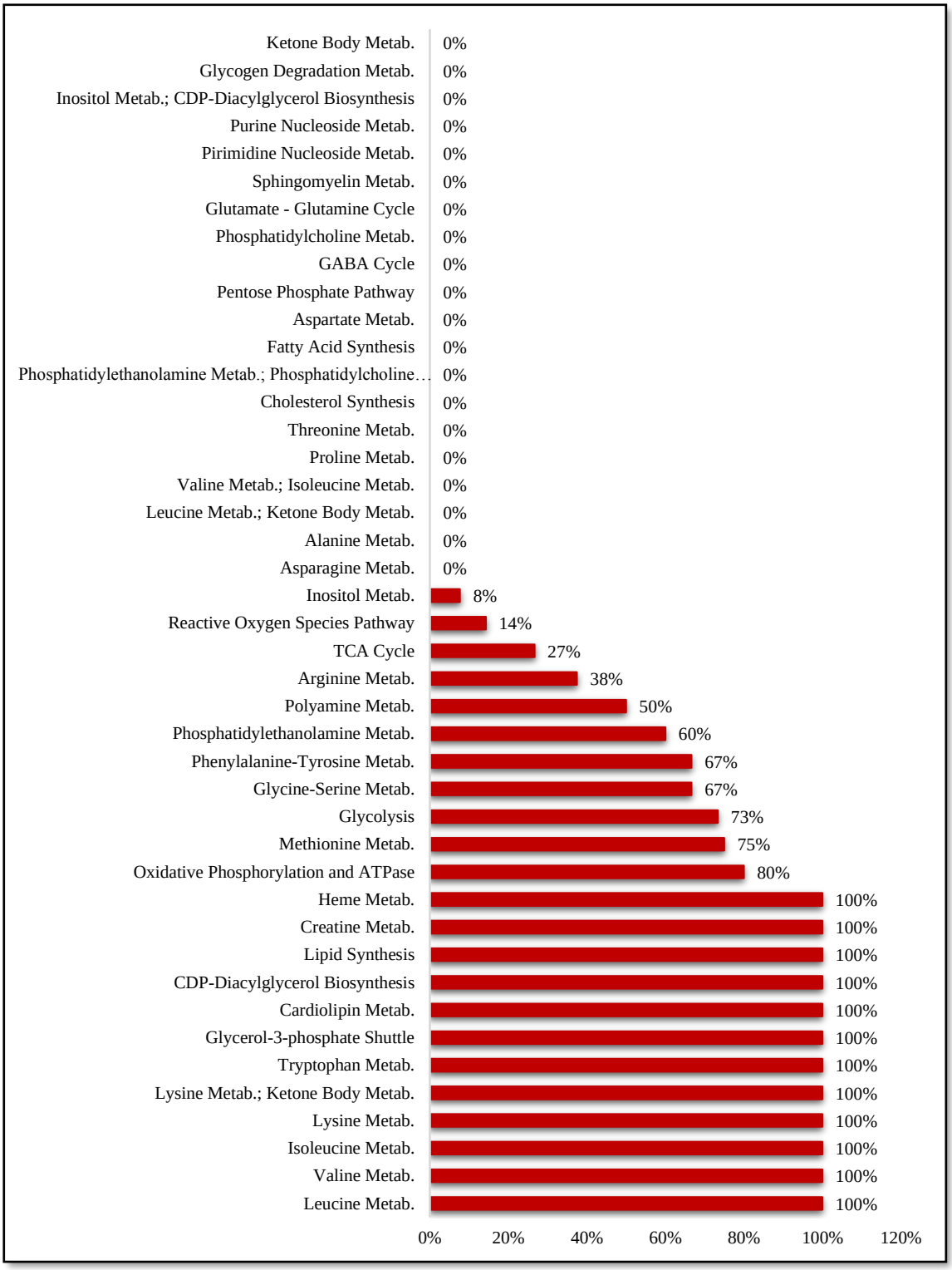

Figure 4.11. The percentages of significant reactions in neuron for each subsystem.

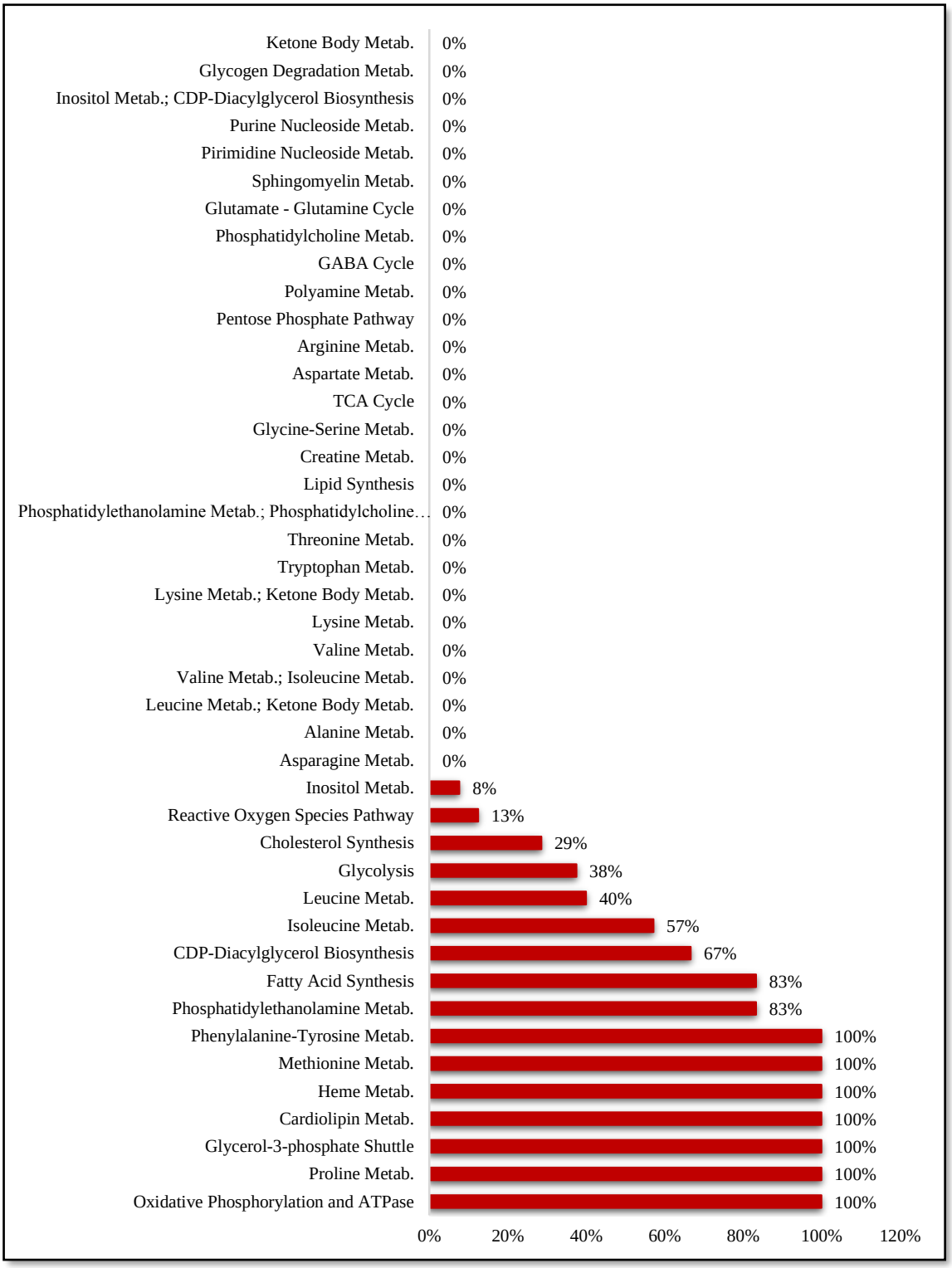

Figure 4.12. The percentages of significant reactions in astrocyte for each subsystem.

Therefore, it is pertinent to consider that MB cells decrease leucine and isoleucine productions from glutamate, take up them externally, and use them up for important biological processes like cell division, nucleotide, and protein production (Cormerais *et al*., 2018). Both lysine uptake and lysine metabolism reactions were also found to be lower in the MB model compared to ones in the healthy model.

73% of glycolysis reactions in neuron were also detected as statistically important owing to the high glucose uptake and abnormal lactate production of malignant cells compared to normal cells (Tech *et al*., 2015), (Warburg, 1925). 38% of glycolysis reactions were identified as significantly different in astrocyte. Figure 4.13 and Figure 4.14 show the flux sampling results for lactate production in astrocyte and neuron, respectively. While the black asterisk on the red histogram indicates the flux result obtained using FBA for MB, the red asterisk on the blue histogram shows the flux rate for the healthy model.

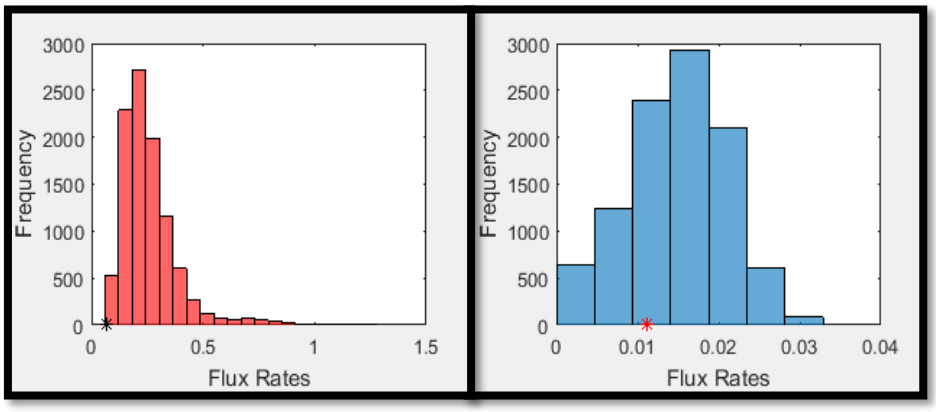

Figure 4.13. Lactate production (R11) in glycolysis for astrocyte. Flux sampling results for MB are shown in red while the results for healthy are shown in blue.

In the sampling approach, lactate production in astrocyte was determined to be higher than the one in the healthy model (See Figure 4.13). Similarly, lactate production result obtained with FBA was found almost six times higher in MB than the flux rate for healthy. Lactate production reaction was determined to be one of the significantly different reactions in the neuron. In both FBA and flux sampling, lactate production was found to be significantly higher compared to the results for the healthy model (See Figure 4.14).

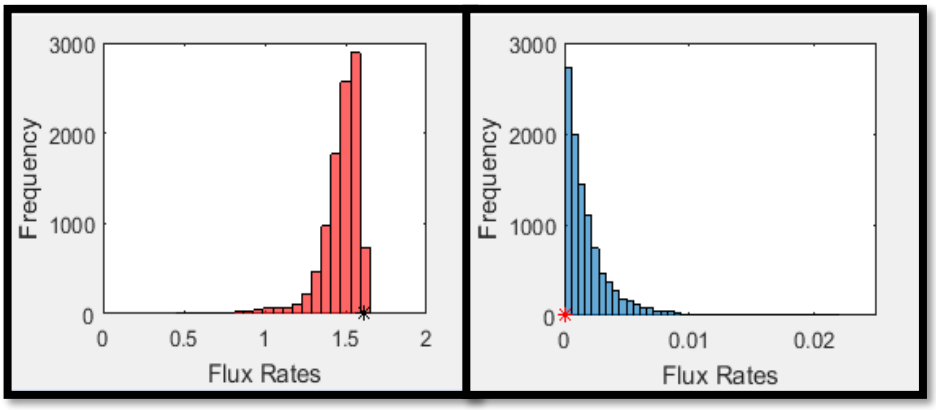

Figure 4.14. Lactate production (R56) in glycolysis for neuron. Flux sampling results for MB are shown in red while the results for healthy are shown in blue.

Consistent with the previous findings in this study and experimental outcomes, 80% and 100% of OXPHOS pathway reactions were found to be significant for neuron and astrocyte, respectively. Although ATP generation in OXPHOS was detected to be remarkably lower in the MB model than the healthy model in both approaches, the ATP generation rates obtained in FBA were observed to be lower relative to flux sampling mean values in astrocyte and neuron (See Figure 4.15 and Figure 4.16).

Unlike FBA, flux sampling is employed without defining an objective (Herrmann *et al*., 2019).

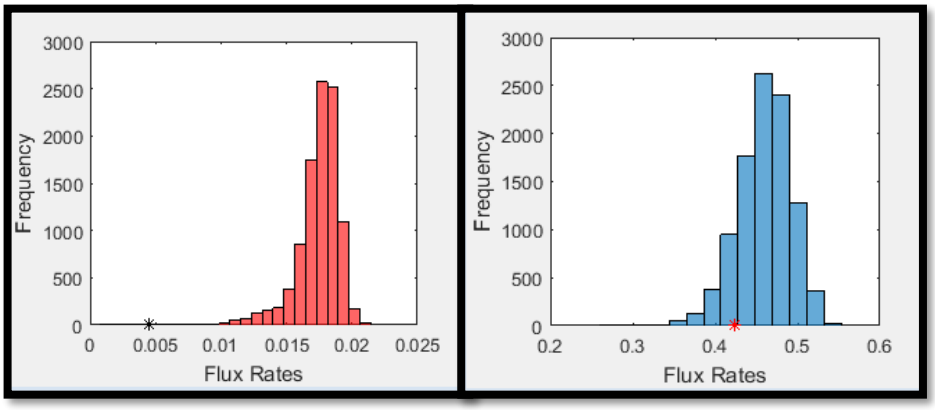

Figure 4.15. ATP production (R45) in OXPHOS for astrocyte. Flux sampling results for MB are shown in red while the results for healthy are shown in blue.

The difference in the activity of OXPHOS in both approaches indicates that when growth reaction was taken into consideration like in FBA, MB reduces the OXPHOS activity much more to promote its growth. Therefore, there is a correlation between the low activity of OXPHOS and growth in MB. Taken together with both FBA and sampling approaches, the MB model captured the Warburg effect successfully.

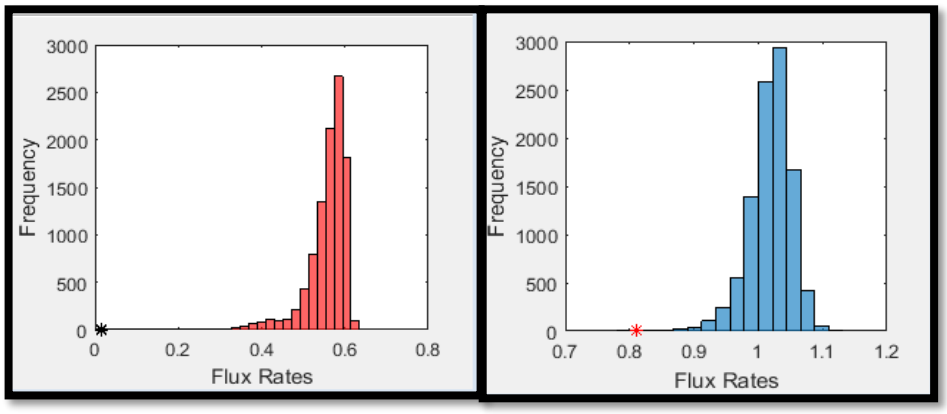

Figure 4.16. ATP production (R88) in OXPHOS for neuron. Flux sampling results for MB are shown in red while the results for healthy are shown in blue.

Since the first reaction of PPP in the healthy model was constrained to the values found by Sertbaş et al. for flux sampling, histograms for the healthy model were not shown in Figure 4.17 and Figure 4.18.

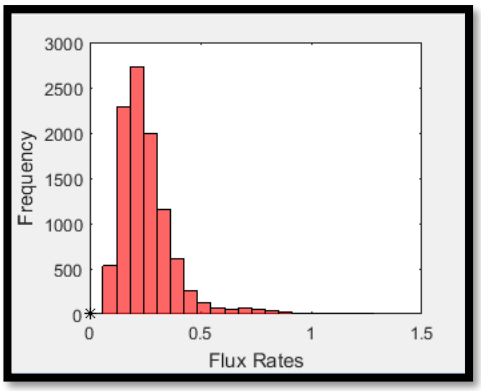

Figure 4.17. 6-phosphogluconate production (R17) in pentose phosphate pathway for astrocyte. Flux sampling results for MB are shown in red.

For astrocyte, the first reaction flux of PPP in MB was found to be twice of the result obtained for the healthy model in FBA. On the other hand, the mean of the flux sampling results of the same reaction was detected to be almost ten times lower than the FBA result of the reaction in healthy model. Similarly, for neuron, the FBA result was observed to be almost ten times higher than the mean of flux sampling results in the MB model, which indicates MB utilizing PPP to support its proliferation (See Figure 4.18). However, with both methods, increased activity in PPP was determined for the neuron in MB compared to its healthy counterpart.

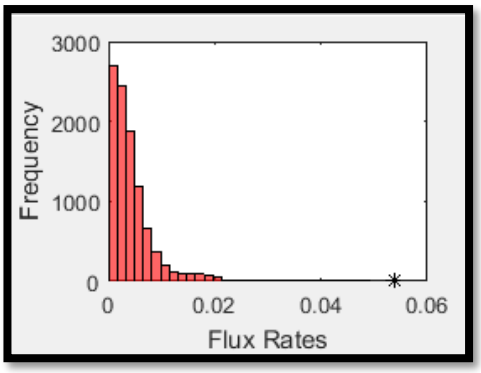

Figure 4.18. 6-phosphogluconate production (R61) in the pentose phosphate pathway for neuron. Flux sampling results for MB are shown in red.

TCA cycle activity was estimated to be decreased in FBA analyses due to the Warburg effect. In flux sampling analysis, 27% of TCA cycle reactions were also assessed to be important in agreement with the FBA results in this study and experimental findings. Citrate production reaction, which is the first step of the TCA cycle, was relatively activated in FBA analysis because of its use in the generation of acetyl-CoA. Still, its flux rate was found to be lower than the flux rate in the healthy model. Conversely, the means of flux sampling results for MB and healthy were estimated to be very similar to each other in both astrocyte and neuron (See Figure 4.19 and Figure 4.20).

One of the reactive oxygen pathway reactions where oxidized glutathione is produced from H_2O_2 and reduced glutathione was also found as a significantly changed reaction in neuron and astrocyte. In MB, the mean of the fluxes for this reaction was found to be negative in flux sampling analysis.

Similarly, in the FBA approach, the flux of this reaction was zero while much higher flux values were obtained in both methods for the healthy model.

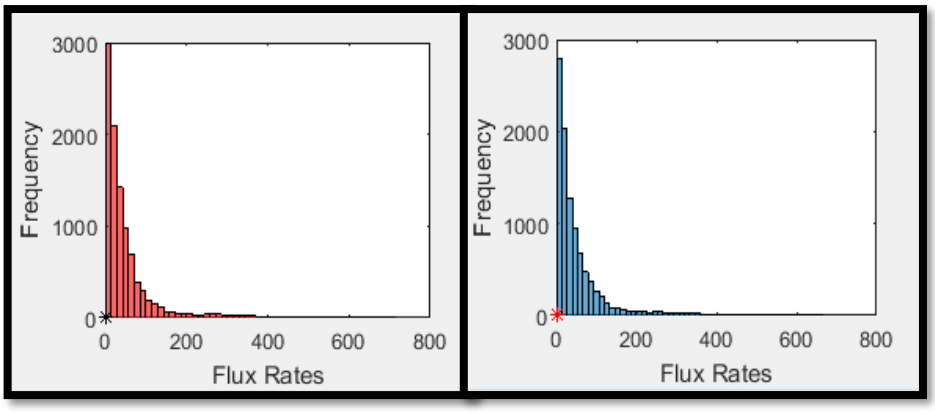

Figure 4.19. Citrate production (R25) in the TCA cycle for astrocyte. Flux sampling results for MB are shown in red while the results for healthy shown in blue.

Considering the high level of ROS found in many cancer types leading to stimulation of PPP-related enzymes to activate this pathway and promote cancer growth, inhibition of this reaction in the MB model is quite plausible (Liou and Storz, 2010), (Stincone *et al*., 2015). Low flux values, found in both techniques, show that there is an accumulation of H_2O_2 in MB as found in many cancer types (Liou and Storz, 2010).

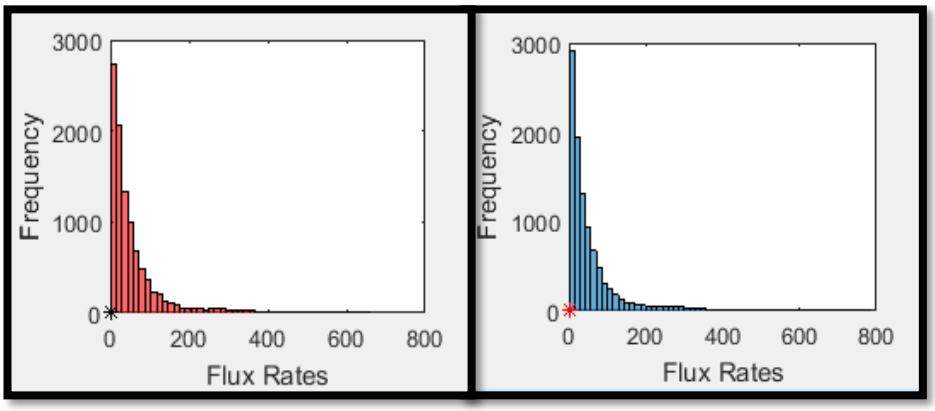

Figure 4.20. Citrate production (R69) in the TCA cycle for neuron. Flux sampling results for MB are shown in red while the results for healthy are shown in blue.

Compatible with lots of studies that found low inositol activity in many cancer types including astrocytoma and lung cancer, inositol uptake reactions for neuron and astrocyte were found to be lower compared to the fluxes in the healthy model (Badodi *et al*., 2021), (Castillo *et al*., 2000), (Ren *et al*., 2017), (Vucenik, 2019).

4.5. Regulation

The aim of this section is to identify which reactions are metabolically, transcriptionally, and post-transcriptionally are regulated using flux sampling results and GSE expression levels for two cases. First, sampling algorithm was used to obtain a set of flux distributions satisfying the constraints in solutions space for each reaction. Means and standard deviations of the reactions present in both models were calculated using the results obtained from sampling algorithm. In order to determine the significance of change between MB and healthy conditions, Z-scores were calculated (ZF-Z scores for metabolic fluxes, ZG-Z scores for expression data).

201 reactions out of 594 common reactions found in both MB and healthy models were removed because both ZF and ZG scores of these reactions were found to be lower than 1.96 or higher than -1.96. 240 of the remaining reactions were detected to be regulated metabolically since only the ZF score of these reactions are significantly different suggesting that there are other factors other than gene expression level affecting their flux rates. 80 of them were determined to be controlled transcriptionally as both ZF and ZG values of these reactions are significant. 73 reactions were estimated to be regulated post-transcriptionally since there is a remarkable change in gene expression of their related genes whereas there is no important change in their flux rates compared to the healthy model. Figure 4.21 shows the number of the reactions regulated, metabolically, transcriptionally, and post-transcriptionally in both neuron and astrocyte based on the pathway, they are carried out. M, T, and PT stand for metabolically, transcriptionally, and post-transcriptionally reactions. For example, in glycolysis metabolism, 16, 2, and 4 reactions are controlled metabolically, transcriptionally, and post-transcriptionally, respectively. Some of the pathways like pyrimidine nucleoside metabolism were removed from Figure 4.21 because no significantly differential reactions were detected in these pathways.

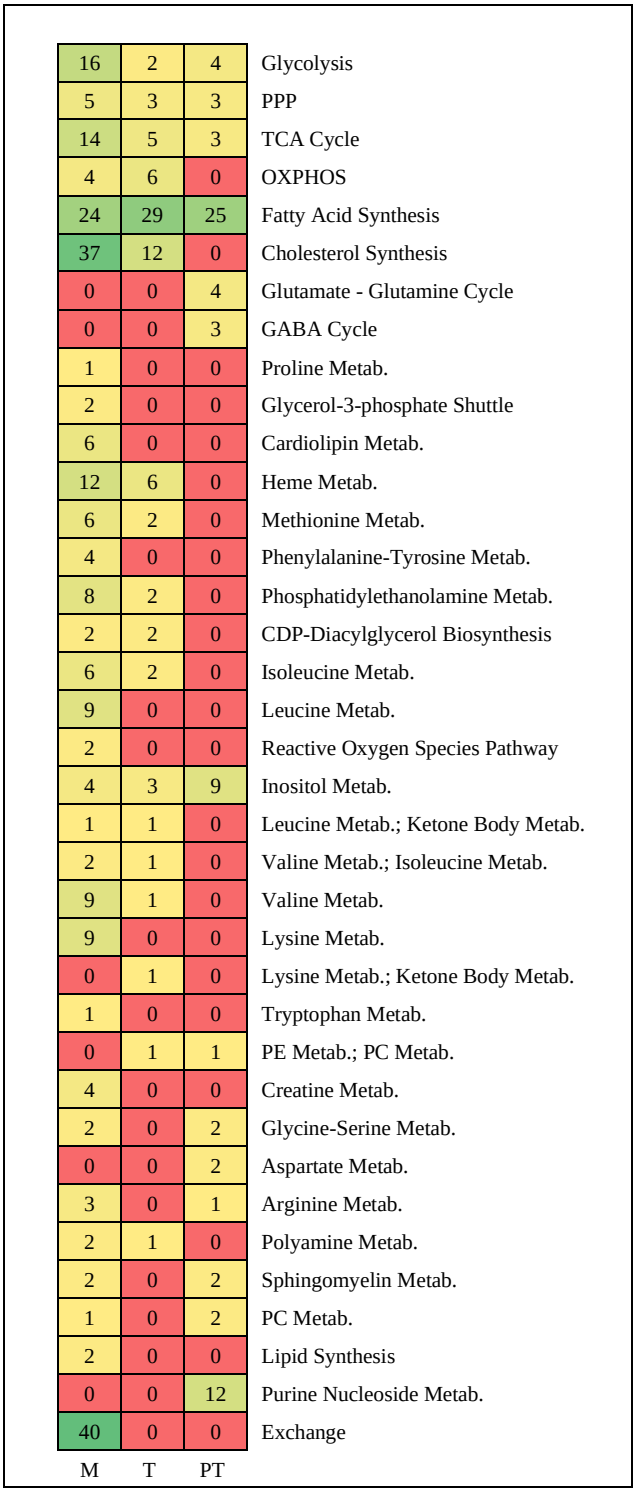

Figure 4.21. The number of the reactions regulated metabolically (M), transcriptionally (T), and post-transcriptionally (PT) in both neuron and astrocyte for each pathway.

In metabolic engineering, it is important to identify transcriptionally regulated reactions (TRR) whose flux rate changes stem from gene expression alterations. Variations in gene expression are frequently utilized to change metabolic fluxes in the desired way. In other words, the genes controlling TRR can be used as therapeutic targets. When fluxes and gene expression levels of reactions do not differ similarly, the genes related to these reactions can not be used to change flux rates by the means of gene expression.

Figure 4.22 demonstrates the genes whose associated reactions were found to be significantly different in MB model compared to ones in the healthy model . The red color indicates whether the genes are associated with metabolically or transcriptionally or post-transcriptionally reactions. Glycolysis, PPP, TCA, OXPHOS, fatty acid synthesis pathways do not include the genes detected in only astrocyte because it was aimed to find the genes whose perturbation affects both cells or only neuron where MB occurs (Northcott *et al*., 2019). Since the cholesterol pathway is realized in astrocyte, the genes related to significantly differential reactions in this pathway were included.

As seen in Figure 4.21, the pathway with the highest TRR ratio was fatty acid synthesis with more than one-third of reactions. 2 TRR's realized in both neuron and astrocyte are regulated by ACOT2, ACOT4, ACOT7, FADS1, FADS2, FADS6, SCD5, and SCD (See Figure 4.22). While ACOT2, ACOT4, ACOT7 genes are responsible for the production of stearate from stearoyl-CoA, FADS1, FADS2, FADS6, SCD, and SCD5 genes control the generation of oleoyl-CoA from stearoyl-CoA. The expression values of ACOT2, ACOT4, FADS1, and FADS6 were not included in the GSE datasets used in this study. Therefore, their ZG scores were not calculated. ZF score of SCD5 was found to be insignificant. However, both ZG and ZF scores of ACOT7, FADS2, and SCD genes were estimated to be significantly lower than the critical value (-1.96) determined for this work. These results suggest that the oleoyl-CoA synthesis is downregulated in MB. Importantly, oleoyl-CoA is converted to oleic acid which has been shown by many studies to have anti-cancer properties (Li *et al*., 2014), (Natali *et al*., 2007), (Ruggiero *et al*., 2014), (Zhu *et al*., 2005).

Based on the significantly low ZF and ZG scores, it can be deduced that there is a reduction in oleic acid amount in MB compared to the normal brain.

Consistently, according to a recent paper conducted by Anna et al, oleic acid production was found to be lower expressed in brain tumors including MB based on the results obtained in the Raman technique (Anna *et al*., 2017). Therefore, lower production of oleic acid may be a phenotype of MB metabolism. Application of oleic acid on MB might be a potential therapeutic strategy considering its anti-tumor effects on NB and GBM (Zhu *et al*., 2005), (Natali *et al*., 2007).

Interestingly, oleic acid was also detected in two separate analyzes performed in the present study. Firstly, it was found in the GeneCards database due to its relation to the FASN gene which was identified as one of eight common essential genes in gene essentiality analysis (See Section 4.8.1). Secondly, it was determined as a potential antimetabolite in the DrugBank database because of its similarity to linoleate and arachidonate with 0.90 and 0.83 similarity scores, respectively (See Section 4.8.2). In this part of the work, inhibition of the reactions where linoleate and arachidonate are substrates led to a decrease of 80% and 79%, respectively in the growth reaction of the MB model. In the same study performed by Anna et al, the peaks detected for linoleate and arachidonate were the same as the ones obtained for brain tumors in the Raman technique suggesting the upregulation of these metabolites (Anna *et al*., 2017).

Based on experimental findings and results obtained in this study, the effect of extraneous oleic acid on MB should be investigated in further studies because it might suppress the conversion of arachidonate from linoleate as an antimetabolite and prevent tumor progress with anticancer effects simultaneously. However, it is important to note that keeping oleic acid and stearic acid proportion at a normal level is crucial because an imbalance between these two fatty acids disrupts the membrane structure which is known as a cancer-specific feature (Habib *et al*., 1987).

Most of the reactions in cholesterol synthesis were identified as metabolically regulated reactions (MRR) (See Figure 4.21). 12 TRRs related to cholesterol synthesis are controlled by 10 genes (See Figure 4.22). 5 of these including HMGCS1, HMGCS2, HMGCR, PMVK, and MVD are associated with the mevalonate pathway.

HMGCR, PMVK, and MVD were also identified in the group of eight potential genes in gene essentiality analysis (See Section 4.8.1). Many metabolites whose enzymes could be used as therapeutic targets were also found to be related to mevalonate pathway genes (See Section 4.8.2).

Despite the contribution of this pathway to growth, both ZG and ZF scores of reactions related to HMGCS1, HMGCR, PMVK, and MVD were estimated to be significantly low in this analysis. ZG score for HMGCS2 was found to be insignificant. The reactions related to other genes including, LSS, NSDHL, and DHCR7 have also remarkably low ZF and ZG scores. Additionally, ZF and ZG scores of reactions associated with FDFT1 and SQLE which are identified as essential genes are significantly lower than the critic value (-1.96). Despite low expressions of these genes relative to the healthy brain, cholesterol is one of the main structural lipids forming cell membranes (Maxfield and van Meer, 2010). Therefore, to survive, MB cells have to produce metabolites related to cholesterol synthesis even in the low levels. Considering numerous studies which show that inhibition of cancer cells by interfering cholesterol pathway and the essentiality of many cholesterol genes in this study, perturbating cholesterol pathway might be a promising approach for MB (Dimitroulakos *et al*., 2000), (Girgert *et al*., 1999), (Hindler *et al*., 2006), (Jiang *et al*., 2014), (Mahmoud *et al*., 2016), (Shellman *et al*., 2005), (Song *et al*., 2014), (Larner *et al*., 1998), (Kim *et al*., 2001).

In glycolysis, most of the reactions are not affected by the expression levels of the genes controlling them (See Figure 4.21). Probably, an extreme level of glucose internalized by glucose carriers leads to activations of the enzymes in the glycolysis pathway. Only fructose-1-6-biphosphate producing reaction whose ZF and ZF scores both significantly alter can be classified as a TRR. This reaction is controlled by PFKL, PFKM, and PFKP genes (See Figure 4.22). ZG score of fructose-6-phosphate production reaction is lower than the critical value (-1.96), in agreement with the literature (Moreno-Sanchez *et al*., 2009). ZF score is remarkably higher than the critical value (1.96). Although both z scores change significantly, there is a huge difference between them. The high flux value of this reaction in this case probably stems from abnormal glucose uptake of MB cells (Tech *et al*., 2015). It was observed that lactate production reaction in glycolysis has a high ZF score while its ZG score is considerably lower.

Perhaps, this reaction is also affected by external concentrations. A high amount of pyruvate accumulating activates lactate production. ZF score of the reaction where acetyl-CoA is produced from pyruvate in glycolysis pathway is lower than the critical value (-1.96). Therefore, less acetyl-CoA is generated in glycolysis compared to the healthy case since most of the pyruvate is used in the production of lactate in the MB model.

Consistent with p values obtained for PPP, ZF values for the reactions in PPP were also estimated to be unimportant (See Figure 4.21). ZG values of G6PD and TKTL1 genes, on the other hand, were found to be significantly lower than the critical value (-1.96) which makes their associated reactions post-transcriptionally regulated (See Figure 4.22). Even though there is an insignificant change in ZF values of these reactions, ZF values are higher than zero suggesting that there is a small increase in these reaction rates compared to the healthy brain. Therefore, significantly lower expressions of G6PD and TKTL1 genes, do not affect the flux rates of the reactions controlled by them. While G6PD is responsible for the production of 6-phosphogluconate, the TKTL1 gene plays role in the generation of fructose-6-phosphate and glyceraldehyde-3-phosphate with other genes which are TKTL2 and TKT. The reaction controlled by G6PD is the first reaction of PPP and it is known to be affected by many factors such as oxidative stress and lower activation of PFK in brain tumors (Moreno-Sanchez *et al*., 2009), (Stincone *et al*., 2015). These factors may be the reason for the noncorrelation between ZG and ZF.

The first reaction of the TCA cycle where oxaloacetate and acetyl-CoA are converted to citrate by CS and SLC35G3 is regulated post-transcriptionally (See Figure 4.22). On the other hand, the following two reactions where cis aconitate and isocitrate production are controlled by ACO1 and ACO2 genes are transcriptionally regulated reactions. It was observed that ZF scores of these reactions were significantly lower than the critical value (-1.96) because of the low activity of the TCA cycle in cancer (Warburg, 1925). Other reactions wherein only ZF score changes significantly, are metabolically regulated reactions because of the insufficient amount of substances produced in the first steps of TCA.

One other reason for low ZF scores of MRR's in the TCA cycle may be the aberrant consumption of the pyruvate for lactate production in the glycolysis pathway.

Consequently, less acetyl-CoA and oxaloacetate are synthesized from pyruvate in the glycolysis pathway and this affects the first reaction of TCA where citrate is produced from these metabolites.

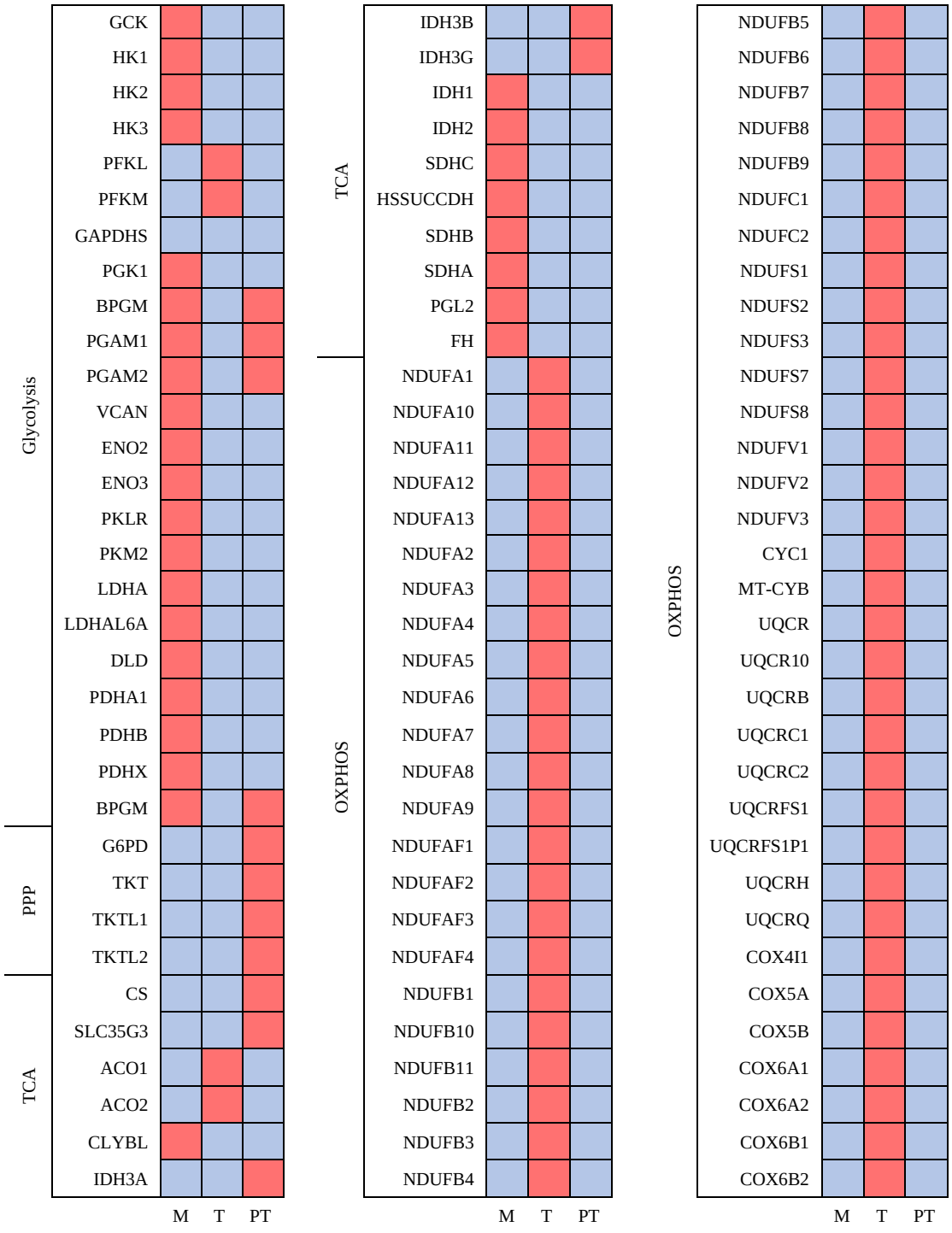

Figure 4.22. The genes whose associated reactions are significantly different in MB compared to the reactions in the healthy model based on pathways.

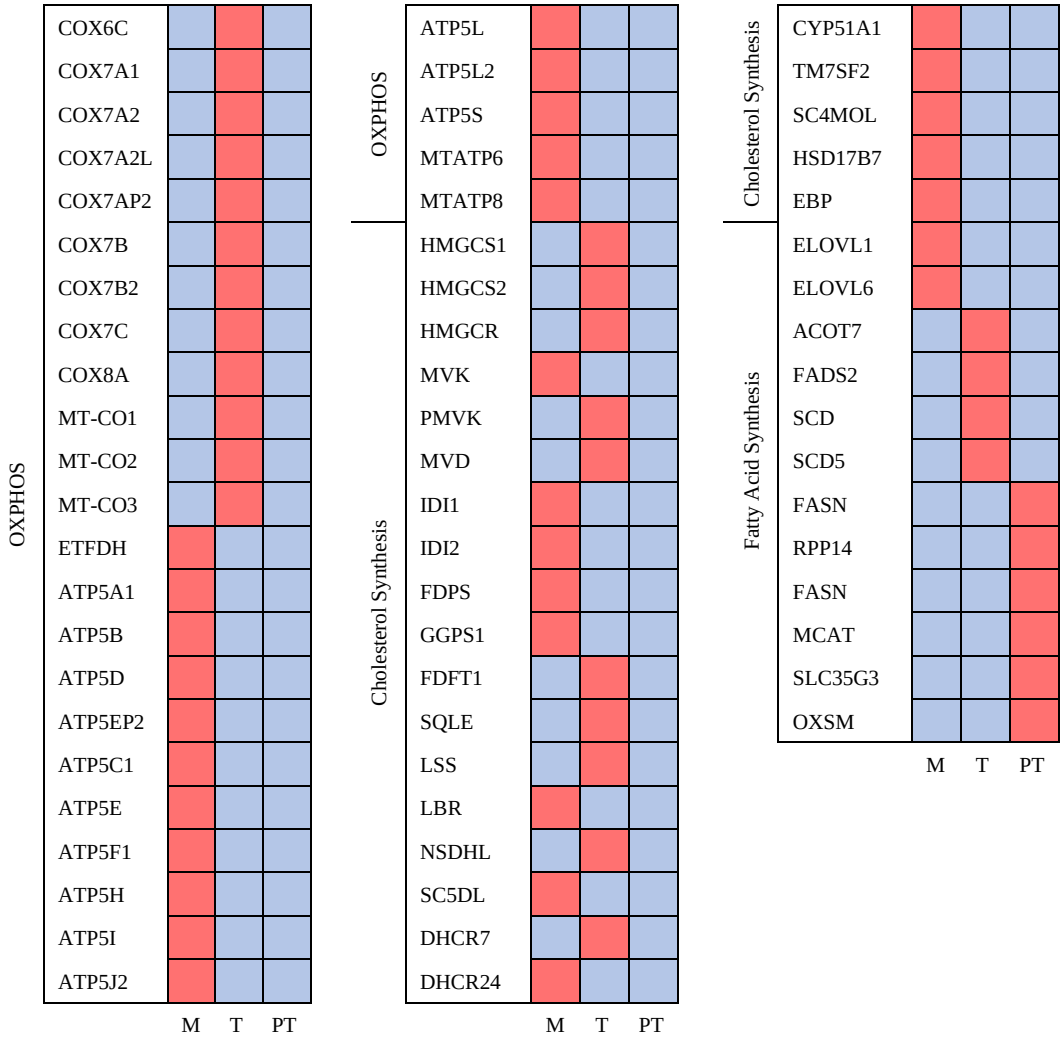

Figure 4.22. The genes whose associated reactions are significantly different in MB compared to the reactions in the healthy model based on pathways.

While the first three reactions of OXPHOS are regulated transcriptionally, the last two are regulated metabolically (See Figure 4.22). It was observed that all ZF scores in OXPHOS reactions including the ZF score of the third reaction where CytCox and Hc are produced and oxygen is consumed are significantly lower than the critical value (-1.96) which is in agreement with the fact that cancer cells take low oxygen even in the presence of oxygen (Kim *et al*., 2012).

4.6. Flux Coupling Analysis

The purpose of this section is to obtain the reactions that are fully coupled, partially coupled and directionally coupled to biomass reaction using Flux coupling analysis. The reactions coupled with growth are considered as putative drug targets to reduce tumor growth. In order to find the reactions coupled with biomass reaction, flux coupling analysis was performed. It was estimated that 158 reactions are related to biomass reaction. 32 reactions out of 158 reactions are fully coupled to growth reaction. Only 6 of them are partially connected to biomass reaction, while 120 of them are directionally linked to biomass rection. Naturally, all the reactions in which the metabolites from the neuron and astrocyte combine and participate in the biomass reaction were found to be fully related to the biomass reaction. In addition, uptake reactions of lysine, phenylalanine, and histidine which are not synthesized in the human body (Buford, 2008) were found to be fully connected to biomass reaction suggesting that any perturbation on these reactions influence growth reaction tremendously. Reciprocally, any change in growth also affects the uptake of these amino acids. Lysine was detected to be internalized abundantly by breast cancer cells (Vazquez Rodriguez *et al*., 2020). Limiting lysine in diets was also suggested to support cancer treatment (Kang, 2020).

LAT1 carrier which internalizes isoleucine, phenylalanine, histidine, and leucine, was also found to be upregulated in MB (Wei *et al*., 2021), (Cormerais *et al*., 2018), (Munford, 2019). These experimental findings and the results of the present work indicate that the inhibitory effect of essential amino acid uptake reactions on MB should be investigated in further studies. Since arginine is taken up by neuron via astrocyte (Sertbaş *et al*., 2014), the transport reaction of arginine between two cells is also fully connected to the growth reaction. Furthermore, the uracil production reaction from uridine is entirely connected to growth reaction since uracil is one of the main nucleotides used in RNA synthesis (Sertbaş *et al*., 2014).

All reactions partially connected to growth are related to nucleotide exchange reactions including guanosine, uridine, and cytidine uptakes. In gene essentiality analysis, the PNP and ADK genes which are responsible for the guanine and adenosine monophosphate syntheses were also found as essential.

Both analyses indicate that nucleotide metabolism is directly related to growth. Indeed, there are various chemotherapeutic agents targeting nucleotide production (Marie and Shinjo, 2011).

The related pathways of 120 reactions associated with growth directionally are shown in Figure 4.23. The reactions directionally related to growth include nucleoside metabolism reactions like guanine synthesis from guanosine. Additionally, ribose-5-phosphate production from ribose-1-phosphate was detected as a directionally coupled reaction to growth. Ribose-5-phosphate is a precursor metabolite for nucleotide synthesis. In fact, ribose-1-phosphate inhibition led to a 91% decrease in the growth reaction of MB in this study (See Section 4.8.2).

Exchange reactions related directly to growth include isoleucine, methionine, threonine, and oxygen uptake reactions. In addition, tyrosine and ornithine intakes were found to be directly related to biomass reaction. Tyrosine can be also synthesized from phenylalanine which is an essential amino acid. Ornithine is a precursor non-essential amino acid for the production of polyamines including spermidine, spermine, and putrescine associated with cell growth (Casero *et al*., 2018). Choices of cells to get isoleucine, methionine and threonine are limited, because these amino acids are not synthesized in the human body (Buford, 2008). Overall, the MB model detected essential amino acid uptake reactions and reactions related to amino acids produced from another essential amino acid like tyrosine. Oxygen intake is vital for OXPHOS. Even though cancer cells are prone to meet their ATP need mostly from glycolysis, it was shown that they need to generate energy in OXPHOS to survive (Moreno-Sanchez *et al*., 2009). Naturally, lipid synthesis which is one of the important reactions forming the main biomass reaction was also estimated in this analysis. While lipid synthesis reaction was found as directionally related to growth, protein reaction was detected to be fully coupled to growth. That probably stems from higher protein content found in the cerebellum relative to lipid (See Section 3.1.2). Therefore, a computational change in biomass reaction influences protein metabolism more than lipid metabolism. The reactions related to the production of cardiolipin which is known to take part in the structure of the cell membrane (Nielson and Rutter, 2018) are directly related to growth (See Figure 4.23). Consistently, cardiolipin synthesis genes, CRLS1 and PGS1 were also found to be essential genes in this study (See Section 4.7).

Cardiolipin is formed with the combination of cytidine diphosphate diacylglycerol (CDP diacylglycerol) and glycerol-3-phosphate (Sertbaş *et al*., 2014). Glycerol-3-phosphate syntheses reactions are detected in this analysis since this metabolite is used in both cardiolipin and CDP diacylglycerol syntheses (See Figure 4.23). GPD1 and GPD2 genes which control glycerol-3-phosphate syntheses were also found as essential genes (See Section 4.7). CDP diacylglycerol is the main metabolite in the productions of cardiolipin and phosphatidyl-inositol (Blunsom and Cockcroft, 2020). Indeed, the reactions in CDP diacylglycerol metabolism were estimated as partially linked reactions to growth (See Figure 4.23).

89% of reactions in fatty acid synthesis are directly linked to growth in agreement with other analyses done for this work (See Figure 4.23). The reaction directly related to cholesterol metabolism is the one where cholesterol is transported from astrocyte to neuron because its synthesis is only carried out in astrocyte (See Figure 4.23). Consistent with other analyses, cholesterol production is coupled to growth reaction.

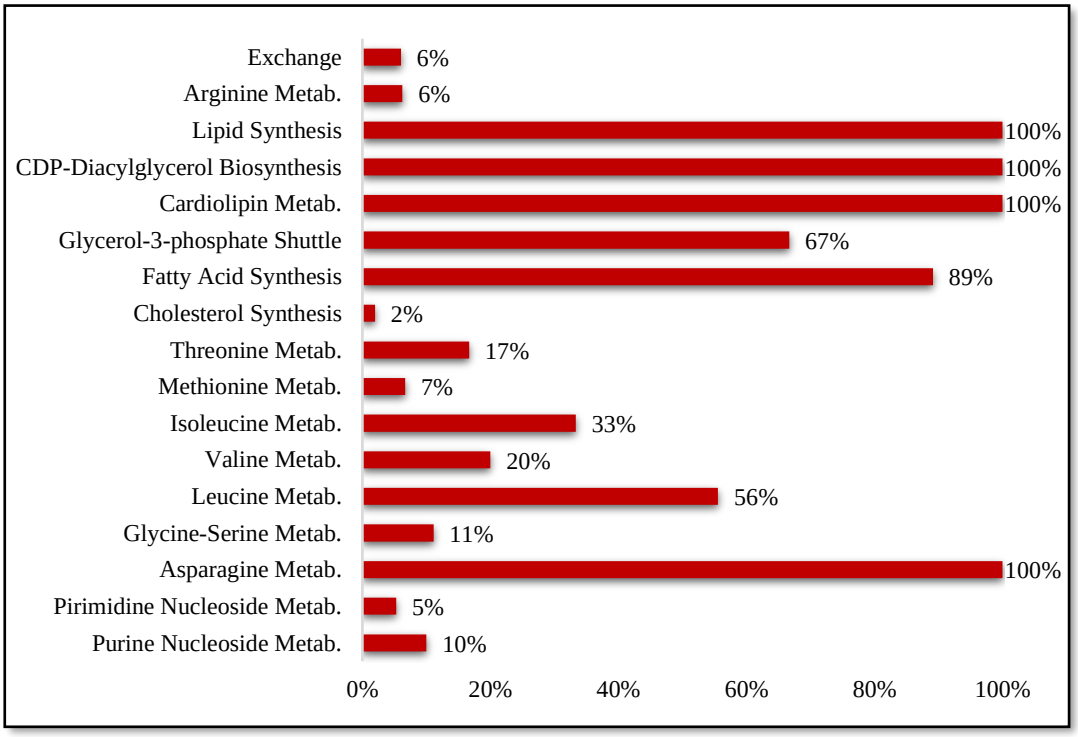

Figure 4.23. The distribution of reactions directionally coupled to growth based on the pathway.

Other reactions directly coupled to growth are related to amino acid metabolisms including isoleucine, valine, leucine, glycine, serine, and asparagine. Isoleucine, valine, and leucine are transported to astrocyte and they are converted to keto-beta-methyl valeric acid (KMV), alpha-ketoisovalerate (KIV) ketoisocaproate (KIC), respectively (Sertbaş *et al*., 2014). Then KMV, KIV, and KIC are transported to neuron and transformed to isoleucine, valine, and leucine. The reactions where KMV, KIV, and KIC are internalized by neuron and then converted back to isoleucine, valine, and leucine were found to be directly related to growth. It is known that intermediates of these three amino acids and lysine are converted to acetyl-CoA which is benefited by histone proteins (Lieu *et al*., 2020). Histone proteins are linked to proliferation and they are frequently deregulated in cancer (Lieu *et al*., 2020), (Wei *et al*., 2021). Isoleucine, valine, and leucine are also converted to alpha-ketoglutarate which also contributes to tumor survival by refilling the TCA cycle (Lieu *et al*., 2020).

Serine transport reaction from astrocyte to neuron was also detected as a reaction related to growth (See Figure 4.23). Serine is a non-essential amino acid produced in astrocyte (Sertbaş et al., 2014) Serine is also known to promote proliferation in cancer cells (Yang and Vousden, 2016). It was shown that a decrease in serine level caused suppression of growth of several cancers (Maddocks *et al*., 2013). In addition, serine is necessary for glycine production. Once serine is synthesized in astrocyte, it is transported to neuron to be converted into glycine with tetrahydrofolate (Yang and Vousden, 2016). This finding is quite compatible with the literature considering one of the characteristics of MB is high glycine concentration (Bennet, 2018).

The reaction where glutamine and aspartate are consumed to produce asparagine and glutamate was detected in coupling analysis (See Figure 4.23). ASNS gene controlling this reaction was also detected in essentiality analysis (See Section 4.7). Increased activity of ASNS was determined in several cancer types like pancreatic, ovarian, and prostate (Panosyan *et al*., 2014). Moreover, it was found that decreased amount of asparagine in brain metabolism increased the impact of chemotherapy significantly in DAOY, MB cell line by enhancing the sensitivity of MB cells (Panosyan *et al*., 2014). Thus, ASNS which was found by the MB model in both analyses could be a potential therapeutic target for MB.

4.7. Essentiality Analyses

Single gene deletion, double gene deletion, and reaction deletion analyses were performed to determine potential therapeutic targets for MB. In single gene and reaction deletion analyses, all genes and reactions found in the model are extracted one by one, and flux rates of a determined reaction are calculated after each extraction. If the flux rate of specified reaction falls below a certain value as a result of gene or reaction deletion, these genes or reactions are assumed to be essential for the system.

In this part of the study, the genes or reactions whose removal decrease the flux rate of biomass reaction below 10^{-6} mmol/gDW*hour were accepted as essential for the MB model. As a result of single-gene deletion analysis, 45 essential genes were detected in the MB model. 3 of 45 essential genes are shown in Table 4.2. These 3 genes were detected in only the single deletion analysis, while 42 of them were identified in reaction deletion analysis as well. These 42 essential genes are demonstrated in Table 4.3.

As seen from Table 4.2 and 4.3, almost 60% of essential genes detected by the MB model regulate reactions in pathways such as cholesterol, phosphatidylethanolamine, sphingomyelin, phosphatidyl-inositol, glycosphingolipid, and fatty acid metabolism coupled to main lipid reaction. These findings indicate that lipid production is essential for MB cell growth and they are compatible with experimental results where a high amount of lipid was found in MB (Bennett *et al*., 2018).

Table 4.2. Essential genes in MB model and their associated pathways.

Essential gene	Pathway
SC5DL	Cholesterol Synthesis
DHCR7	Cholesterol Synthesis
DHCR24	Cholesterol Synthesis

Table 4.3. Essential genes detected in both analyses and their associated pathways.

Essential genes	Pathway
GPI	Glycolysis
TPI1	Glycolysis
RPE	Pentose phosphate pathway
TALDO1	Pentose phosphate pathway
FH	TCA cycle
ETFDH	Oxidative Phosphorylation
ASNS	Asparagine metabolism
QDPR	Phenylalanine-Tyrosine Metabolism
TH	Phenylalanine-Tyrosine Metabolism
DDC	Phenylalanine-Tyrosine Metabolism
GCAT	Threonine Metabolism
HMGCR	Cholesterol Synthesis
MVK	Cholesterol Synthesis
PMVK	Cholesterol Synthesis
MVD	Cholesterol Synthesis
FDFT1	Cholesterol Synthesis
SQLE	Cholesterol Synthesis
LSS	Cholesterol Synthesis
CYP51A1	Cholesterol Synthesis
SC4MOL	Cholesterol Synthesis
NSDHL	Cholesterol Synthesis
HSD17B7	Cholesterol Synthesis

Table 4.3. Genes detected in both analyses and their associated pathways. (cont.)

Essential genes	Pathway
EBP	Cholesterol Synthesis
FASN	Fatty Acid Synthesis
GPD1	Glycerol-3-phosphate Shuttle
GPD2	Glycerol-3-phosphate Shuttle
PCYT2	Phosphatidylethanolamine Metabolism
PTDSS2	Phosphatidylethanolamine Metabolism
PISD	Phosphatidylethanolamine Metabolism
PGS1	Cardiolipin Metabolism
CRLS1	Cardiolipin Metabolism
SPTLC1	Sphingomyelin Metabolism
KDSR	Sphingomyelin Metabolism
DEGS2	Sphingomyelin Metabolism
CDIPT	Inositol Metabolism
INPP1	Inositol Metabolism
GSS	Reactive Oxygen Species Pathway
AMD1	Polyamine Metabolism
SMS	Polyamine Metabolism
SMOX	Polyamine Metabolism
ADK	Purine Nucleoside Metabolism
PNP	Purine Nucleoside Metabolism

Glycolysis pathway genes, glucose-6-phosphate isomerase (GPI) and triosephosphate isomerase 1 (TPI1), and PPP genes, ribulose-5-phosphate-3-epimerase (RPE), and transaldolase 1 (TALDO1) were detected as essential genes because they all take part in vital pathways for MB and cancer cells. GPI and TPI1 are responsible for fructose-6-phosphate and glyceraldehyde-3-phosphate productions (Sertbaş *et al*., 2014). Therefore, silencing these genes leads to the termination of the production of pyruvate used in syntheses of significant metabolites like alanine, acetyl CoA, and lactate alongside ATP generation in glycolysis. RPE regulates the reversible reaction where xylulose-5-phosphate is produced from ribulose-5-phosphate in PPP (Liang *et al*., 2011). TALDO1 controls the reversible reaction where fructose-6-phosphate and erythrose-4-phosphate are synthesized from sedoheptulose-7-phosphate and glyceraldehyde-3-phosphate (Sertbaş *et al*., 2014). The metabolites like fructose 6-phosphate, glyceraldehyde 3-phosphate, and erythrose 4-phosphate produced in PPP are required for the generations of the ATP and aromatic amino acids (Liang *et al*., 2011). It was also shown that RPE contributes to decreasing oxidative stress because it controls the reaction involved in NADPH generation (Liang *et al*., 2011).

In the TCA cycle, the fumarate hydratase (FH) gene that is responsible for the production of malate from fumarate was also found as an essential gene in both single gene and reaction deletion analyses. That stems from the fact that malate is used in the production of oxaloacetate which is utilized in glycolysis, TCA, and aspartate pathways to synthesize phosphoenol-pyruvate, citrate, and aspartate, respectively (Sertbaş *et al*., 2014). Malate is also utilized in the production of pyruvate which is a crucial metabolite used in lactate and alanine syntheses.

Electron transfer flavoprotein dehydrogenase (ETFDH) which is responsible for the production of ubiquinol and flavin adenine dinucleotide (FAD) from reduced flavin adenine dinucleotide (FADH2) and ubiquinone, is also identified as an essential gene by the MB model. FAD, which is responsible for transporting electrons, is a crucial molecule for the electron transfer chain (Le and Ou, 2016). In the TCA cycle, FAD is converted to FADH2 by accepting two electrons. In leucine, valine, and isoleucine metabolisms, FAD is utilized as a cofactor (Brody, 1999).

Although the identification of these vital genes related to glycolysis, PPP and OXPHOS in both essentiality analyses supports the robustness of the MB model, inhibitions of the genes in these pathways might cause deleterious effects on healthy cells as well.

Asparagine synthetase (ASNS) regulates asparagine production from glutamine and aspartate. High activity of ASNS was related to various malignancies including ovarian, pancreatic, and prostate cancers (Panosyan *et al*., 2014). ASNS was also detected in flux coupling analysis.

Glycerol-3-phosphate dehydrogenase 1 (GPD1) and glycerol-3-phosphate dehydrogenase 2 (GPD2) control the productions of glycerol-3-phosphate, NAD, and FAD. GPD2 takes part in glycolysis, glycerol, lipid, and gluconeogenesis metabolisms. Glycerol-3-phosphate is used in cardiolipin metabolism to synthesize cardiolipin which forms 20% of mitochondrial membrane (Nielson and Rutter, 2018). GPD2 was found to be overexpressed in many cancers (Lu *et al*., 2020). Moreover, GPD2 suppression resulted in anti-cancer effects in a prostate cancer cell line (Singh, 2014). GPD1 and GPD2 genes and their related reactions were detected in both single gene deletion and flux coupling analyses by the MB model.

Polyamines including spermine, spermidine, and putrescine participate in main biological activities such as survival, apoptosis, and cell growth (Casero *et al*., 2018). Decreased levels of polyamines lead to inhibition of growth (Casero *et al*., 2018). Putrescine is synthesized from ornithine by ornithine decarboxylase 1 (ODC1). S-adenosyl-L-methionine produced in methionine metabolism is converted to S-adenosyl-L-methioninamine by adenosylmethionine decarboxylase 1 (AMD1) which was found as an essential gene by the MB model (Casero *et al*., 2018). Subsequently, spermidine is generated by spermidine synthase (SRM) by using putrescine and S-adenosyl-L-methioninamine (Casero *et al*., 2018). Afterward, spermine synthase (SMS) which is an essential gene carries out the production of spermine from spermidine. Spermine can be converted to spermidine releasing H_2O_2 by spermine oxidase (SMOX) which is also an essential gene (Sertbaş *et al*., 2014). Polyamine metabolism is generally disrupted in cancer (Casero *et al*., 2018).

SMOX was found to be overexpressed leading to overproduction of H_2O_2 in several cancers including liver, lung, colon, prostate, and stomach (Casero *et al*., 2018). Depleting the activity of SMOX caused an important reduction in ROS generation and thus decreased oxidative damage in gastric and colon cancers (Casero *et al*., 2018). It was demonstrated that SHH, which is dysregulated in the SHH type of MB, also triggers polyamine production (D'Amico *et al*., 2015). Some studies demonstrated that a reduction in polyamines resulted in tumor suppression (Coni *et al*., 2019). It was determined that with the deactivation of the polyamine pathway, MB growth in a mouse model was notably disrupted (Casero *et al*., 2018). Therefore, SMS, SMOX, and AMD1 which play important roles in polyamine synthesis and are also associated with cancer were successfully detected by the MB model.

Nucleotide production has been inhibited to prevent cancer growth recently (Marie and Shinjo, 2011). There are chemotherapeutic compounds known to target nucleotide synthesis (Marie and Shinjo, 2011). Consistently, purine nucleoside phosphorylase (PNP) which regulates the production of guanine from guanosine, and adenosine kinase (ADK) which controls the adenosine monophosphate synthesis from adenosine were identified as essential genes by the MB model.

In reaction deletion analysis, 312 essential reactions were identified in the MB model. The controlling genes of 116 essential reactions were also determined in single deletion gene analysis. The distribution of common essential genes detected in both analyses is shown based on the associated metabolic pathways (See Figure 4.24). The pathway including most of the common essential genes was found as cholesterol synthesis.

Apart from the genes identified in both analyses, in reaction deletion analysis, reaction 55, pyruvate, and ATP producer in neuron was identified as an essential reaction for the system because of its contributions to lactate, acetyl-CoA, and alanine productions (Marie and Shinjo, 2011). In agreement with the experimental results where a high amount of lipid found in MB, reaction 69 was also detected as an essential reaction because this reaction produces citrate which can be transported from the mitochondrial membrane, and then citrate is converted to acetyl- CoA that is used for the lipid synthesis (Bennett *et al*., 2018).

Like glucose, glutamine is also an important metabolite for tumors. GLS enzyme produces glutamate and ammonia by consuming glutamine. It was detected that GLS1 is upregulated in all MB subgroups in comparison to the healthy brain (Munford, 2019). Consistent with that information, reaction 96 where glutamate is produced, was found as an essential reaction.

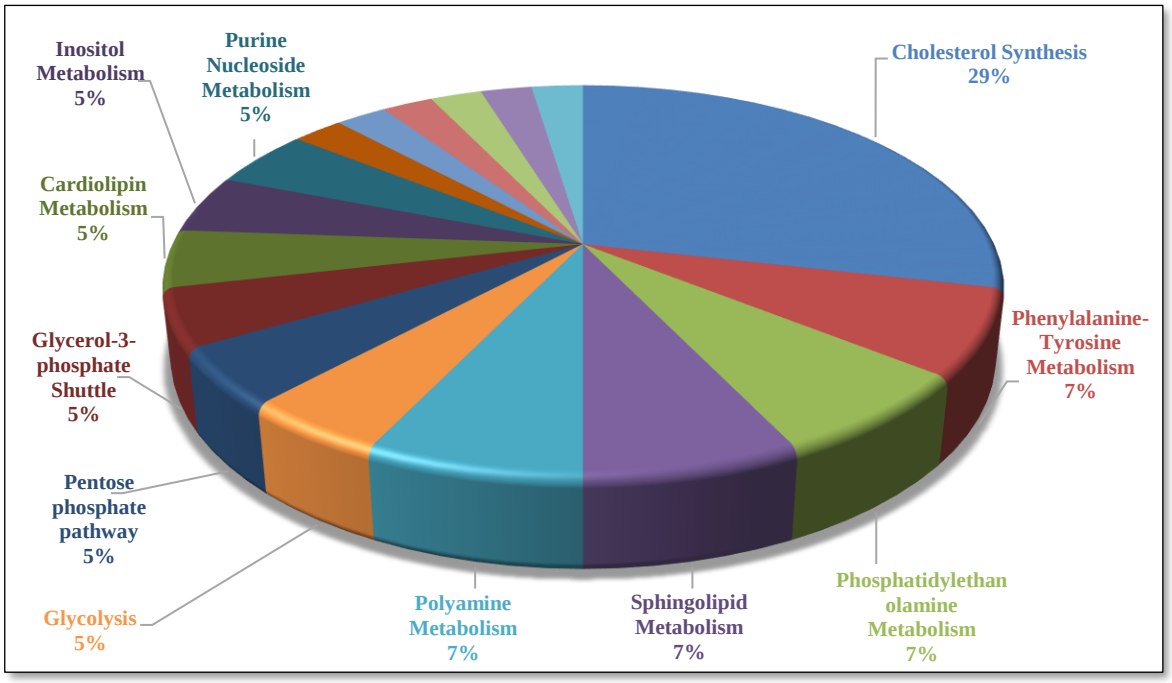

Figure 4.24. The distribution of common essential genes estimated in single-gene deletion and reaction deletion analyses based on associated pathways.

After performing single gene deletion and reaction deletion analyses, double gene deletion analysis was performed. In double gene deletion analysis, combinations of gene pairs are sequentially removed from the model, and the flux rate of a specified reaction is estimated after each removal. If the flux rate of the determined reaction falls below a certain value as a result of double gene deletion, these gene combinations are assumed to be essential for the system. In this analysis, the gene combinations whose removal reduces the flux of biomass reaction below10^{-6} mmol/gDW*hour were accepted as essential for the MB model.

One of the gene combinations detected is the pair of ACL and FASN which was also detected in single gene deletion analysis.

Inhibition of ACL which carries out the production of acetyl CoA in the TCA cycle led to a decrease in the growth of lung cancer cells (Hatzivassiliou *et al*., 2005), (Marie and Shinjo, 2011). FASN deactivation also resulted in suppression of tumor-specific features like lipid synthesis in multiple cancers like pancreatic, ovarian, and lung tumors (Ventura *et al*., 2015). Additionally, it was determined that the deactivation of ACL and FAS genes restricted cancer cell division (Marie and Shinjo, 2011). Consistent with the literature, the combination of ACL and FASN genes was estimated by the MB model in double gene deletion analysis.

When essential genes obtained from single gene deletion analysis were removed from the results obtained as a result of double gene analysis, 26 pairs of genes remained. These gene combinations are demonstrated in Figure 4.25. The combinations whose removal reduces the biomass below 10^{-6} mmol/gDW*hour, are shown in green, while others are shown in blue.

The number of gene combinations based on the pathway is shown in Figure 4.26. For instance, there is one gene combination in the TCA cycle and both genes take part in the TCA cycle. There are four gene pairs which include eight genes taking part in GABA and TCA cycle. That is why, 4 is written in the square where TCA and GABA pathways intersect, in Figure 4.26.

In MB, the activity in the GABA cycle decreases compared to normal cells (Munford, 20). It was found that GABA transaminase (ABAT) which converts GABA and alpha-ketoglutarate to glutamate and SuccinateSAL is downregulated in primary MB relative to healthy cerebellum (Martirosian *et al*., 2021). It was also detected that ABAT activity is lower in malignant GR3 and GR4 subgroups than SHH and WNT. Moreover, upregulated ABAT was found to trigger apoptosis and decrease cancer proliferation in rats with MB (Martirosian *et al*., 2021). However, recently Martirosan et al found that the expression of ABAT is remarkably higher in metastatic MB samples than primary MB since they need to meet its energy requirement by catabolizing GABA (Martirosan *et al*., 2021). Metastatic tumor cells were observed to divert OXPHOS to generate sufficient energy and survive under hard conditions.

Moreover, the ABAT gene was determined to be vital for metastatic cells since ABAT replenishes metabolites used in the TCA cycle and OXPHOS by contributing to NADH and succinate syntheses (Figure 4.27).

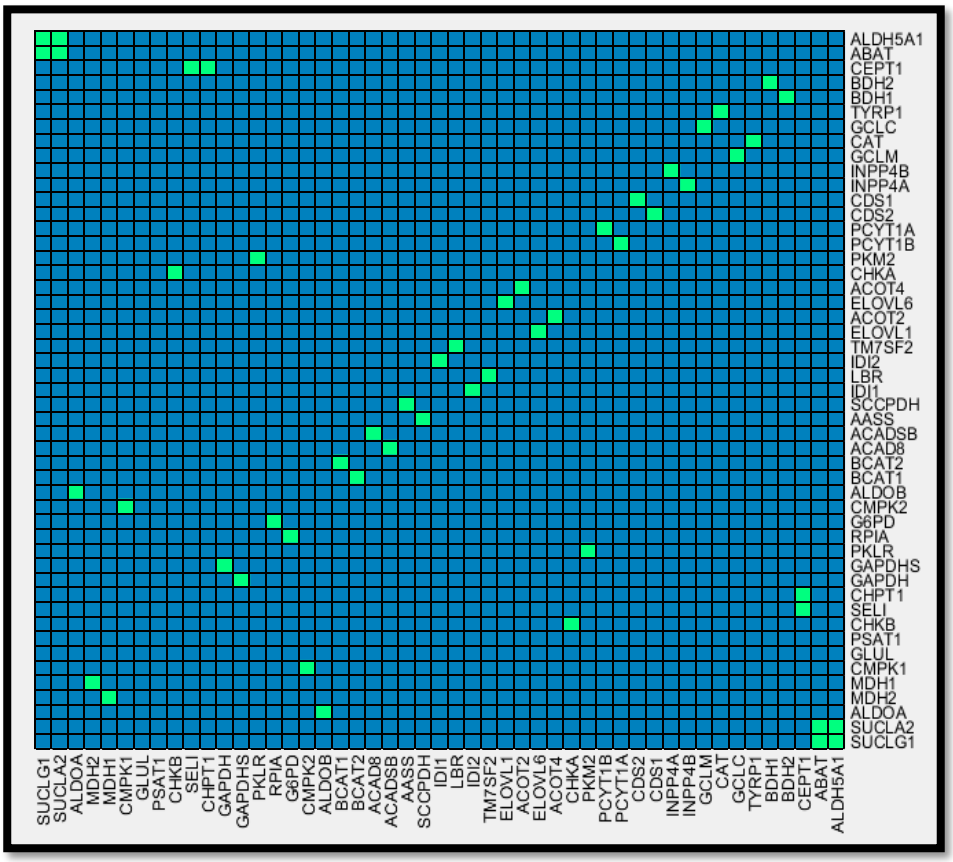

Figure 4.25. The interrelationship of the genes found in double gene deletion analysis. The gene combinations whose removal affects biomass significantly are shown in green.

In GABA metabolism, glutamate is converted to GABA in neuron and then they are transported to astrocytes (See R97 in Figure 4.27). Then GABA and alpha-ketoglutarate form glutamate and succinate SAL by GABA transaminase regulated by ABAT (See R99 and R101 in Figure 4.27). Afterward, succinate and NADH were produced from succinate SAL and NAD by aldehyde dehydrogenase 5 family member A1 (ALDH5A1) (See R100 and R102 in Figure 4.27). Then in the TCA cycle, FAD and succinate are converted to $FADH_2$ and fumarate. FAD is transformed to $FADH_2$ by accepting two electrons and these electrons are transferred to electron transfer chain (Le and Ou, 2016).

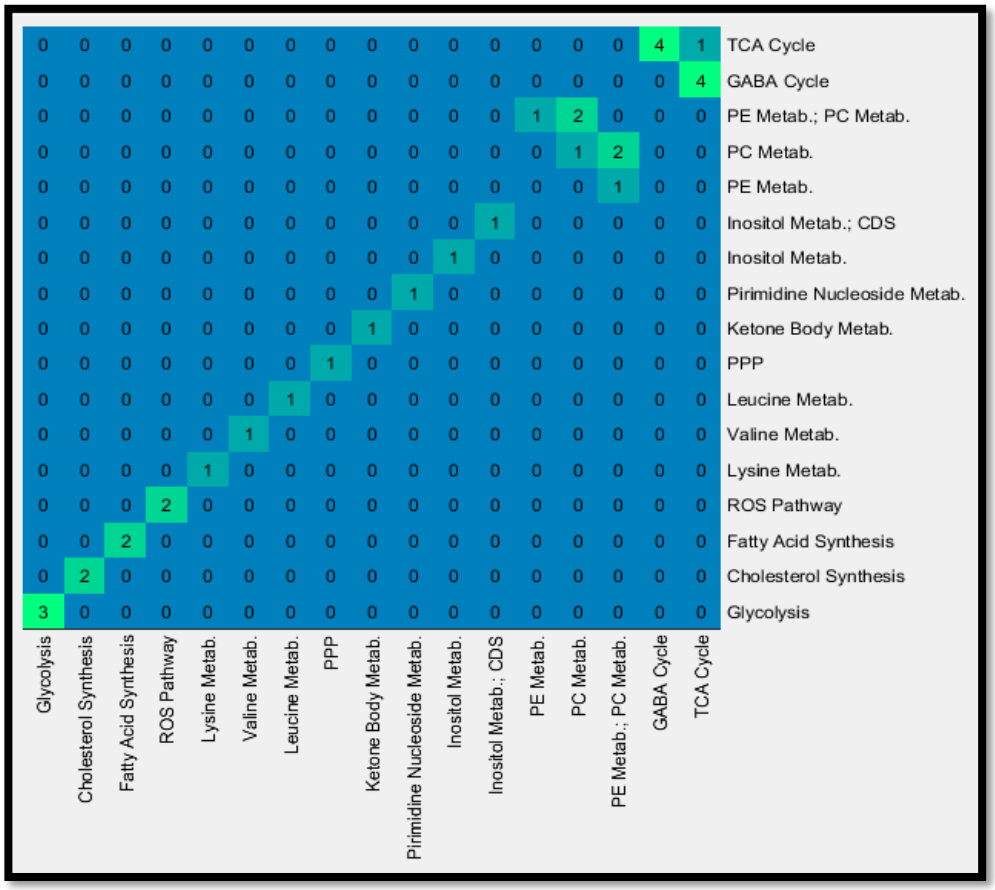

Figure 4.26. The number of gene combinations obtained in double gene deletion analysis and their related pathways.

Overexpression of succinate is also related to cancer (Jiang, 2017). Abnormalities related to Succinate dehydrogenase (SDH) which produces fumarate from succinate was estimated in some cancer types because an increase in succinate leads to hypoxia-inducible factor 1-alpha (HIF-alpha) stabilization and HIF-alpha regulates the genes inducing cell proliferation (Jiang, 2017). This study shows targeting the genes that regulate succinate production is a promising therapeutic approach.

Congruent with experimental results, ABAT gene with both succinate-CoA ligase ADP-forming subunit beta (SUCLA2) and succinate-CoA ligase GDP/ADP-forming subunit alpha (SUCLG1) genes producing succinate from succinyl-CoA in TCA cycle were detected by MB model.

Various compounds targeting these three genes and their interaction with each other were investigated from GeneCards and DrugBank (Stelzer *et al.*, 2016), (Wishart, 2006). The Food and Drug Administration (FDA) approved Acyclovir, which is utilized for herpes, targets both SUCLA2 and SUCLG1 genes (Stelzer *et al.*, 2016).

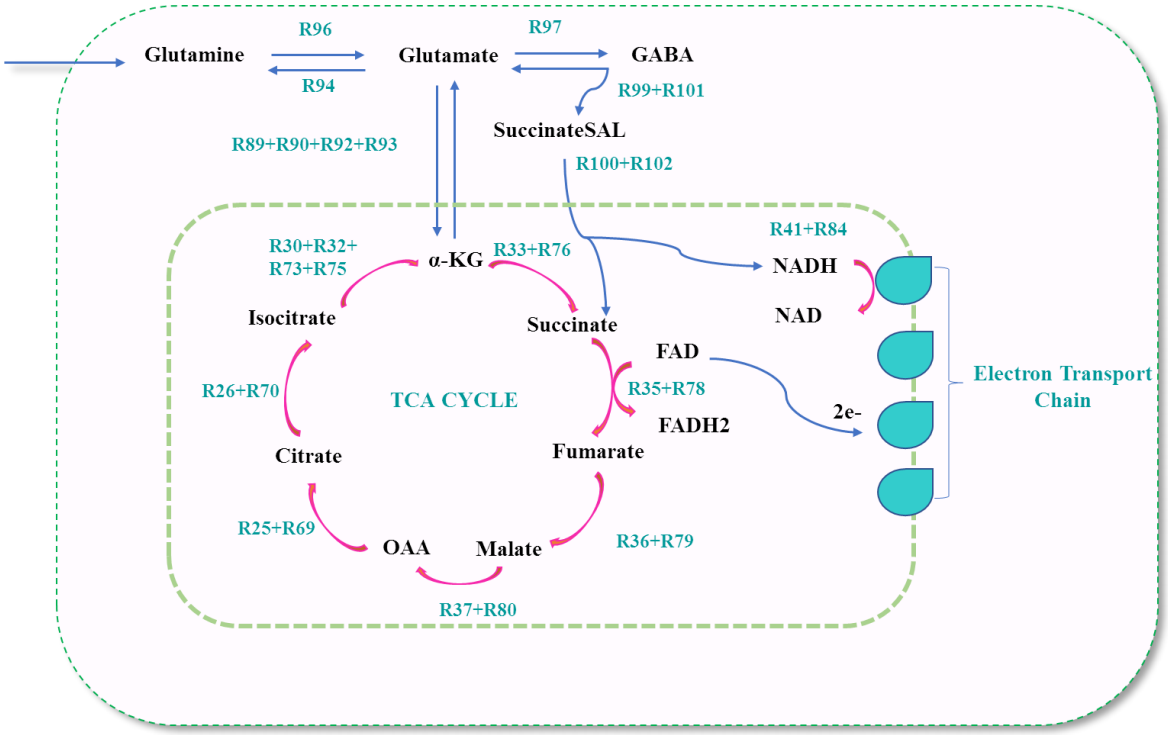

Figure 4.27. The relation between GABA shunt, TCA cycle and electron transfer chain.

Acyclovir was shown to reduce the growth of glioblastoma cell lines by 68.3% whilst it reduced healthy cells by 38.3% (Kominsky *et al.*, 2000). A similar study also demonstrated that Acyclovir was effective on glioblastoma (Özdemir and Göktürk, 2019). Phenelzine and Vigabatrin are compounds approved by FDA and they both inhibit ABAT (Puniya *et al.*, 2021). While Phenelzine is used as an antidepressant, Vigabatrin is an antiepileptic drug (Wishart, 2006). Both cross the blood-brain barrier (BBB) (Wishart, 2006). Phenelzine which also targets Monoamine Oxidase A (MAOA) was found effective for prostate tumor cells (Gross *et al.*, 2021). The side effects of Phenelzine were detected to be low but important cardiovascular effects were estimated infrequently (Gross *et al.*, 2021). However, the interaction of Acyclovir with Phenelzine may reduce the secretion of Phenelzine (Wishart, 2006).

Vigabatrin was detected to be a promising drug for brain tumors and effective for metastatic brain tumors in vivo (Hung *et al*., 2021), (Schnepp *et al*., 2017). According to a recent study conducted in glioblastoma cell lines, Vigabatrin was shown to suppress ion channels which ease aggressive migration and contribute to cell proliferation (Hung *et al*., 2021). Unlike interaction between Phenelzine and Acyclovir, no toxic effects were found for the interaction between Acyclovir and Vigabatrin (Wishart, 2006). Based on the experimental results obtained for Acyclovir and Vigabatrin in different cancer types, the synergistic effect of two drugs targeting SUCLA2, SUCLG1, and ABAT on MB should be investigated.

In addition to DrugBank and GeneCards databases, the Connectivity map database which includes disease, drug, and gene relations was examined for the compounds that inhibit SUCLA2, SUCLG1, and ABAT genes (Jiang *et al*., 2021), (Subramanian *et al*., 2017). While no extra compounds were found for SUCLA2 and SUCLG1 genes, natural compound vanillin was detected to reduce activities of both ABAT and ALDH5A1 genes (Tao *et al*., 2006). Moreover, vanillin was found to be transported through BBB (Wishart, 2006). However, unlike Vigabatrin and Phenelzine inhibiting ABAT, vanillin is still being investigated experimentally.

It is important to note that upregulation of the ABAT gene has reverse effects on non-metastatic MB, unlike metastatic MB (Martirosan *et al*., 2021). Therefore, it is significant to deliver these agents only in metastatic cases.

4.8. Therapeutic Targets for Medulloblastoma

4.8.1. Common Essential Genes for Three Critical Parameters

The aim of this section is to detect the essential genes required for growth, lactate, and ATP productions for the survival of MB cells (by repeating the above analysis for lactate and ATP syntheses). Targeting the genes that are essential for three parameters was expected to enhance the efficacy of the treatment.

Figure 4.28 shows the number of essential genes obtained for each of the three analyses. The intersection of essential genes found in three analyses is also shown in Figure 4.28. These 32 common genes were examined in detail. 32 common essential genes and the results where these genes were silenced in both models are also included in Appendix E.

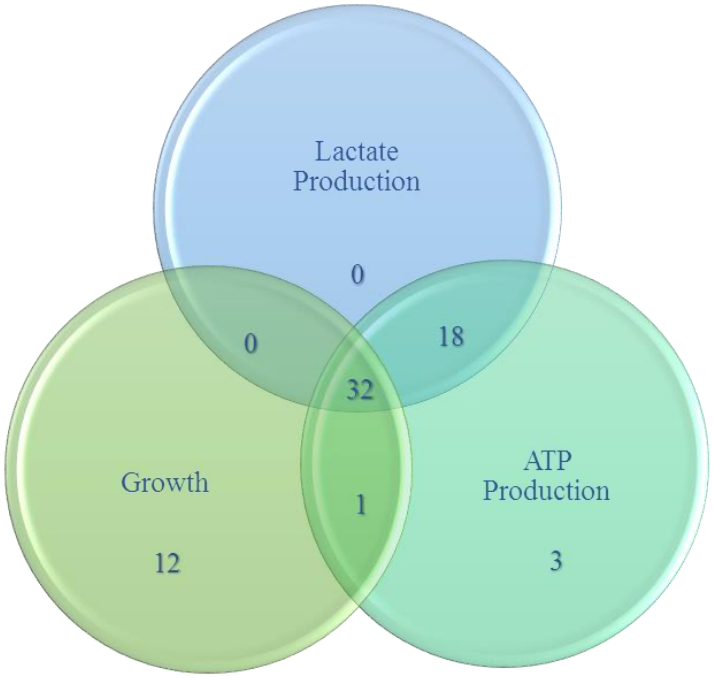

Figure 4.28. The number of essential genes obtained for each of the three cases.

After the reactions related to these 32 essential genes were removed one at a time from the healthy brain model, the genes whose removal does not have an impact on the main functions of the normal cell were identified. The results were compared with healthy model FBA results and the genes whose removal cause the healthy cell to fail to fulfill vital tasks were left out. For instance, after TPI1 gene knockout, solution space reduced with new constraints, and no solution was obtained as a result of FBA analysis. These types of genes were left out because their removal affected the system significantly. It was predicted that biologically, their inhibition would damage healthy cells alongside cancer cells. However, here, it is aimed to determine genes whose removal causes as minimum side effects as possible of therapeutic means on healthy cells. The genes whose removal do not affect the MB model significantly were also eliminated. For example, FH gene knockout did not affect MB growth at all. After Quinoid Dihydropteridine Reductase (QDPR) gene knockout, the growth reaction in MB only decreased by 26% of its previous value.

That is why these essential genes were removed. However, after the 3-Hydroxy-3-Methylglutaryl-CoA Reductase (HMGCR) gene knockout in the MB model, the growth reaction in MB decreased 100% of its previous value. This gene and similar genes were considered as good therapeutic targets. Based on these criteria, the essential gene list was narrowed down to 8 from 32. Eight essential genes whose removal does not affect or slightly affect the healthy model and affect the MB model more than 40% were identified. Table 4.4 demonstrates potential therapeutic genes (HMGCR, MVK, PMVK, MVD, FDFT1, CRLS1, FASN and SQLE) and the results where they were silenced in healthy model.

In the first column of table 4.4, eight common essential genes were shown while in the second one, the pathways related to these essential genes are shown. The third column of Table 4.4 includes information about how metabolic activities in the healthy cell changed after essential gene knockout.

For all 32 essential genes common to growth, lactate, and ATP productions, the drugs and potential compounds (approved, experimental, investigational) were also compiled from the DrugBank and GeneCards databases (Wishart, 2006), (Stelzer *et al*., 2016). There are 206 compounds detected in databases. Out of 206 drug compounds, 26 are approved, while 61 of them are at experimental status. 9 of 206 drugs are at investigational status. The rest of the compounds have either no status or have more than one status.

The appropriate compounds determined for eight essential genes were tabulated (Tables 4.5-9) with the help of DrugBank and GeneCard databases. 54 compounds were detected for eight potential therapeutic genes (HMGCR, MVK, PMVK, MVD, FDFT1, CRLS1, FASN, SQLE). The number of total compounds, whose drug status is available, is 47 for eight potential therapeutic genes. 10 compounds out of 47 are approved while 19 of them are at experimental status. 5 drug compounds out of 47 are at investigational status. Other compounds have more than one status. In Figure 4.29 the number of compounds for eight potential therapeutic genes based on the approved, investigational, experimental status and the ones with more than one status is demonstrated. 1 drug compound whose drug status is Vet-approved was not included in Figure 4.29.

Table 4.4. Eight potential therapeutic genes for medulloblastoma.

Gene	Pathway	The Effects of Gene Knockout on The Healthy Model
HMGCR	Cholesterol metabolism	Mild change in Glycolysis, PPP, Oxidative Phosphorylation and ATPase.
		Moderate change in TCA Cycle and Glutamate - Glutamine Cycle.
		Significant change in Cholesterol Synthesis and Fatty Acid Synthesis.
MVK	Cholesterol metabolism	Mild change in Glycolysis, PPP, Oxidative Phosphorylation and ATPase.
		Moderate change in TCA Cycle and Glutamate - Glutamine Cycle.
		Significant change in Cholesterol Synthesis and Fatty Acid Synthesis.
PMVK	Cholesterol metabolism	Mild change in Glycolysis, PPP, Oxidative Phosphorylation and ATPase.
		Moderate change in TCA Cycle and Glutamate - Glutamine Cycle.
		Significant change in Cholesterol Synthesis and Fatty Acid Synthesis.

Table 4.4. Eight potential therapeutic genes for medulloblastoma. (cont.)

Gene	Pathway	The Effects of Gene Knockout on The Healthy Model
MVD	Cholesterol metabolism	Mild change in Glycolysis, PPP, Oxidative Phosphorylation and ATPase.
		Moderate change in TCA Cycle and Glutamate - Glutamine Cycle.
		Significant change in Cholesterol Synthesis and Fatty Acid Synthesis.
FDFT1	Cholesterol metabolism	Mild change in Glycolysis, PPP, Oxidative Phosphorylation and ATPase.
		Moderate change in TCA Cycle and Glutamate - Glutamine Cycle.
		Significant change in Cholesterol Synthesis and Fatty Acid Synthesis.
SQLE	Cholesterol metabolism	Mild change in Glycolysis, PPP, Oxidative Phosphorylation and ATPase.
		Moderate change in TCA Cycle and Glutamate - Glutamine Cycle.
		Significant change in Cholesterol Synthesis and Fatty Acid Synthesis.

Table 4.4. Eight potential therapeutic genes for medulloblastoma. (cont.)

Gene	Pathway	The Effects of Gene Knockout on The Healthy Model
FASN	Fatty acid synthesis	No change in PPP.
		Mild change in Glycolysis, Oxidative Phosphorylation and ATPase.
		Moderate change in TCA Cycle, Glutamate - Glutamine Cycle.
		Significant change in Cholesterol Synthesis and Fatty Acid Synthesis.
CRLS1	Cardiolipin metabolism	No change in PPP.
		Mild change in Glycolysis, Oxidative Phosphorylation and ATPase.
		Moderate change in TCA Cycle, Glutamate-Glutamine Cycle.
		Significant change in Cholesterol Synthesis, Fatty Acid Synthesis.

24 compounds out of 54 drugs are related to cancer, and (including ones whose status is not available) the MB model successfully help us find them. The Drugs/Compounds expected to give satisfactory results in MB were investigated in detail.

The production of mevalonate from 3-hydroxy-3 methylglutaril-CoA carried out by HMGCR is the key rate-determining reaction in cholesterol synthesis (Feltrin *et al*., 2020).

HMGCR inhibitors (Table 4.5) known as statins are normally utilized in cholesterol-related problems and cardiovascular diseases. Statins might be beneficial for cancer owing to their relations to important biological processes, like cell proliferation (Hindler *et al*., 2006). Statins have been detected to suppress tumor growth and trigger cell death in leukemia, neuroblastoma (NB), melanoma, and glioma cell lines (Dimitroulakos *et al*., 2000), (Girgert *et al*., 1999), (Shellman *et al*., 2005), (Song *et al*., 2014).

Figure 4.29. The Number of Drugs/Compounds based on their status.

Lovastatin which is also one of the statins, (See Table 4.5), has been utilized as a potential anticancer drug in several studies related to glioblastoma, astrocytoma, gastric adenocarcinoma, and breast cancer (Larner *et al*., 1998), (Kim *et al*., 2001), (Mahmoud *et al*., 2016). Macaulay et al observed that Lovastatin reduces cell growth and stimulates apoptosis in MB cells (Macaulay *et al*., 1999). Sheikholeslami et al. found that Simvastatin, another statin, initiates apoptosis in MB cell lines (Sheikholeslami *et al*., 2019).

Atorvastatin, one other statin was studied on a glioma model (Bayat *et al*., 2016). They detected that tumor-specific features of glioblastoma substantially alleviated after Atorvastatin application.

In another study conducted by Kumar et al, Mevastatin significantly reduced the NB cells viability (Kumar *et al*., 2002). In the same study, pravastatin was not found as effective as Mevastatin. In another study, Jiang et al examined the impact of various statin agents (Lovastatin, Cerivastatin, Rosuvastatin Simvastatin, Atorvastatin, Fluvastatin, Pitavastatin, Mevastatin, and Pravastatin) which reduce the activity of mevalonate synthesis on brain cancer cells (See Table 4.5) (Jiang *et al*., 2014). They detected that Pitavastatin, Fluvastatin, and Cerivastatin were the most effective drugs in glioblastoma cell lines. However, Cerivastatin was removed from the market, because of its unwanted effects on the human body (Wishart, 2006).

Sławinska-Brych et al. studied the impact of Fluvastatin on rat glioma cells (Sławińska-Brych *et al*., 2014). They detected that Fluvastatin remarkably decreased cell viability and demonstrated anti-cancer characteristics. Moreover, Fluvastatin did not affect healthy neurons.

Cannabidiol is found in cannabis and utilized to alleviate pain (See Table 4.5) (Wishart, 2006). Nabiximols is also a plant-derived agent obtained from cannabis (See Table 4.5) (Wishart, 2006). Medical cannabis decreases nausea caused by chemotherapy according to early studies (See Table 4.5) (Borgelt *et al*., 2013). Many studies detected that they have anti-tumor features (Andradas *et al*., 2021). A brain tumor-related study realized in a mouse model of glioblastoma showed that Cannabidiol enhanced mouse survival when it was applied with chemotherapy temozolomide (López-Valero *et al*., 2018). Andradas et al. studied the behaviors of D9-tetrahydrocannabinol and cannabidiol in MB and ependymoma (EP). They found that cannabinoids have detrimental impacts on MB and EP, but they did not observe any change in mouse survival (Andradas *et al*., 2021). Moreover, cannabinoids did not affect chemotherapy at all in MB.

Table 4.5. Drugs/ Compounds for HMGCR.

HMGCR - Cholesterol Pathway	
Drug	**Status (Wishart, 2006)**
Lovastatin	Approved, Investigational
Cerivastatin	Approved, Withdrawn
Simvastatin	Approved
Atorvastatin	Approved
Rosuvastatin	Approved
Fluvastatin	Approved
Pravastatin	Approved
Mevastatin	Experimental
Pitavastatin	Approved
Meglutol	Experimental
Cannabidiol	Approved, Investigational
Nabiximols	Investigational
Medical Cannabis	Experimental, Investigational

Lots of studies have detected that Farnesol decreases aberrant cell division and stimulates apoptosis in cancer cells (See Table 4.6) (Adany *et al*., 1994), (Rioja *et al*., 2000), (Yazlovitskaya and Melnykovych, 1995). Tumor cells were usually observed to be more sensitive to Farnesol than healthy cells. Rioja et al. examined the effects of Farnesol on leukemic cell lines (Rioja *et al*., 2000). They observed that Farnesol leads to apoptosis of leukemic cell lines while it does not affect normal cells.

Preliminary works revealed that apoptosis initiation and the mitigation in cell proliferation by Farnesol might be associated with the reduction in the activity of 3-hydroxy-3-methylglutaryl CoA (HMG-CoA) reductase (Joo and Jetten, 2010). Another work showed that deactivation of HMG-CoA reductase causes endoplasmic reticulum (ER) stress, which is related to apoptosis (Chen *et al*., 2008).

TAK-475 is another cholesterol regulator (See Table 4.7) (Wishart, 2006). But instead of suppressing HMG-CoA reductase like statins, this agent reduces the activity of squalene synthase which is a downstream step of cholesterol synthesis (Wishart, 2006). Benakanakere et al used cholesterol regulators including TAK-475 to evaluate their impacts on leukemia cell lines (Benakanakere *et al*., 2014). Their study revealed that inhibition of squalene synthase increased the susceptibility of cancer cells to chemoimmunotherapy.

Squalene is an organic substance found abundantly in shark liver and produced in the cholesterol synthesis in humans (See Table 4.7) (Gunes, 2013). Because squalene has anti-cancer features, it is mainly utilized as an additional treatment in many cancer types.

Squalene is considered to affect the formation of cancer by suppressing the production of mevalonate from HMG-CoA, reducing the enzymatic synthesis of xenobiotics, and lastly removing free radicals (Gunes, 2013). Furthermore, squalene was found to protect healthy cells from the detrimental effects of chemotherapy (Das *et al*., 2003). Similarly, squalene protected healthy bone cells from harmful impacts of anti-cancer agents whereas it did not protect NB cells (Das et al., 2008). According to another study conducted on colon cancer, 1% squalene diet decreased aberrant cell genesis by 46% (Rao *et al*., 1998).

It was also detected Roidex that has squalene hindered cancer growth in mice. In the same study, Roidex led to remission in cancer progression (Desai *et al*., 1996).

Orlistat is an agent utilized for obesity (See Table 4.8). Orlistat is also known to cease cancer progress by restricting fatty acid metabolism and stimulating apoptosis. Another study performed on prostate cancer demonstrated that this agent suppresses tumor growth in vivo (Kridel *et al*., 2004). Grube et al found that Orlistat suppressed fatty acid biosynthesis, decreased growth by approximately 64%, and lowered cell viability in glioblastoma cells (Grube *et al*., 2014).

Table 4.6. Drugs/ Compounds for MVK and MVD.

MVK - Cholesterol Pathway	
Drug	**Status (Wishart, 2006)**
Farnesol	Experimental
Scopolamine	Approved, Investigational
Isopentenyl pyrophosphate	Experimental

Isoniazid is utilized to cure tuberculosis (See Table 4.8). Studies on the use of isoniazid as an anticancer drug have been observed to be very few. In a study carried out by Lv et al, isoniazid depleted MAOA which is related to prostate cancer progress and dissemination (Lv *et al*., 2019).

Oleic Acid is frequently used in drugs and it demonstrates anticancer features when it interacts with lactoferrins and α-lactalbumin proteins (See Table 4.8) (Ruggiero *et al*., 2014). That is why, Ruggiero et al. combined oleic acid and Gc protein-derived macrophage activating factor (GcMAF) (Ruggiero *et al*., 2014). That complex with a special diet rich in protein and including low carbohydrate nutrients was applied to cancer patients. The study has resulted in the inhibition of tumor growth by 25% (Ruggiero *et al*., 2014).

Stearic acid is a substance used in skin products (See Table 4.8). Habib et al studied the effect of stearic acid on cancer progress in vivo and in vitro (Habib *et al*., 1987). A reduction in membrane rigidity is one of the properties of cancer cells. It stems from the disruption in the proportion of oleic acid to stearic acid. By keeping the proportion of cell membrane at a normal level, tumor growth in the mouse model could be restrained (Habib *et al*., 1987).

Cerulenin is an antifungal drug that hinders sterols and fatty acids generations (See Table 4.8) (Volpe *et al*., 1976). It also suppresses HMG-CoA synthase in cholesterol synthesis (Ohno *et al*., 1974). Slade et al. studied the influence of cerulenin on childhood cancer cell lines including MB, NB, retinoblastoma, and rhabdoid tumor and they observed that cerulenin triggers apoptosis (Slade *et al*., 2003). Decreasing the activity of squalene epoxidase lessened cholesterol generation significantly (Feltrin *et al*., 2020). Butenafine which is a SQLE inhibitor is an antifungal substance utilized for dermatologic diseases (See Table 4.9) (Wishart, 2006).

Naftifine is also an antifungal drug (See Table 4.9) (Wishart, 2006). It is known that abnormal initiation of WNT/β-catenin signaling leads to many diseases including the WNT subtype of MB (Raabe and Eberhart, 2013), (Schmeel *et al*., 2015). Schmeel et al. tested Naftifine which has similar properties to WNT inhibitors, to observe its effect on lymphoma and myeloma cell lines (Schmeel *et al*., 2015). They detected that Naftifine lessened cell viability in lymphoma and myeloma cell lines. Moreover, they observed that the influence of Naftifine on normal cells was very mild.

Table 4.7. Drugs/ Compounds for FDFT1.

FDFT1 - Cholesterol Pathway	
Drug	**Status (Wishart, 2006)**
TAK-475	Investigational
Squalene	Vet approved

Terbinafine which is very similar to Butenafine also decreases SQLE activity (See Table 4.9) (Porras *et al*., 2018). Unlike other antifungal agents like Butenafine and Naftifine, there are more studies that focus on the anti-cancer features of Terbinafine. Chien et al, investigated the influence of Terbinafine on oral cancer (Chien *et al*., 2012). Terbinafine suppressed growth substantially in oral cancer cell lines.

Ellagic acid (EA) is found in berries, walnuts, grapes, and pomegranates (See Table 4.9) (Ceci *et al*., 2018). In the last decades, Ellagic acid (EA) has been examined for its anticancer characteristics in various tumors such as colon cancer, lung cancer, ovarian cancer, melanoma, and GBM (Ceci *et al*., 2018). Both studies related to GBM revealed that EA caused an important reduction in cell division and stimulated apoptosis (Wang *et al*., 2016), (Wang *et al*., 2017). Studies carried out in GBM revealed that the tumor-suppressive impact of EA was related to the deactivation of NOTCH1 and the Akt signaling pathway (Ceci *et al*., 2018). Notch signaling is significant for cerebellar development (Kahn *et al*., 2018). The genes controlling the NOTCH1 pathway are overexpressed in MB. Kahn et al uncovered that NOTCH1 is the main reason for Group 3 MB metastasis (Kahn *et al*., 2018).

Table 4.8. Drugs/ Compounds for FASN.

FASN - Fatty Acid Synthesis	
Drug	**Status (Wishart, 2006)**
Orlistat	Approved, Investigational
Isoniazid	Approved, Investigational
Oleic acid	Approved, Investigational, Vet approved
Stearic acid	Approved, Experimental
Cerulenin	Experimental

Liranaftate is another SQLE drug used for fungal-related diseases (See Table 4.9) (Kim *et al*., 2021). However, there are no cancer-related studies based on this inhibitor. NB-598 is another compound that targets SQLE and it is utilized to regulate cholesterol generation (See Table 4.9) (Feltrin *et al*., 2020). Lately, it was shown that reducing SQLE activity is a promising approach in cancer. It was found that lung cancer cells are affected significantly by NB-598 because of excessive squalene accumulation (Mahoney *et al*., 2019).

Table 4.9. Drugs/ Compounds for SQLE.

SQLE - Cholesterol Pathway	
Drug	**Status (Wishart, 2006)**
Butenafine	Approved
Naftifine	Approved
Terbinafine	Approved, Investigational, Vet_approved
Ellagic acid	Investigational
Liranaftate	
NB-598	

4.8.2. Potential Metabolite-Antimetabolite Pairs

The objective of this section is to determine potential antimetabolites which might decrease the use of chosen natural metabolites in cells by creating competitive inhibition.

Firstly, the compounds similar to metabolites in the brain model were searched in DrugBank Database by using the structural information (SMILES code of each metabolite). Then, the metabolic reactions related to these metabolites were determined. Drug effect was simulated in both healthy and medulloblastoma models by inhibiting these reactions.

Once 315 Flux Balance Analyses where drug effects were simulated, were completed for the healthy model, the same procedure was performed for the MB model. The results where vital tasks were not realized in the healthy model and the ones in which the growth rate reduced by less than 40% in the MB model were removed. As a result, 114 natural substrates whose enzymes could be used as drug targets are detected by both MB and healthy models (See Table 4.10). These substrates are shown in the first column of Table 4.10 and related pathways of the substrates are included in the second column. The third column of Table 4.10 includes the number of similar compounds found in the DrugBank Database (Wishart, 2006).

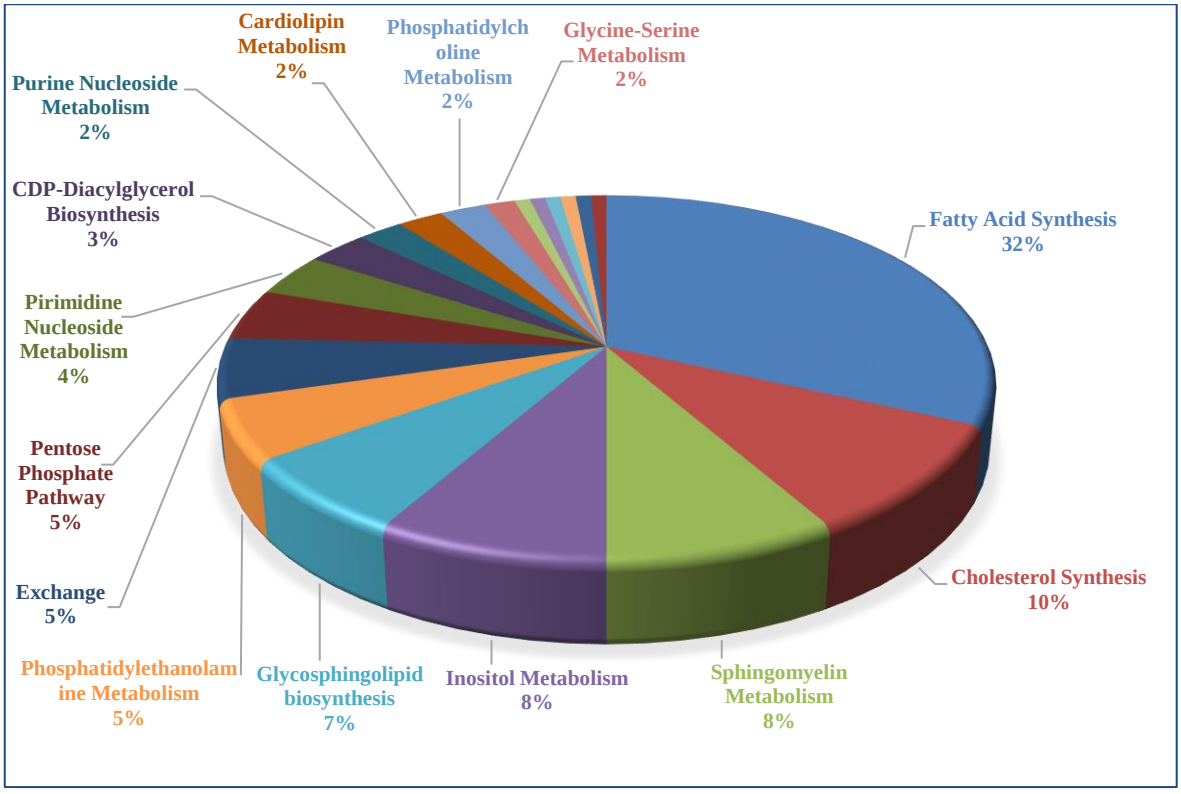

Figure 4.30. The distribution of substrates detected in FBA analysis according to their related pathways.

In other words, this column contains the number of potential antimetabolites for therapeutic purposes. The last column indicates how much MB growth rate decreased as a percentage in the presence of the drug.

For example, 3 compounds similar to 6-phosphogluconate were found in DrugBank Database (Wishart, 2006). And, the inhibition of reactions where 6-phosphogluconate is the substrate, reduced the growth rate by 100% in the MB model. No similar compounds were found from DrugBank Database for several metabolites like threonine (Wishart, 2006). Natural substrates related to sphingomyelin and glycosphingolipid metabolisms are shown in the next section. The total number of drug-metabolite pairs that could be used for therapeutic purposes, is 544.

The distribution of detected substrates based on their related pathways was calculated (Figure 4.30). Most of the metabolites whose enzymes are potential drug targets are linked to fatty acid synthesis (32%), cholesterol synthesis (10%), sphingomyelin metabolism (8%), inositol metabolism (8%), and glycosphingolipid metabolism (7%).

Indeed, fatty acid synthesis (FAs) was investigated as a target for malignancies by many researchers since lipids are used in many metabolic pathways which are vital for cancer progress (Röhrig and Schulze, 2016). After Warburg et al. found that tumors have glucose avidity and they carry out glycolysis whether oxygen is available, Medes et al. detected that tumors use acetate or glucose to produce lipids (Warburg, 1925), (Medes *et al*., 1953). Afterward, Fatty acid synthase was found to be an antigen in breast cancer (Kuhajda *et al*., 1994). FASN was also found to be upregulated in the SHH subtype of MB (Tech and Gerson, 2015).

Several agents such as Cerulenin, C75 have been examined for FASN suppression (Röhrig and Schulze, 2016). Cerulenin, normally used as a fungal drug, is being investigated as a cancer drug based on the findings that it triggers apoptosis and inhibits uncontrolled cell division (Röhrig and Schulze, 2016), (Slade *et al*., 2003). C75 also reduced cancer growth and enhanced the survival of mice with MB (Bhatia *et al*., 2012).

Table 4.10. The substrates whose enzymes could be used as drug targets.

Metabolites	Pathway	The Number of Compounds Found Similar to Metabolite	Decrease in Growth Rate in The Presence of Drug (%)
6-Phosphogluconate	Pentose Phosphate Pathway	3	100
Ribulose-5-Phosphate	Pentose Phosphate Pathway	3	100
Xylulose-5-Phosphate	Pentose Phosphate Pathway	3	100
Sedoheptulose-7-Phosphate	Pentose Phosphate Pathway	11	100
Erythrose-4-Phosphate	Pentose Phosphate Pathway	6	100
Histidine	Histamine Metabolism, Exchange	2	76
3_Phospho_Serine	Glycine-Serine Metabolism	5	48
Serine	Glycine-Serine Metabolism, Sphingomyelin Metabolism	8	92

Table 4.10. The substrates whose enzymes could be used as drug targets. (cont.)

Metabolites	Pathway	The Number of Compounds Found Similar to Metabolite	Decrease in Growth Rate in The Presence of Drug (%)
Leucine	Leucine Metabolism	7	90
Valine	Valine Metabolism, Exchange	5	90
Lysine	Lysine Metabolism, Exchange	1	90
Threonine	Threonine Metabolism, Exchange	0	88
R-Mevalonate	Cholesterol Synthesis	4	79
Mevalonate-5-Phosphate	Cholesterol Synthesis	0	79
Mevalonate-Diphosphate	Cholesterol Synthesis	0	79
Isopentenyl_Diphosphate	Cholesterol Synthesis	3	79
Dimethylallyl_ Diphosphate	Cholesterol Synthesis	0	80

Table 4.10. The substrates whose enzymes could be used as drug targets. (cont.)

Metabolites	Pathway	The Number of Compounds Found Similar to Metabolite	Decrease in Growth Rate in The Presence of Drug (%)
Geranyl_Diphosphate	Cholesterol Synthesis	2	80
2E_6E_Farnesyl_Diphosphate	Cholesterol Synthesis	2	79
Presqualene_Diphosphate	Cholesterol Synthesis	0	79
Squalene	Cholesterol Synthesis	0	79
S_2_3_Epoxysqualene	Cholesterol Synthesis	0	79
Lanosterol	Cholesterol Synthesis	13	79
Desmosterol	Cholesterol Synthesis	12	100
Cholesterol	Cholesterol Synthesis	12	79
Acetoacetyl-Acp	Fatty Acid Synthesis	0	91
R-3-Hydroxybutanoyl-Acp	Fatty Acid Synthesis	0	91
Crotonyl-Acp	Fatty Acid Synthesis	0	91

Table 4.10. The substrates whose enzymes could be used as drug targets. (cont.)

Metabolites	Pathway	The Number of Compounds Found Similar to Metabolite	Decrease in Growth Rate in The Presence of Drug (%)
Butyryl-Acp	Fatty Acid Synthesis	0	91
Malonyl-Coa	Fatty Acid Synthesis	48	91
3-Oxo-Hexanoyl-Acp	Fatty Acid Synthesis	0	91
R-3-Hydroxyhexanoyl-Acp	Fatty Acid Synthesis	0	91
Trans_Hex-2-Enoyl-Acp	Fatty Acid Synthesis	0	91
Hexanoyl-Acp	Fatty Acid Synthesis	0	91
3-Oxo-Octanoyl-Acp	Fatty Acid Synthesis	0	91
R-3-Hydroxyoctanoyl-Acp	Fatty Acid Synthesis	0	91
Trans_Oct-2-Enoyl-Acp	Fatty Acid Synthesis	0	91
Decanoyl-Acp	Fatty Acid Synthesis	0	91
Trans_Dodec-2-Enoyl-Acp	Fatty Acid Synthesis	0	91
Dodecanoyl-Acp	Fatty Acid Synthesis	0	91
3-Oxo-Myristoyl-Acp	Fatty Acid Synthesis	0	91

Table 4.10. The substrates whose enzymes could be used as drug targets. (cont.)

Metabolites	Pathway	The Number of Compounds Found Similar to Metabolite	Decrease in Growth Rate in The Presence of Drug (%)
R-3-Hydroxypalmitoyl-Acp	Fatty Acid Synthesis	0	91
Trans_Hexadecenoyl-Acp	Fatty Acid Synthesis	0	91
Palmitoyl-Acp	Fatty Acid Synthesis	0	91
Acetyl-Acp	Fatty Acid Synthesis	0	91
Palmitoyl-Coa	Fatty Acid Synthesis, Sphingomyelin Metabolism	44	91
Amp	Purine Nucleoside Metabolism	19	91
3-Oxo-Stearoyl-Coa	Fatty Acid Synthesis	23	91
Oleoyl-Coa	Fatty Acid Synthesis	23	91
Linoleate	Fatty Acid Synthesis	10	80

Table 4.10. The substrates whose enzymes could be used as drug targets. (cont.)

Metabolites	Pathway	The Number of Compounds Found Similar to Metabolite	Decrease in Growth Rate in The Presence of Drug (%)
Arachidonate	Fatty Acid Synthesis	10	79
Linolenate	Fatty Acid Synthesis	9	79
Decosahexenoate	Fatty Acid Synthesis	1	79
Octanoyl-Acp	Fatty Acid Synthesis	0	91
3-Oxo-Decanoyl-Acp	Fatty Acid Synthesis	0	91
R-3-Hydroxydecanoyl-Acp	Fatty Acid Synthesis	0	91
Trans-Delta2-Decenoyl-Acp	Fatty Acid Synthesis	0	91
3-Oxo-Dodecanoyl-Acp	Fatty Acid Synthesis	0	91
R-3-Hydroxydodecanoyl-Acp	Fatty Acid Synthesis	0	91
3R-3-Hydroxymyristoyl-Acp	Fatty Acid Synthesis	0	91
Trans_Tetradec-2-Enoyl-Acp	Fatty Acid Synthesis	0	91
Myristoyl-Acp	Fatty Acid Synthesis	0	91
3-Oxo-Palmitoyl-Acp	Fatty Acid Synthesis	0	91

Table 4.10. The substrates whose enzymes could be used as drug targets. (cont.)

Metabolites	Pathway	The Number of Compounds Found Similar to Metabolite	Decrease in Growth Rate in The Presence of Drug (%)
Palmitate	Fatty Acid Synthesis	7	91
Malonyl-Acp	Fatty Acid Synthesis	0	91
3-Hydroxy-Stearoyl-Coa	Fatty Acid Synthesis	22	91
Trans-2-3-Stearoyl-Coa	Fatty Acid Synthesis	0	91
Stearoyl-Coa	Fatty Acid Synthesis	21	91
Fatty acid	CDP-Diacylglycerol Biosynthesis	0	91
Ctp	Phosphatidylethanolamine Metabolism, Phosphatidylcholine Metabolism, Inositol Metabolism; CDP-Diacylglycerol Biosynthesis, Pirimidine Nucleoside Metabolism	20	91
CDP-Ethanolamine	Phosphatidylethanolamine Metabolism	21	90

Table 4.10. The substrates whose enzymes could be used as drug targets. (cont.)

Metabolites	Pathway	The Number of Compounds Found Similar to Metabolite	Decrease in Growth Rate in The Presence of Drug (%)
1_2-Diacylglycerol	Phosphatidylethanolamine Metabolism, Phosphatidylcholine Metabolism, Inositol Metabolism	1	90
Phosphatidyl-Ethanolamine	Phosphatidylethanolamine Metabolism; Phosphatidylcholine Metabolism	0	90
Cmp	Pirimidine Nucleoside Metabolism	23	91
Phosphatidyl-Serine	Phosphatidylethanolamine Metabolism	5	90
Ethanolamine	Phosphatidylethanolamine Metabolism	0	90

Table 4.10. The substrates whose enzymes could be used as drug targets. (cont.)

Metabolites	Pathway	The Number of Compounds Found Similar to Metabolite	Decrease in Growth Rate in The Presence of Drug (%)
Phosphoryl-Ethanolamine	Phosphatidylethanolamine Metabolism	0	90
CDP-Diacylglycerol	Cardiolipin Metabolism, Inositol Metabolism	0	100
Phosphatidylglycerol-Phosphate	Cardiolipin Metabolism	0	100
Phosphatidyl-Glycerol	Cardiolipin Metabolism	0	100
Phosphatidate	Inositol Metabolism; CDP-Diacylglycerol Biosynthesis	0	91
1-Acyl-Sn-Glycerol-3-Phosphate	CDP-Diacylglycerol Biosynthesis	0	91
Myo-Inositol	Inositol Metabolism, Exchange	6	100

Table 4.10. The substrates whose enzymes could be used as drug targets. (cont.)

Metabolites	Pathway	The Number of Compounds Found Similar to Metabolite	Decrease in Growth Rate in The Presence of Drug (%)
Phosphatidyl-Inositol	Inositol Metabolism	6	90
Phosphatidyl-1D-Myo-Inositol-4-Phosphate	Inositol Metabolism	0	90
Phosphatidyl-1D-Myo-Inositol-4-5-Bisphosphate	Inositol Metabolism	0	90
Myo-Inositol-(1-4-5)-Trisphosphate	Inositol Metabolism	11	90
Myo-Inositol-(1-4)-Bisphosphate	Inositol Metabolism	17	90
Myo-Inositol-(4)-Monophosphate	Inositol Metabolism	17	90
Arginine	Arginine Metabolism	0	90
Guanosine	Purine Nucleoside Metabolism	5	91
Ribose-1-Phosphate	Purine Nucleoside Metabolism	5	91
Uridine	Pirimidine Nucleoside Metabolism	3	92

Table 4.10. The substrates whose enzymes could be used as drug targets. (cont.)

Metabolites	Pathway	The Number of Compounds Found Similar to Metabolite	Decrease in Growth Rate in The Presence of Drug (%)
Cytidine	Pirimidine Nucleoside Metabolism	3	100
Cdp	Pirimidine Nucleoside Metabolism	7	91
Taurine	Exchange	0	90

In analyses related to fatty acid synthesis in healthy model, no changes were detected in PPP and OXPHOS while severe changes were observed in the acetyl-CoA, alpha-ketoglutarate, succinate, fumarate, and malate production reactions in the TCA cycle. In Fatty acid synthesis, moderate changes were observed.

Most of the metabolites detected in cholesterol synthesis are intermediates of the mevalonate pathway. HMGCR, MVK, PMVK, and MVD genes that control mevalonate (MVA) metabolism were also determined in gene essentiality analyses by the MB model. MVA metabolism which converts acetyl-CoA into isoprenoids and sterols is known to be crucial for malignant cells (Mullen *et al*., 2016). It was observed that the oncogenic signaling pathways stimulate the MVA metabolism in order to promote cancer-related properties such as abnormal proliferation.

Interfering with this characteristic of malignant cells is one of the promising therapeutic alternatives (Mullen *et al*., 2016).

In analyses related to cholesterol synthesis in healthy model, moderate changes were observed in flux values of fatty acid synthesis. Severe changes were observed in acetyl-CoA and alpha-ketoglutarate production reactions of the TCA cycle and all reactions in cholesterol synthesis.

In addition to the fatty acid and cholesterol synthesis metabolites, ones related to inositol pathway enzymes were also detected by the MB model. Inositols are known to be responsible for the physiological functions of the cell (Badodi *et al.*, 2021). Energy generation is controlled by Akt/mTOR pathways where inositol pyrophosphates and phosphoinositides are mainly involved. Abnormal changes related to inositol metabolism have been detected in malignant tumors (Badodi *et al.*, 2021). Studies showed that there was a decrease in the amount of inositol in several tumors like astrocytoma and lung cancer (Castillo *et al.*, 2000), (Ren *et al.*, 2017). Moreover, inositol metabolism intermediates were found to be lower in human disseminated osteosarcoma tumor cells than low metastatic cells (Ren *et al.*, 2017).

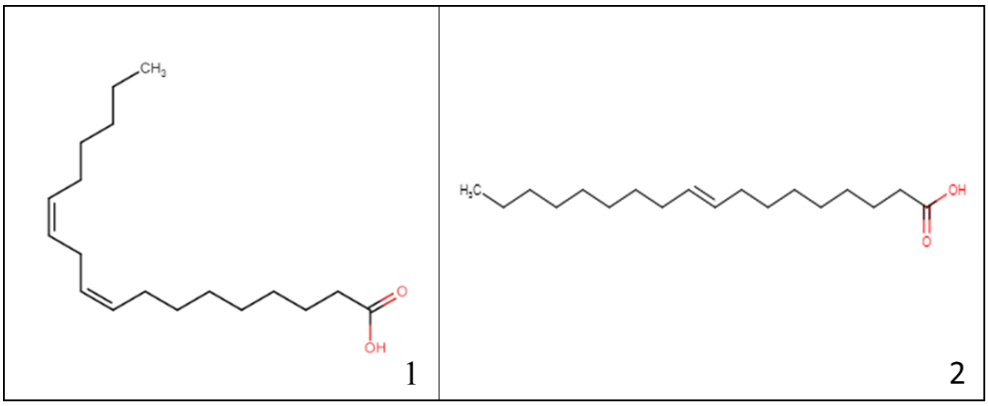

Figure 4.31. Metabolite and antimetabolite pair with 0.90 similarity score. Number 1 and number 2 represent linoleate and oleic acid, respectively (Wishart, 2006).

After determining the natural substrates whose enzymes could be used as drug targets, these metabolite-drug pairs were examined in terms of their toxicity and permeability through the BBB, and several compounds were selected regarding whether they cross the BBB and they are carcinogenic. Figure 4.31-4.37 show chemical structures of potential metabolites and drugs/compounds with similarity scores.

Both arachidonate and linoleate are very similar to oleic acid, and they have common ligands (See Figure 4.31 and 4.32). Oleic Acid is utilized in various drugs due to its antibacterial features (Wishart, 2006). Oleic acid was observed to stimulate apoptosis in human NB cell lines (Zhu *et al*., 2005).

Figure 4.32. Metabolite and antimetabolite pair with 0.83 similarity score. Number 1 and number 2 represent arachidonate and oleic acid, respectively (Wishart, 2006).

Oleic acid was also detected to inhibit cholesterol and fatty acid metabolisms in glioma cells by decreasing HMGCR and ACC1 impacts (Natali *et al*., 2007). It was also found that Oleic acid reduced the growth of cancer cells in breast and gastric cancer cell lines (Li *et al*., 2014).

After the production of gamma-linolenic acid from linoleate by fatty acid desaturase 2, arachidonate is synthesized from gamma-linolenic acid in fatty acid synthesis (Hanna and Hafez, 2018). Aside from the fact that oleic acid showed anti-cancer properties in previous studies (Zhu *et al*., 2005), (Natali *et al*., 2007), (Li *et al*., 2014), it can be presumed that oleic acid which is very similar to linoleate, might bind fatty acid desaturase 2 and inhibit this enzyme by causing competitive inhibition.

Icosapent is an omega-3 fatty acid that is very similar to arachidonate and linoleate (See Figure 4.33 and 4.34) (Wishart, 2006).

Icosapent is currently being investigated for cancer and Alzheimer's. It was found that icosapent uptake for 6 months decreased distinctly the size of benign polyposis (West *et al*., 2010). Considering the molecular similarity between icosapent, arachidonate, and linoleate, and the results where MB growth rate was decreased by 79% and 80% as the results of inhibitions of arachidonate and linoleate producing enzymes, our results suggest that the use of icosapent as an antimetabolite in cancer should be investigated in detail.

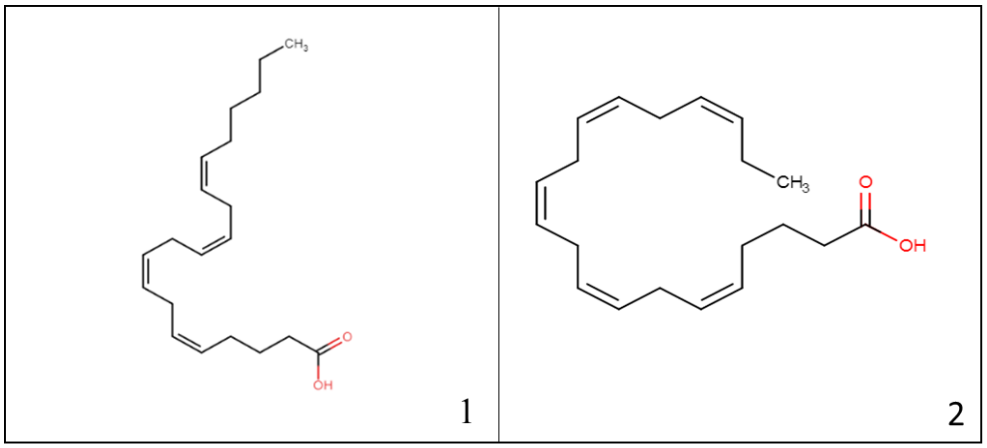

Figure 4.33. Metabolite and antimetabolite pair with 0.95 similarity score. Number 1 and number 2 represent arachidonate and icosapent, respectively (Wishart, 2006).

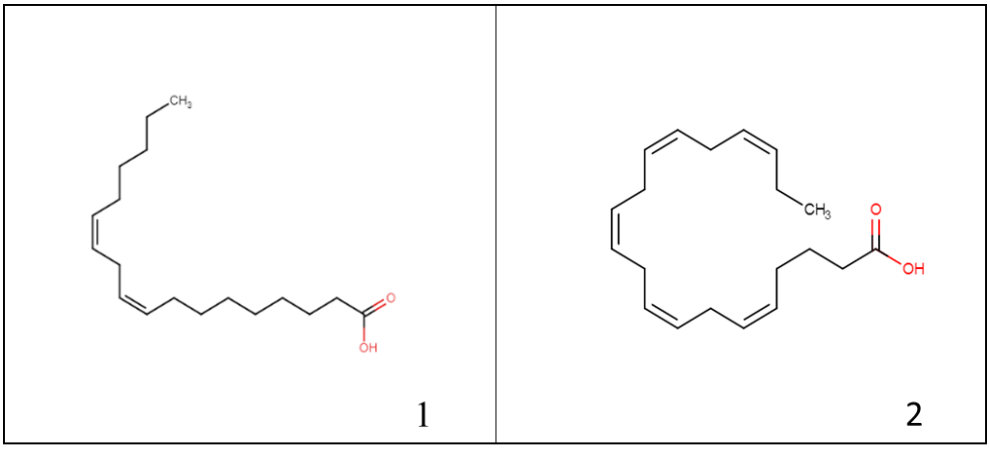

Figure 4.34. Metabolite and antimetabolite pair with 0.88 similarity score. Number 1 and number 2 represent linoleate and icosapent, respectively (Wishart, 2006).

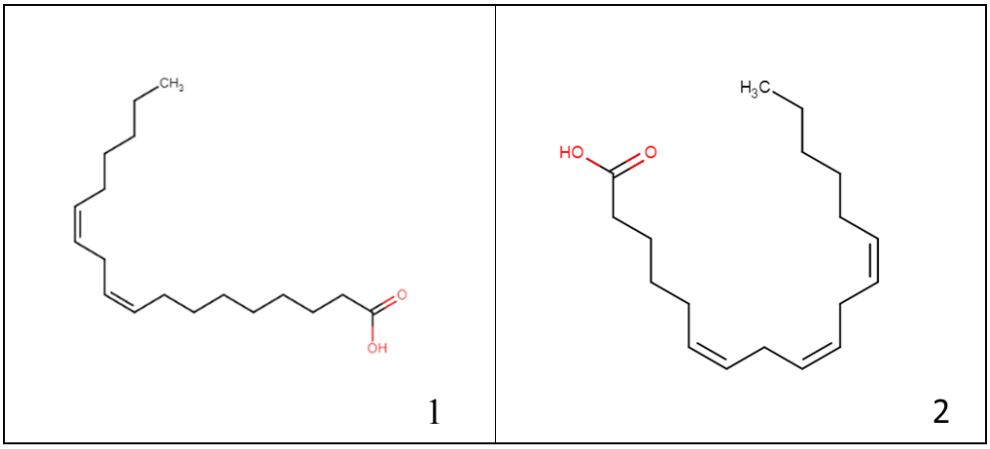

Figure 4.35. Metabolite and antimetabolite pair with 0.97 similarity score. Number 1 and number 2 represent linoleate and gamolenic acid, respectively (Wishart, 2006).

Another potential antimetabolite candidate is Gamolenic acid (GLA) which is similar to both linoleate and arachidonate (See Figure 4.35 and 4.36). Gamolenic acid showed high toxicity in cancer by inhibiting abnormal cell division in NB and colon tumor cell lines (Hrelia *et al.*, 1996). In another study about breast cancer, tamoxifen and GLA were given to a group of patients, while only tamoxifen was given to others (Kenny *et al.*, 2000). As a result, patients who received both GLA and tamoxifen responded more quickly to treatment by one and a half months. Our results show that Gamolenic acid should be investigated as an antimetabolite in further studies due to its similarity to certain metabolites in fatty acid synthesis.

Statins are known to target the mevalonate pathway, decrease tumor growth and induce apoptosis (Girgert *et al.*, 1999), (Song *et al.*, 2014), (Shellman *et al.*, 2005), (Dimitroulakos *et al.*, 2000), (Feltrin *et al.*, 2020). In addition to statins, Meglutole should be investigated experimentally in further studies since its similarity to mevalonate might make it a desirable antimetabolite for the treatment of MB even though there are no comprehensive studies regard of its effects on cancer cells. As seen from Figure 4.37, both substances have the same ligands and their similarity score is 0.97 which is really high.

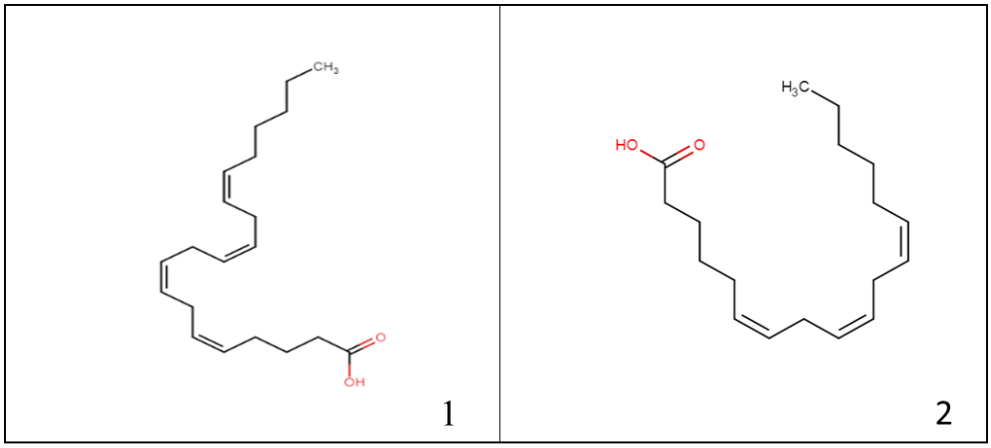

Figure 4.36. Metabolite and antimetabolite pair with 0.95 similarity score. Number 1 and number 2 represent arachidonate and gamolenic acid, respectively (Wishart, 2006).

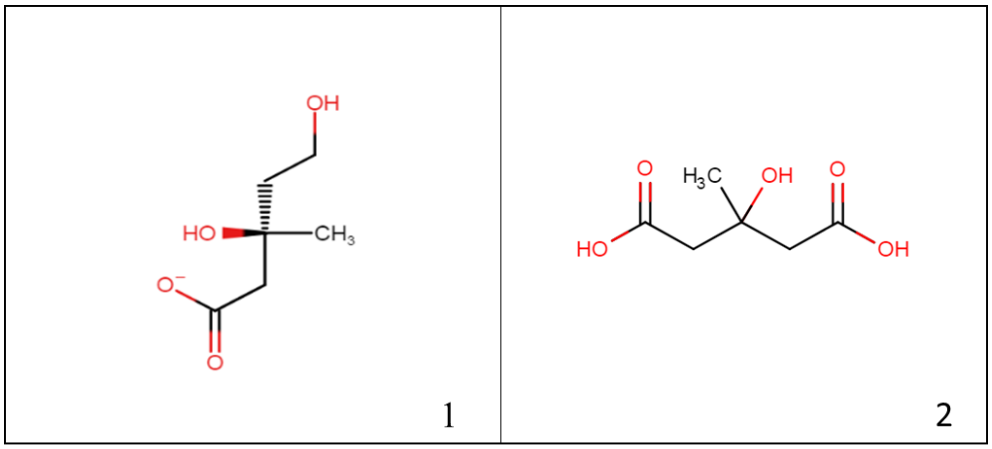

Figure 4.37. Metabolite and antimetabolite pair with 0.97 similarity score. Number 1 and number 2 represent R-mevalonate and meglutol, respectively (Wishart, 2006).

Sphingomyelin and glycosphingolipid metabolism will be examined in the next section in detail.

4.8.3. Investigation of Sphingolipid Metabolism

This section includes the effects of intermediates of sphingolipid metabolism on cancer and MB metabolism and therapeutic suggestions based on the results of FBA analyses where drug effect was created and gene essentiality analyses.

In the first step of the sphingolipid metabolic pathway, dehydrosphinganine was synthesized with the combination of palmitoyl CoA and serine metabolites (Figure 4.38). Then sphinganine is generated from dehydrosphinganine by 3-ketosphinganine reductase encoded by the KDSR gene (Lahiri and Futerman, 2007), (Sertbaş *et al*., 2014). Sphingosine kinase produces sphinganine 1-phosphate from sphinganine (Kanehisa *et al*., 2021). Sphinganine 1-phosphate is converted to phosphoryl-ethanolamine which is used in phosphatidylethanolamine metabolism (Lahiri and Futerman, 2007), (Kanehisa *et al*., 2021). After sphinganine is converted to dihydroceramide by dihydroceramide synthase, ceramide synthesis is carried out by dihydroceramide reductase encoded by the DEGS2 gene (Lahiri and Futerman, 2007), (Sertbaş *et al*., 2014). The production of ceramide is triggered by radiation and chemotherapy since it directs the cell to apoptosis (Ogretmen, 2018).

Afterward, ceramidase synthesizes sphingosine, and sphingosine kinase (SPHK1) produces sphingosine-1-phosphate (S1P) using sphingosine (Lahiri and Futerman, 2007), (Kanehisa *et al*., 2021). Subsequently, phosphoryl-ethanolamine is generated from sphingosine-1-phosphate. Galactosyl ceramide, ceramide-1-phosphate, sphingomyelin, sphingosine, and glucosylceramide are synthesized from ceramide (Lahiri and Futerman, 2007), (Kanehisa *et al*., 2021). Glucosylceramide is a precursor of more than 300 glycosphingolipids (GSL), whereas galactosylceramide is used only to produce a couple of GSLs (Ichikawa and Hirabayashi, 1998).

Next, lactosylceramide is synthesized with the combination of glucosylceramide and galactose (Schömel *et al*., 2020). Lactosylceramide is known to have critical roles in metastasis and cell division (Schömel *et al*., 2020).

Afterward, the several GSL series which are named Globo, Ganglio, Lacto/neo-Lacto, and neutral are formed from lactosylceramide (Schömel *et al*., 2020), (Kanehisa *et al*., 2021). GSLs are important constituents of the cell membrane and regulate various biological activities (D'Angelo *et al*., 2013).

Since cancer cells desire to keep ceramide levels low, they increase ceramide breakdown and restrict its generation (Oskouian and Saba, 2010). Indeed, 50% less ceramide was detected in collateral cancer compared to its healthy counterpart (Selzner *et al*., 2001).

Moreover, inhibition of ceramidase, the enzyme that produces fatty acids from ceramide, enhanced the ceramide level in malignancies and led to the initiation of apoptosis (Oskouian and Saba, 2010). Consistent with the literature, inhibition of ceramide degradation reaction led to a reduction in growth rate by 91% (See Table 4.11).

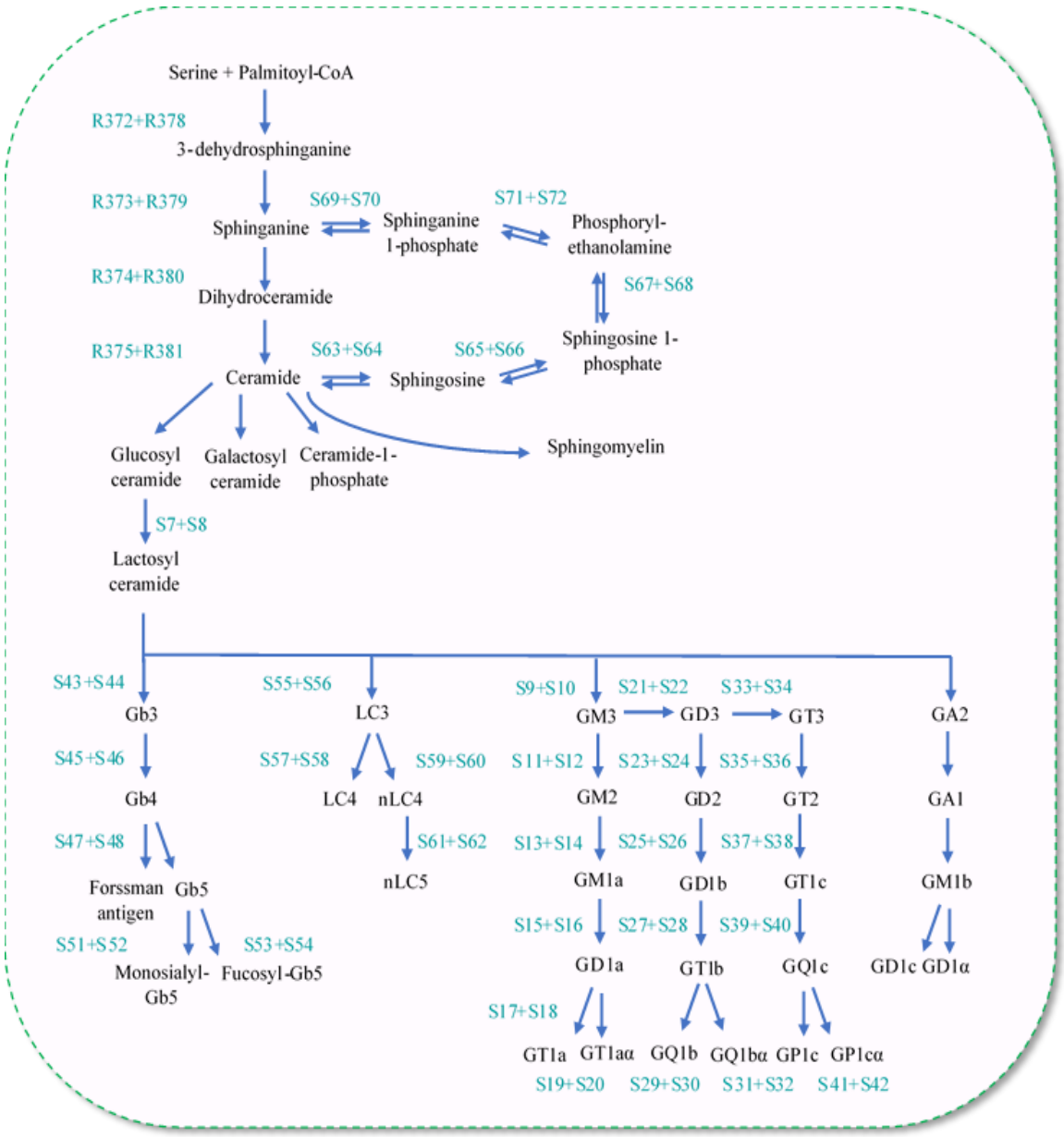

Figure 4.38. Sphingolipid Metabolism.

Like ceramide, S1P is also known to be linked to pivotal metabolic processes like growth, apoptosis, and proliferation. Unlike ceramide which leads to cell apoptosis, S1P supports cell survival, thus cancer cells generate S1P from ceramide to avoid cell arrest (Ogretmen, 2018), (Hawkins *et al*., 2020).

In glioblastoma (GBM), a higher level of S1P was determined while a reduction was detected in ceramides relative to the normal brain (Hawkins *et al*., 2020). In addition, overexpression of S1P is associated with the uncontrolled cell division and metastasis of GBM (Hawkins *et al*., 2020). To initiate apoptosis in GBM cells, ceramide synthesis from sphingomyelin is promoted with radiation and chemotherapy therapies. However, cells divert ceramide to the generation of S1P, which triggers survival effects, consequently reducing the effectiveness of these treatments (Ogretmen, 2018), (Hawkins *et al*., 2020).

Cellular signal is controlled with the interplay of GSLs with receptors and other components found on the cell (Schömel *et al*., 2020). GSLs expressions alter based on cell types and tissues (Zhuo *et al*., 2018). Abnormalities seen in GSL metabolism have been linked to malignancies (Ogretmen, 2018). It is known that the changes realized throughout early development also occur in oncogenic alteration (Russo *et al*., 2018). Aberrations related to GSLs metabolism were studied in many malignancies including renal, breast, gastric, colorectal, leukemia, melanoma, lung, prostate, bladder, ovarian (Zhuo *et al*., 2018). Some GSLs as tumor markers were also investigated for cancer therapy (Zhuo *et al*., 2018). Interestingly, the impacts of GSLs change based on the type of cancer. For instance, GM3 is downregulated in many malignancies, whereas it is upregulated in kidney cancer (Zhuo *et al*., 2018).

Globotetraosylceramide (Gb4) is known to be overexpressed in malignancies. In breast and colon cancer cell lines, it increases proliferation by triggering the mitogen-activated protein kinase (MAPK) pathway which has important roles in apoptosis and cell division (Schömel *et al*., 2020), (Pearson *et al*., 2001).

In the WNT subtype of Medulloblastoma (MB) the gene controlling Gb4 production, B3GALNT1, is upregulated in the GSE62600 dataset (Hooper *et al*., 2014).

GM3 is a precursor in the synthesis of more intricate gangliosides (Schömel *et al*., 2020). The gene controlling GM3 production was detected to be abnormally expressed in several types of malignancies (Zhuo *et al*., 2018**)**. While GM3 was observed to be upregulated in renal and leukemia cancers, it was determined to be downregulated in colon, ovarian, and bladder cancers (Zhuo *et al*., 2018**).** In glioma cells, GM3 initiates apoptosis and reduces migration of malignant cells in vivo and in vitro (Fujimoto *et al*., 2005).

Furthermore, GM3 has anticancer effects and decreases growth in astrocytoma (Seyfried and Mukherjee, 2010). Growth factor proteins controlled by gangliosides are generated abundantly in cancer leading to an increase in proliferation (Krengel and Bousquet, 2014). Various malignancies are also associated with overexpression of growth factor proteins. The GM3 ganglioside is known to suppress growth factor proteins (Krengel and Bousquet, 2014). Conversely, GM3 synthase knockout decreased the cell invasion in lung metastasis of mouse breast tumor (Gu *et al*., 2008).

In MB, GM3 was found as one of the prominent gangliosides in the both DAOY and TE-671 cell lines (Chang *et al*., 1997), (Gottfries *et al*., 1989). In the study realized by Hooper et al, the gene controlling GM3 production was detected to be upregulated in all subtypes relative to the control group (Hooper *et al*., 2014). Especially GM3 production was found to be overexpressed in the GR4 subtype of MB in comparison to the samples taken from other subgroups and control group in both datasets integrated into the MB model (Hooper *et al*., 2014), (Robinson *et al*., 2012).

GM2 ganglioside induces tumor growth using the immune escape system (Schömel *et al*., 2020). It was found that in all subtypes, the gene controlling GM2 production, was lower expressed compared to the control group (Hooper *et al*., 2014). On the other hand, Chang et al detected that GM2 composes almost 66% of all gangliosides in MB (Chang *et al*., 1997). A recent study also supported Chang's results by detecting ample GM2 in MB (Ermini *et al*., 2017).

GD3 which is a precursor of GD1b, enhances growth and metastasis, whereas GD1b is known to trigger apoptosis by promoting caspase in breast cancer.

GD1b also suppresses uncontrolled cell division in melanoma (Kanda *et al*., 2001), (Hamamura and Furukawa, 2017), (Ha *et al*., 2016).

GD2 is overexpressed in lung cancer, osteogenic sarcoma, and malignant melanoma (Hamamura and Furukawa, 2017).

Both GQ1b and GT1b decrease growth in melanoma cells (Kanda *et al*., 2001). The genes which control GD3 and GQ1b productions are downregulated in all subgroups of MB (Hooper *et al*., 2014).

GT3 are upregulated in WNT and GR4 subtypes of MB (Hooper *et al*., 2014).

4.8.3.1. Detection of Antimetabolites in Sphingolipid (SL) Metabolism.

Once the sphingomyelin and glycosphingolipid reactions were added to the brain model, the same analyses performed for all metabolites in MB and healthy models were carried out for these new SL metabolites. Table 4.11 contains metabolites whose enzymes could be therapeutic targets in sphingolipid metabolism.

As mentioned in section 4.8.2, 8% of all metabolites in the model MB are found to be related to the sphingomyelin pathway while 7% of them are linked to the glycosphingolipid pathway. Therefore 15% of substrates whose enzymes could be utilized as drug targets are associated with sphingolipid metabolism. This outcome renders sphingolipid metabolism the second most important pathway therapeutically after fatty acid synthesis where 32% of substrates are detected (See Figure 4.30). Correspondingly, intermediates and enzymes related to sphingolipid metabolism were determined to play substantial roles in cell metabolism as mentioned at the beginning of this section. Ceramide and sphingosine-1-phosphate are key intermediates whose productions determine whether the cell will go to apoptosis or survive.

Table 4.11. The substrates whose enzymes could be used as drug targets in sphingomyelin metabolism and glycosphingolipid biosynthesis-ganglio series.

Metabolites	Pathway	The Number of Compounds Found Similar to Metabolite	Decrease in Growth Rate in The Presence of Drug (%)
Serine	Glycine-Serine Metabolism, Sphingomyelin Metabolism	8	92
3-Dehydrosphinganine	Sphingomyelin Metabolism	1	90
Sphinganine	Sphingomyelin Metabolism	1	90
Dihydroceramide	Sphingomyelin Metabolism	0	90
Ceramide	Sphingomyelin Metabolism	0	91
Sphingomyelin	Sphingomyelin Metabolism	0	99
Phosphatidyl-Choline	Sphingomyelin Metabolism	0	91
Palmitoyl-Coa	Fatty Acid Synthesis, Sphingomyelin Metabolism	44	91
Galactose	Exchange, Sphingomyelin Metabolism	21	
Glucosylceramide	Sphingomyelin Metabolism	2	
Lactosylceramide	Glycosphingolipid biosynthesis-ganglio series	1	

Table 4.11. The substrates whose enzymes could be used as drug targets in sphingomyelin metabolism and glycosphingolipid biosynthesis-ganglio series. (cont.)

Metabolites	Pathway	The Number of Compounds Found Similar to Metabolite	Decrease in Growth Rate in The Presence of Drug (%)
GM3	Glycosphingolipid biosynthesis-ganglio series	4	70
GM2	Glycosphingolipid biosynthesis-ganglio series	4	52
GM1	Glycosphingolipid biosynthesis-ganglio series	1	85
GD1a	Glycosphingolipid biosynthesis-ganglio series	0	78
GD3	Glycosphingolipid biosynthesis-ganglio series	4	85
GD2	Glycosphingolipid biosynthesis-ganglio series	4	63
GD1b	Glycosphingolipid biosynthesis-ganglio series	4	85
GT1b	Glycosphingolipid biosynthesis-ganglio series	4	78
GD3	Glycosphingolipid biosynthesis-ganglio series	4	78

Moreover, it is known that sphingolipids partake in cell membranes and contribute to the cell signaling mechanism. A change in ganglioside production might lead to cell arrest or an increase in tumor-promoting activities.

The major obstacle of targeting ganglioside-associated enzymes is their impacts on cells might be very different depending on the cancer type and tissue. Therefore, their effects on MB and other cancer types were investigated in detail before making any conclusion. Like Table 4.10, Table 4.11 includes the substrates whose enzymes could be potential targets. The antimetabolite candidates identified from DrugBank and GeneCards databases were investigated in terms of their toxicity and permeability through the BBB.

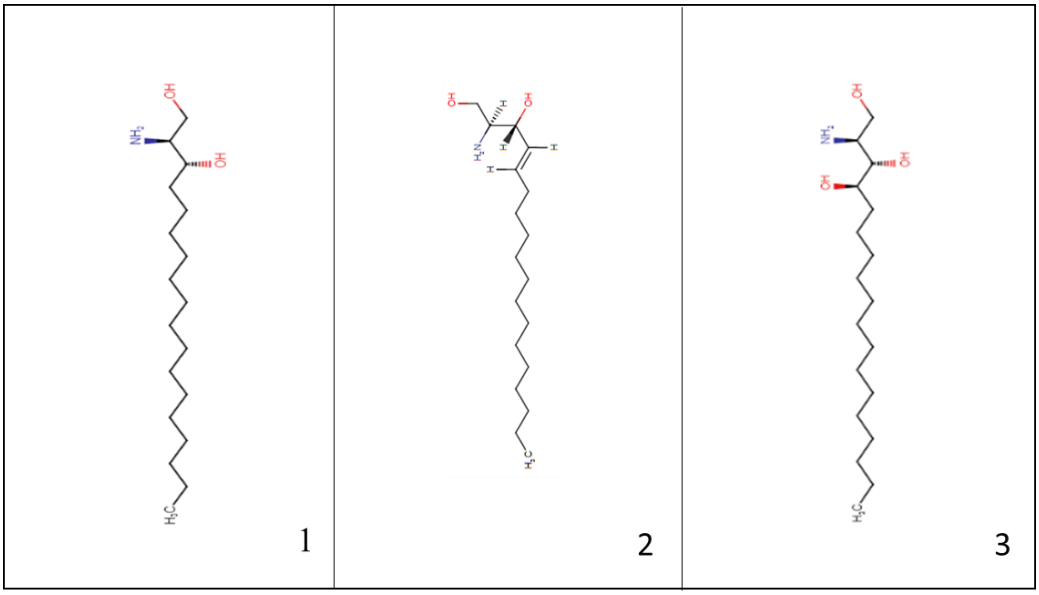

Figure 4.39. Sphinganine and phytosphingosine with 0.825 similarity score. Number 1, number 2 and number 3 represent Sphinganine, Sphingosine and Phytosphingosine, respectively (Wishart, 2006).

Phytosphingosine was found in the DrugBank database due to its molecular similarity to sphinganine metabolite which is the reactant of both sphinganine-1-phosphate and dihydroceramide production reactions (See Figure 4.39) (Wishart, 2006), (Lahiri and Futerman, 2007). Phytosphingosine is ample in nature (Nagahara *et al*., 2005). Phytosphingosine is also available in white blood cells and microvilli in the small bowel of mammals (Nagahara *et al*., 2005). According to literature, phytosphingosine is known as an analog of sphingosine in addition to its molecular similarity to sphinganine (Park *et al*., 2003a), (Nagahara *et al*., 2005), (Kang *et al*., 2017).

However, phytosphingosine was not detected in the DrugBank database when similar compounds for sphingosine were investigated (Wishart, 2006). That is why the similarity score for these two metabolites was not included in Figure 4.39.

According to recent research conducted on colorectal cancer, sphinganine and sphingosine trigger apoptosis (Ahn *et al*., 2006). Additionally, sphinganine was determined to initiate apoptosis in leukemia cells (Ryland *et al*., 2011). Fingolimod which is an agent chemically similar to sphingosine was also found to trigger apoptosis in several cancer types including glioma (Ryland *et al*., 2011). According to studies realized in lung cancer and lymphoma cells, phytosphingosine initiates apoptosis stimulating caspase 8 (Nagahara *et al*., 2005), (Park *et al*., 2003a). In the same study conducted on lung cancer and lymphoma cells, it was aimed to observe the impact of phytosphingosine on the activity of mitochondria which leaks out cytochrome c that is associated with apoptosis (Park *et al*., 2003a). They concluded their study by finding an increase in cytochrome c secretion. When cytochrome c excretion increases, caspase 9 was stimulated leading to the initiation of caspase 3. Subsequently, caspase 3 carries out apoptosis causing the cell to decrease in size (Park *et al*., 2003a), (Nagahara *et al*., 2005).

After this study, the same group performed various studies that showed the therapeutic effects of phytosphingosine on cancer cells (Park *et al*., 2005), (Park *et al*., 2007), (Moon *et al*., 2007). For example, in their subsequent study, Park et al studied the effect of mitogen-activated protein kinases (MAPKs) when phytosphingosine initiates cell arrest (Park *et al*., 2003b). They found that phytosphingosine deactivates ERK1/2, which is an antiapoptotic pathway and promotes p38 MAPK which activates cytochrome c secretion (Park *et al*., 2003b). In another study performed on lymphoma by the same group, it was detected that phytosphingosine and γ-radiation together trigger apoptosis of the cells resistant to radiation (Park *et al*., 2005).

Next, Kang et al demonstrated that in breast cancer, phytosphingosine can decrease the transformation of epithelial cells to mesenchymal cells which may enhance the aggressiveness of cancer (Kang *et al*., 2017). They also indicated that phytosphingosine inhibits lung metastasis in vivo models (Kang *et al*., 2017).

Although there is no information about the permeability of phytosphingosine through the BBB in both the DrugBank Database and the literature, it is known that Sphingosine, a molecular analog of phytosphingosine, crosses BBB (Wishart, 2006).

According to a recent study that tested the permeability of phytoceramides through the BBB for Alzheimer's, plant-based ceramides were found to move across BBB in vivo and in vitro (Eguchi *et al*., 2020). Overall, considering the permeability of its analogs through the BBB and its potential to trigger apoptosis in cancer (Wishart, 2006), (Eguchi *et al*., 2020), (Nagahara *et al*., 2005), (Park *et al*., 2003a, b), (Park *et al*., 2005), (Kang *et al*., 2017**)**, phytosphingosine should be investigated for MB in further studies.

4.8.3.2. Gene Deletion Analyses in Sphingolipid Metabolism.

Both single and double gene deletion analyses were performed to identify essential genes after the addition of sphingolipid reactions and the glycosphingolipid pathway. KDSR and DEGS2 genes which control both sphinganine and ceramide production reactions were determined in sphingomyelin metabolism as a result of single deletion analysis. In addition to other genes detected in previous analyses, B4GALNT1, B3GALT4, ST8SIA5, ST8SIA1, and ST3GAL5 genes related to glycosphingolipid biosynthesis-ganglio series were identified.

In double gene deletion analyses, the SGPL1 gene which is responsible for reversible phosphoryl-ethanolamine production from sphingosine 1-phosphate was also detected with both KDSR and DEGS2 genes. Sphingosine-1-phosphate is an anti-apoptotic metabolite that intensifies cancer (Ogretmen, 2018). This result shows that the MB model successfully detected the SGPL1 gene whose activation might lead to the production of sphingosine 1-phosphate even if KDSR or DEGS2 genes were inhibited. Since ceramide is the precursor of both sphingomyelin and GM3, inhibition of the genes that control their productions might result in the accumulation of ceramide which triggers apoptosis (Lahiri and Futerman, 2007). Consistently, SAMD8, SGMS1, and SGMS2 genes, sphingomyelin production genes, were identified by our model with ST3GAL5 gene which controls GM3 generation.

Drugs/compounds related to essential genes in GeneCards and DrugBank Databases were determined (Stelzer *et al*., 2016), (Wishart, 2006). However, these compounds were not found appropriate since most of them do not permeate the BBB and some of them induce cancer instead of inhibiting them (Wishart, 2006).

All these genes were detected successfully by our model because they all contribute to the growth of cancer cells. However, some of the metabolites produced by these genes have a pivotal role in controlling apoptotic or anti-apoptotic signals in the cell (Ogretmen, 2018), (Zhuo *et al*., 2018), (Schömel *et al*., 2020). For example, inhibition of the B3GALT4 gene causes a reduction in GD1b which triggers apoptosis in melanoma (Ha *et al*., 2016), (Kanda *et al*., 2001).

ST3GAL5 gene controlling GM3 production was detected by our model as an essential gene. When the activity of GM3 synthase controlled by the ST3GAL5 gene was reduced, also attenuated cell development and dissemination in metastatic samples of breast cancer (Gu *et al*., 2008). In a study realized by Nusinovich et al, GM3 synthase suppression led to a 70% reduction in all gangliosides in the MB cell line (Nusinovich and Ladisch, 2008). However, over time, the ganglioside level returned to its previous amount. Then they deduced that there is another system that compensates for the reduced ganglioside. Conversely, abnormal cell division in breast and collateral cancer cells diminished remarkably when they suppressed GM3 synthase in the same study (Nusinovich and Ladisch, 2008). GM3 was detected abundantly in MB in several studies (Chang *et al*., 1997), (Gottfries *et al*., 1989), (Fredman, 1994). Especially in GR4, one of the MB subtypes, the ST3GAL5 gene was overexpressed relative to the control group and other subtypes (Hooper *et al*., 2014), (Brandon *et al*., 2012). Therefore, an analysis specifically for the MB-GR4 model was performed. Inhibition of GM3 production by simulating drug effect resulted in a 95% decrease in growth of GR4 (See Figure 4.40). However, many studies indicated that GM3 has anticancer properties as mentioned in previous sections (Zhuo *et al*., 2018), (Fujimoto *et al*., 2005), (Seyfried and Mukherjee, 2010), (Krengel and Bousquet, 2014). Furthermore, it is known that GM3 suppresses growth factor receptors (Krengel and Bousquet, 2014).

All in all, silencing GM3 synthase have anticancer effects on MB and some other cancer types, however, GM3 also shows apoptotic properties in various cancer types (Gu *et al*., 2008), (Nusinovich and Ladisch, 2008), (Zhuo *et al*., 2018), (Fujimoto *et al*., 2005), (Seyfried and Mukherjee, 2010), (Krengel and Bousquet, 2014).

B4GALNT1 which is responsible for GM2, GD2, and GT2 productions, is another essential gene detected by our model (Kanehisa *et al*., 2021). Precursors of these gangliosides are GM3, GD3, and GT3, respectively (Schömel *et al*., 2020). GM2 which is known to trigger tumor growth is the most and the second most abundant ganglioside in DAOY and TE-671 MB cell lines, respectively (Schömel *et al*., 2020), (Chang *et al*., 1997), (Ermini *et al*., 2017), (Gottfries *et al*., 1989), (Vrionis *et al*., 1989). Like GM2, GD2 was estimated higher in MB compared to the healthy brain (Longee *et al*., 1991). Another study conducted recently found that only MB has a high level of GD2 among nine other pediatric cancers (Balis *et al*., 2020). Cinatl et al evaluated the impact of L-cycloserine, an inhibitor, on the MB cell line (Cinatl *et al*.,1999). L-cycloserine reduced GM2 and GD2 expressions and led to a 60% decrease in growth in vivo (Cinatl *et al*., 1999). In agreement with the literature, we found a 97% decrease in growth when drug effect was created in the MB-GR4 model by inhibiting both GD2 and GM2 productions.

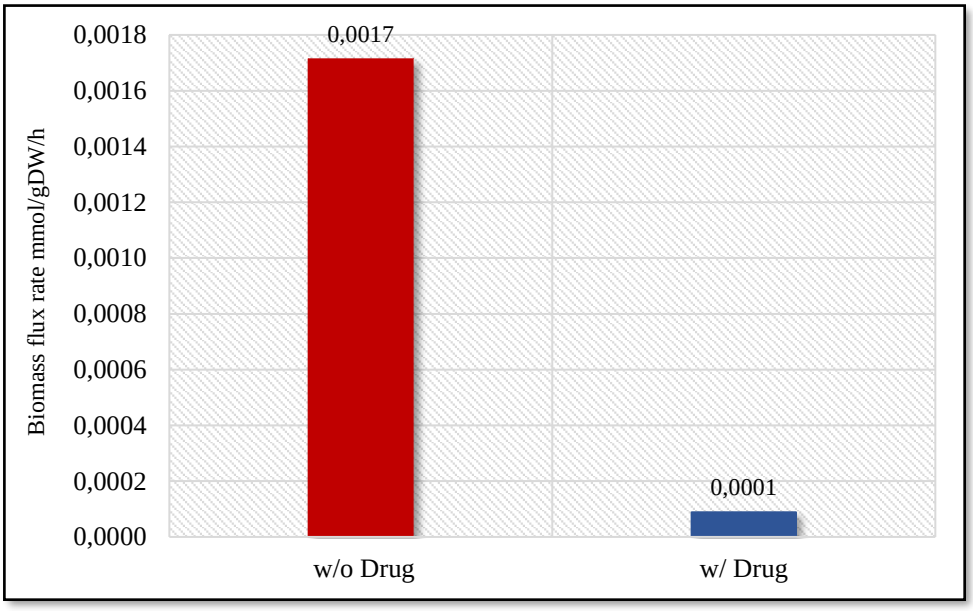

Figure 4.40. The biomass reaction rate without and with drug effect in MB-GR4 model.

B3GALT4 gene detected by MB model produces GM1 from GM2. Inhibition of this gene might not result well as expected since it might cause accumulation of GM2 which is known to trigger tumor growth in MB (Cinatl *et al*., 1999).

Inhibition of ST8SIA5 might cause an increase in GD1a which promotes angiogenesis (Yu *et al*., 2011). While a lower amount of GM3 over GD1a increases cancer growth in ependymoblastoma, a higher ratio decreases cancer growth in astrocytoma (Mukherjee *et al*., 2008). GM3 was claimed to be an angiogenesis inhibitor, whereas GD1a triggers angiogenesis (Yu *et al*., 2011). GD1a is also the third ample ganglioside detected in MB (Chang *et al*., 1997), (Ermini *et al*., 2017).

ST8SIA1 which produces GD3 and GT3 from GM3 was also identified as an essential gene by the MB model. GD3 triggers cell arrest by increasing reactive oxygen species (ROS) generation (Schömel *et al*., 2020). A high level of GD3 in cancer is not lethal, however, GD3 was found to increase abnormal cell division and metastasis (Schömel *et al*., 2020). Gottfries et al did not find any GD3 in MB cell line while high level of GD3 was found in several cancer types (Gottfries *et al*., 1989), (Schömel *et al*., 2020). Furthermore, inhibition of this gene might cause the accumulation of GM3. Although we are not entirely sure about the effects of GM3 on MB due to limited studies, many studies supported that GM3 has anti-cancer properties (Zhuo *et al*., 2018), Fujimoto *et al*., 2005), (Seyfried and Mukherjee, 2010), (Krengel and Bousquet, 2014).

Finally, it would be implausible to reach a definite conclusion because of the limited experimental studies on the inhibition of gangliosides in MB. However, as MB model predicted, targeting B4GALNT1, ST3GAL5, and ST8SIA1 genes can be effective therapeutic approaches for MB based on the previous literature studies and our results.

5. CONCLUSION AND RECOMMENDATIONS

In this study, metabolic alterations specific to medulloblastoma which is the most prevalent pediatric tumor were attempted to capture by using system biology methods. In addition, novel therapeutic approaches on MB were suggested based on the findings of the present work.

In this scope, the growth reactions predefined based on the white matter were modified specifically to the cerebellum in the MB model. The MB model covers 753 metabolic reactions controlled by 601 genes and 44 pathways including taurine synthesis and glycosphingolipid metabolism.

Three GSE data were integrated into the MB model by the GIMME algorithm to obtain MB-specific models and find a correlation between metastasis and the Warburg effect. The flux rates of the reactions found in MB-specific models were estimated by utilizing Flux balance analysis combined with MOMA and the results were compared with the experimental and healthy model findings. Consistent with the Warburg effect, glycolysis activity was significantly higher in MB-specific models relative to those in the healthy model. Conversely, the flux rates in TCA and OXPHOS pathways were observed to be much lower than those in the healthy model. In agreement with the literature, the flux rates of lipid and nucleotide precursor reactions in the TCA cycle and PPP, respectively, were higher than the same flux rates in healthy case. Additionally, the ratio of glutamate to glutamine flux in MB was found to be very similar to experimental results.

Moreover, FBA was used to find from which pathway the MB cells meet their energy demand in the absence of glucose and glutamine. It was observed that MB which normally obtains its energy from glycolysis, was prone to producing ATP in the TCA cycle by using glutamine in the lack of glucose. When MB patient suffered from both glucose and glutamine deficiency, MB metabolism was diverted to OXPHOS, which was the only way for energy generation.

These results support the idea that the use of the ketogenic diet targeting the glucose pathway by depleting the necessary metabolites, might be a potential therapeutic approach. Therefore, the effects of this non-toxic diet should be tested on MB patients as well.

The relation between the Warburg effect and metastasis was investigated in MB using FBA and GSE data containing metastatic and non-metastatic samples. Warburg effect was observed to be increased tremendously as metastasis intensifies. However, although LacR/OCR was slightly enhanced, it did not increase as much as the ATPG/ATPOP indicating that MB uses its energy to promote invasion rather than growth. Indeed, there was no significant change between biomass reactions of MB-M0 and MB-M2 models. Consequently, it is important to apply a different therapeutic strategy for metastatic MB cells.

The Flux sampling approach was performed to acquire all possible flux values that satisfy the given constraints. The results obtained with Flux sampling were compatible with FBA outcomes. Flux sampling results were also employed to compare flux rates statistically in both cases. It was found that more than 70% of glycolysis and OXPHOS reactions in MB were significantly higher and lower, respectively, in comparison to the reactions in the healthy model consistent with the findings of the present study and the literature. Sampling results and gene expression levels were also used to obtain ZF and ZG scores in regulation analysis to detect especially transcriptionally regulated reactions. Almost half of the 80 TRR’s were found in fatty acid synthesis and cholesterol metabolism consistent with other analyses performed in this study.

Oleoyl-CoA production that is the precursor reaction for oleic acid, was downregulated in MB. Oleic acid was also encountered in essentiality analysis because of its relation to the FASN gene and it was identified as a promising antimetabolite owing to its similarity to natural intermediates used in fatty acid synthesis. Considering our findings of oleic acid and its inhibitory and anti-cancer behaviors in other brain tumors the effect of this compound on MB should be investigated in future studies.

Flux coupling analysis (FCA) was also performed in the present study to determine the reactions coupled to growth reaction. As a result, 158 reactions were found to be related to growth reaction. Interfering with these reactions may be a potential therapeutic strategy for MB. Many nucleotide exchange reactions were associated with growth reaction. This result indicates that the model makes accurate predictions about cancer metabolism since there are many cancer drugs targeting nucleotide metabolism. As in many analyzes in this study, reactions related to lipid metabolism came to the fore in this analysis. One of the most notable lipids was cardiolipin. Not only cardiolipin production reactions were found in FCA, but also other reactions related to syntheses of required metabolites including CDP diacylglycerol and glycerol-3-phosphate for the cardiolipin generation were detected. More importantly, cardiolipin and glycerol-3-phosphate production reactions and the CRLS1, PGS1, GPD1, and GPD2 genes controlling them were identified as essential in essentiality analyses. Strikingly, the CRLS1 gene was also determined as one of eight essential genes necessary for lactate and ATP production alongside the growth. Therefore, interventions on genes responsible for cardiolipin production or syntheses reactions of metabolites required for cardiolipin production can be important strategies for MB inhibition. One another reaction coupled to growth was the cholesterol transport reaction suggesting that cholesterol production in astrocyte is crucial for neuron. Almost 90% of the fatty acid synthesis reactions are associated with the growth reaction consistent with experimental findings and all analyses in this work. The transportation reactions of isoleucine, valine, and leucine derivatives to neuron from astrocyte and their conversion back to these essential amino acids in neuron were coupled to growth reaction.

Essentiality analyses were conducted to find essential genes and reactions for the MB model. While 45 genes were detected in single-gene deletion analysis, 312 essential reactions were found in reaction deletion analysis. 42 of them were identified in both analyses and almost 60% of essential genes were related to lipid synthesis. Asparagine production reaction and the ASNS gene-regulating this reaction were also found as essential. This reaction was also detected in FCA. Considering the literature results and the findings in this study, the interference with asparagine metabolism might be a beneficial strategy for MB.

Another critical point in essentiality analysis is that the reactions related to polyamine production and SMS, SMOX, and AMD1 genes controlling these reactions were determined as essential. Consequently, targeting polyamine metabolism might also be a promising approach in MB considering the SHH type of MB promoting polyamine synthesis.

Double gene deletion analysis was also performed to uncover gene combinations whose inhibition might be the potential therapeutic approach. After the genes detected in single deletion analysis were removed, 26 gene combinations remained. ABAT gene, which is responsible for catalyzing GABA to produce glutamate and succinate precursor metabolite, succinate SAL, was found in two combinations with SUCLA2 and SUCLG1 which also synthesize succinate in TCA. The fact that succinate overexpression is promoted in cancer and the determination of genes related to succinate production in this study render succinate-associated genes desirable targets for MB treatment. As a result of the literature survey, it was concluded that the combination of (FDA) approved drugs Acyclovir and Vigabatrin have a huge potential. They separately were shown to be effective in GBM in several studies. However, as far as known, the synergistic effect of these drugs has never been studied in MB. Based on the previous findings and results of this work, the combination of these drugs should be tested on MB.

The essentiality analyses (single deletion) were also performed for lactate and energy production. eight out of 32 common essential genes were selected based on whether their inhibitions cause any dysfunction in the healthy model and affect significantly the MB model. These therapeutically potential genes were determined as HMGCR, MVK, PMVK, MVD, FDFT1, SQLE, CRLS1, and FASN. The first 6 genes regulate the mevalonate pathway which is a therapeutically promising pathway in terms of cancer. Statins known as cholesterol regulators, Farnesol, TAK-475, and anti-fungal agents were found as major inhibitors for the mevalonate pathway. Orlistat and Cerulenin were detected to be associated with the FASN gene and they showed anti-cancer effects on several cancers. Inhibiting mevalonate and fatty acid synthesis using these compounds may be a feasible way for MB treatment.

Next, the potential antimetabolites which might reduce the use of substrates in cells were identified. The number of total metabolite-antimetabolite pairs was found as 544. 32%, 15%, and 10% of substrates whose enzymes could be utilized as drug targets were detected in fatty acid synthesis, sphingolipid metabolism, and cholesterol synthesis, respectively. As a result of this work, Linoleate/ Arachidonate - Oleic acid, Arachidonate/ Linoleate - Icosapent, Linoleate/ Arachidonate - Gamolenic acid, and Mevalonate - Meglutol were determined as potential metabolite-antimetabolite pairs because of their similarity to each other. Inhibitions of the reactions whose substrates are Linoleate, Arachidonate, and Mevalonate resulted in a decrease in the growth reaction of MB by 79% for all. Therefore, utilizing these compounds (Oleic acid, Icosapent Gamolenic acid, and Meglutol) as analogs of the natural substrates might be a beneficial strategy for MB.

Once the sphingomyelin pathway was expanded and glycosphingolipid metabolism was included in the MB model, the essentiality analysis and antimetabolite investigation were repeated. It was detected that phytosphingosine which is very similar to sphinganine and sphingosine might prevent MB survival by creating competitive inhibition. Consequently, phytosphingosine might hinder the conversion of sphingosine to S1P which promotes cell survival. Hence, owing to the permeability of its analogs through the BBB, its potential to induce cell death in cancer, and its similarity to sphingosine, the effects of phytosphingosine should be tested on MB in further studies.

The inhibition of B4GALNT1 and ST3GAL5 genes which were identified as essential might be potential therapeutic approaches for MB. Targeting B4GALNT1, which is responsible for GM2, GD2, and GT2 productions can be an effective therapeutic approach for MB because GM2 is known to induce tumor growth. Since suppressing GM3 synthase have anticancer effects and GM3 was found in MB plentifully, interfering with ST3GAL5 gene regulating GM3 production might also be a promising strategy for MB treatment. Because ST3GAL5 was found to be overexpressed in GR4, GM3 production was inhibited in MB-GR4 resulting in a 95% decrease in growth of GR4. However, because of the scarcity of studies about the effects of gangliosides on MB, it would be unreasonable to draw any firm conclusions. Therefore, further research is required to get information about the influence of gangliosides on MB.

In this work, MB model results were compared with the healthy results obtained from the model reconstructed based on general brain metabolism (Sertbaş *et al*., 2014). For further study, constructing a healthy model specific to the cerebellum and finding constraints particularly for this region of the normal brain will allow more realistic predictions and comparisons of MB and healthy models. Moreover, using Quantitative Structure-Activity Relationship (QSAR) models in further studies will provide more detailed and precise information about the toxicity and permeability of compounds detected in the DrugBank database.

REFERENCES

Adany, I., E. M. Yazlovitskaya, J. S. Haug, P. A. Voziyan and G. Melnykovych, 1994, "Differences in Sensitivity to Farnesol Toxicity Between Neoplastically- and Non-Neoplastically-Derived Cells in Culture", *Cancer Letters*, Vol. 79, No. 2 , pp. 175–179.

Agren, R., S. Bordel, A. Mardinoglu, N. Pornputtapong, I. Nookaew and J. Nielsen, 2012, "Reconstruction of Genome-Scale Active Metabolic Networks for 69 Human Cell Types and 16 Cancer Types Using INIT", *PLoS Computational Biology*, Vol. 8, No. 5, p. 1002518.

Ahn, E. H., C. C. Chang and J. J. Schroeder, 2006, "Evaluation of Sphinganine and Sphingosine as Human Breast Cancer Chemotherapeutic and Chemopreventive Agents", *Experimental Biology and Medicine*, Vol. 231, No. 10, pp. 1664–1672.

Andersen, C., 1997, "In Vivo Estimation of Water Content in Cerebral White Matter of Brain Tumour Patients and Normal Individuals: Towards A Quantitative Brain Oedema Definition", *Acta Neurochirurgica*, Vol. 139, No. 3, pp. 249–256.

Anderson, A. C., 2003, "The Process of Structure-Based Drug Design", *Chemistry Biology*, Vol. 10, No. 9, pp. 787–797.

Andradas, C., J. Byrne, M. Kuchibhotla, M. Ancliffe, A. C. Jones, B. Carline, H. Hii, A. Truong, L. C. D. Storer, T. A. Ritzmann, R. G. Grundy, N. G. Gottardo and R. Endersby, 2021, "Assessment of Cannabidiol and Δ9-Tetrahydrocannabiol in Mouse Models of Medulloblastoma and Ependymoma", *Cancers*, Vol. 13, No. 2, p. 330.

Anna, I., P. Bartosz, P. Lech and A. Halina, 2017, "Novel Strategies of Raman Imaging for Brain Tumor Research", *Oncotarget*, Vol. 8, No. 49, pp. 85290–85310.

Baart, G. J. E. and D. E. Martens, 2012, "Genome-Scale Metabolic Models: Reconstruction and Analysis", *Neisseria Meningitidis*, Vol. 799, pp. 107–126.

Badodi, S., N. Pomella, X. Zhang, G. Rosser, J. Whittingham, M. V. Niklison-Chirou, Y. M. Lim, S. Brandner, G. Morrison, S. M. Pollard, C. D. Bennett, S. C. Clifford, A. Peet, M. A. Basson and S. Marino, 2021, "Inositol Treatment Inhibits Medulloblastoma Through Suppression of Epigenetic-Driven Metabolic Adaptation", *Nature Communications*, Vol. 12, No. 1, p. 2148.

Balis, F. M., C. M. Busch, A. V. Desai, E. Hibbitts, A. Naranjo, R. Bagatell, M. Irwin and E. Fox, 2020, "The Ganglioside GD2 As A Circulating Tumor Biomarker for Neuroblastoma", *Pediatric Blood Cancer*, Vol. 67, No. 1.

Banay-Schwartz, M., M. Palkovits and A. Lajtha, 1993, "Heterogeneous Distribution of Functionally Important Amino Acids in Brain Areas of Adult and Aging Humans", *Neurochemical Research*, Vol. 18, No. 4, pp. 417–423.

Bayat, N., S. Ebrahimi-Barough, A. Norouzi-Javidan, H. Saberi, R. Tajerian, M. M. M. Ardakan, S. Shirian, A. Ai and J. Ai, 2016, "Apoptotic Effect of Atorvastatin in Glioblastoma Spheroids Tumor Cultured in Fibrin Gel", *Biomedicine Pharmacotherapy*, Vol. 84, pp. 1959–1966.

Becker, S. A. and B. O. Palsson, 2008, "Context-Specific Metabolic Networks Are Consistent with Experiments", *PLoS Computational Biology*, Vol. 4, No. 5, p. 1000082.

Benakanakere, I., T. Johnson, R. Sleightholm, V. Villeda, M. Arya, R. Bobba, C. Freter and C. Huang, 2014, "Targeting Cholesterol Synthesis Increases Chemoimmuno-Sensitivity in Chronic Lymphocytic Leukemia Cells", *Experimental Hematology Oncology*, Vol. 3, No. 1, p. 24.

Bennett, C. D., S. E. Kohe, S. K. Gill, N. P. Davies, M. Wilson, L. C. D. Storer, T. Ritzmann, S. M. L. Paine, I. S. Scott, I. Nicklaus-Wollenteit, D. A. Tennant, R. G. Grundy and A. C. Peet, 2018, "Tissue Metabolite Profiles for The Characterisation of Paediatric Cerebellar Tumours", *Scientific Reports*, Vol. 8, No. 1, p. 11992.

Bensaad, K., A. Tsuruta, M. A. Selak, M. N. C. Vidal, K. Nakano, R. Bartrons, E. Gottlieb and K. H. Vousden, 2006, "TIGAR, a P53-Inducible Regulator of Glycolysis and Apoptosis", *Cell*, Vol. 126, No. 1, pp. 107–120.

Bhatia, B., C. R. Potts, C. Guldal, S. Choi, A. Korshunov, S. Pfister, A. M. Kenney and Z. A. Nahlé, 2012, "Hedgehog-Mediated Regulation of PPARγ Controls Metabolic Patterns in Neural Precursors and Shh-Driven Medulloblastoma", *Acta Neuropathologica*, Vol. 123, No. 4, pp. 587–600.

Blunsom, N. J. and S. Cockcroft, 2020, "CDP-Diacylglycerol Synthases (CDS): Gateway to Phosphatidylinositol and Cardiolipin Synthesis", *Frontiers in Cell and Developmental Biology*, Vol. 8, p. 63.

Bordbar, A., J. M. Monk, Z. A. King and B. O. Palsson, 2014, "Constraint-Based Models Predict Metabolic and Associated Cellular Functions", *Nature Reviews Genetics*, Vol. 15, No. 2, pp. 107–120.

Bordel, S., R. Agren and J. Nielsen, 2010, "Sampling the Solution Space in Genome-Scale Metabolic Networks Reveals Transcriptional Regulation in Key Enzymes", *PLoS Computational Biology*, Vol. 6, No. 7, p. 1000859.

Borgelt, L. M., K. L. Franson, A. M. Nussbaum and G. S. Wang, 2013, "The Pharmacologic and Clinical Effects of Medical Cannabis. *Pharmacotherapy: The Journal of Human Pharmacology and Drug Therapy*", Vol. 33, No. 2, pp. 195–209.

Brady, S. T., G. J. Siegel, R. W. Albers and D. L. Price, 2012, In *Basic Neurochemistry: Principles of Molecular, Cellular and Medical Neurobiology*.

Brody, T., 1999, *Nutritional biochemistry*. Academic press.

Bronk, R., 1999, *Human Metabolism Functional Diversity and Integration*. *England*.

Brunk, E., S. Sahoo, D. C. Zielinski, A. Altunkaya, A. Dräger, N. Mih, F. Gatto, A. Nilsson, G. A. Preciat Gonzalez, M. K. Aurich, A. Prlić, A. Sastry, A. D. Danielsdottir, A. Heinken, A. Noronha, P. W. Rose, S. K. Burley, R. M. T. Fleming, J. Nielsen and B. O. Palsson, 2018, "Recon3D Enables a Three-Dimensional View of Gene Variation in Human Metabolism", *Nature Biotechnology*, Vol. 36, No. 3, pp. 272–281.

Buford, T., 2008, "Macronutrient Intake for Physical Activity", *Nutritional Supplements in Sports and Exercise*, pp. 95–119.

Burgard, A. P. and C. D. Maranas, 2003, "Optimization-based Framework for Inferring and Testing Hypothesized Metabolic Objective Functions", *Biotechnology and Bioengineering*, Vol. 82, No. 6, pp. 670–677.

Bush, E. C. and J. M. Allman, 2003, "The Scaling of White Matter to Gray Matter in Cerebellum and Neocortex", *Brain, Behavior and Evolution*, Vol. 61, No. 1, pp. 1–5.

Çakır, T., S. Alsan, H. Saybaşılı, A. Akın and K. Ö. Ülgen, 2007, "Reconstruction and Flux Analysis of Coupling Between Metabolic Pathways of Astrocytes and Neurons: Application to Cerebral Hypoxia", *Theoretical Biology and Medical Modelling*, Vol. 4, No. 1, p. 48.

Casero, R. A., T. Murray Stewart and A. E. Pegg, 2018, "Polyamine Metabolism and Cancer: Treatments, Challenges and Opportunities", *Nature Reviews Cancer*, Vol. 18, No. 11, pp. 681–695.

Castillo, M., J. K. Smith and L. Kwock, 2000, "Correlation of Myo-inositol Levels and Grading of Cerebral Astrocytomas", *American Journal of Neuroradiology*, Vol. 21, pp. 1645–1649.

Ceci, C., P. Lacal, L. Tentori, M. De Martino, R. Miano and G. Graziani, 2018, "Experimental Evidence of the Antitumor, Antimetastatic and Antiangiogenic Activity of Ellagic Acid", *Nutrients*, Vol. 10, No. 11, p. 1756.

Chakraborty, A., J. Han, C. Faltas and N. Coleman, 2018, "Brain Tumor Treatment: 2017 Update", *Cancer and Clinical Oncology*, Vol. 7, No. 1, p. 30.

Chandrasekaran, S., N and D. Price, 2010, "Probabilistic Integrative Modeling of Genome-Scale Metabolic and Regulatory Networks in Escherichia Coli And Mycobacterium Tuberculosis", *Proceedings of the National Academy of Sciences of the United States of America*, Vol. 107, No. 41, pp. 17845–17850.

Chang, C. H., E. M. Housepian and C. Herbert, 1969, "An Operative Staging System and a Megavoltage Radiotherapeutic Technic for Cerebellar Medulloblastomas", *Radiology*, Vol. 93, No. 6, pp. 1351–1359.

Chang, F., R. Li, K. Noon, D. Gage and S. Ladisch, 1997, "Human Medulloblastoma Gangliosides", *Glycobiology*, Vol. 7, No. 4, pp. 523–530.

Chavko, M., E. M. Nemoto and J. A. Melick, 1993, "Regional Lipid Composition in the Rat Brain", *Molecular and Chemical Neuropathology*, Vol. 18, No. 1–2, pp. 123–131.

Chen, J. C., M. L. Wu, K. C. Huang and W. W. Lin, 2008, "HMG-CoA Reductase Inhibitors Activate the Unfolded Protein Response and Induce Cytoprotective GRP78 Expression", *Cardiovascular Research*, Vol. 80, No. 1, pp. 138–150.

Chen, Y., B. O. McConnell, V. Gayatri Dhara, H. Mukesh Naik, C. T. Li, M. R. Antoniewicz and M. J. Betenbaugh, 2019, "An Unconventional Uptake Rate Objective Function Approach Enhances Applicability of Genome-Scale Models for Mammalian Cells", *Npj Systems Biology and Applications*, Vol. 5, No. 1, p.25.

Chien, M. H., T. S. Lee, C. Kao, S. F. Yang and W. S. Lee, 2012, "Terbinafine Inhibits Oral Squamous Cell Carcinoma Growth Through Anti-Cancer Cell Proliferation and Anti-Angiogenesis: TB in Treatment of Oral Cancer", *Molecular Carcinogenesis*, Vol. 51, No. 5, pp. 389–399.

Cinatl, J., R. Kotchetkov, P. Pouckova, J. U. Vogel, H. Rabenau, M. Michaelis and B. Kornhuber, 1999, "Cytotoxicity of L-cycloserine against Human Neuroblastoma and Medulloblastoma Cells Is Associated with The Suppression of Ganglioside Expression", *Anticancer Research*, Vol. 19, No. 6.

Colijn, C., A. Brandes, J. Zucker, D. S. Lun, B. Weiner, M. R. Farhat, T. Y. Cheng, D. B. Moody, M. Murray and J. E. Galagan, 2009, "Interpreting Expression Data with Metabolic Flux Models: Predicting Mycobacterium Tuberculosis Mycolic Acid Production", *PLoS Computational Biology*, Vol. 5, No. 8, p. 1000489.

Collins, S. B., E. Reznik and D. Segrè, 2012, "Temporal Expression-Based Analysis of Metabolism", *PLoS Computational Biology*, Vol. 8, No. 11, p. 1002781.

Coni, S., L. Di Magno, S. M. Serrao, Y. Kanamori, E. Agostinelli and G. Canettieri, 2019, "Polyamine Metabolism as a Therapeutic Target in Hedgehog-Driven Basal Cell Carcinoma and Medulloblastoma", *Cells*, Vol. 8, No. 2, p. 150.

Cormerais, Y., M. Pagnuzzi-Boncompagni, S. Schrötter, S. Giuliano, E. Tambutté, H. Endou, M. F. Wempe, G. Pagès, J. Pouysségur and V. Picco, 2019, "Inhibition of the Amino-Acid Transporter LAT1 Demonstrates Anti-Neoplastic Activity in Medulloblastoma", *Journal of Cellular and Molecular Medicine*, Vol. 23, No. 4, pp. 2711–2718.

D'Amico, D., L. Antonucci, L. Di Magno, S. Coni, G. Sdruscia, A. Macone, E. Miele, P. Infante, L. Di Marcotullio, E. De Smaele, E. Ferretti, L. Ciapponi, F. Giangaspero, J. R. Yates, E. Agostinelli, B. Cardinali, I. Screpanti, A. Gulino and G. Canettieri, 2015, "Non-canonical Hedgehog/AMPK-Mediated Control of Polyamine Metabolism Supports Neuronal and Medulloblastoma Cell Growth", *Developmental Cell*, Vol. 35, No. 1, pp. 21–35.

Daneman, R. and A. Prat, 2015, "The Blood–Brain Barrier", *Cold Spring Harbor Perspectives in Biology*, Vol. 7, No. 1, p. 20412.

D'Angelo, G., S. Capasso, L. Sticco and D. Russo, 2013, "Glycosphingolipids: Synthesis and Functions", *FEBS Journal*, Vol. 280, No. 24, pp. 6338–6353.

Das, B., R. Antoon, R. Tsuchida, S. Lotfi, O. Morozova, W. Farhat, D. Malkin, G. Koren, H. Yeger and S. Baruchel, 2008, "Squalene Selectively Protects Mouse Bone Marrow Progenitors Against Cisplatin and Carboplatin-Induced Cytotoxicity In Vivo without Protecting Tumor Growth", *Neoplasia*, Vol. 10, No. 10, p. 1105.

Das, B., H. Yeger, H. Baruchel, M. H. Freedman, G. Koren and S. Baruchel, 2003, "In Vitro Cytoprotective Activity of Squalene on A Bone Marrow Versus Neuroblastoma Model of Cisplatin-Induced Toxicity", *European Journal of Cancer*, Vol. 39, No. 17, pp. 2556–2565.

Davies, N. P., M. Wilson, L. M. Harris, K. Natarajan, S. Lateef, L. MacPherson, S. Sgouros, R. G. Grundy, T. N. Arvanitis and A. C. Peet, 2008, "Identification and Characterisation of Childhood Cerebellar Tumours by *in Vivo* Proton MRS", *NMR in Biomedicine*, Vol. 21, No. 8, pp. 908–918.

Desai, K. N., H. Wei and C. A. Lamartiniere, 1996, "The Preventive and Therapeutic Potential of the Squalene-Containing Compound, Roidex, on Tumor Promotion and Regression", *Cancer Letters*, Vol. 101, No. 1, pp. 93–96.

Dimitroulakos, J., S. Thai, G. H. Wasfy, D. W. Hedley, M. D. Minden and L. Z. Penn, 2000, "Lovastatin Induces a Pronounced Differentiation Response in Acute Myeloid Leukemias", *Leukemia Lymphoma*, Vol. 40, No. 1–2, pp. 167–178.

Dranoff, G., G. B. Elion, H. S. Friedman, G. L. Campbell and D. D. Bigner, 1985, "Influence of Glutamina on the Growth of Human Glioma and Medulloblastoma in Culture", *Cancer Research*, Vol. 45, pp. 4077-4081.

Duarte, N. C., S. A. Becker, N. Jamshidi, I. Thiele, M. L. Mo, T. D. Vo, R. Srivas and B. O. Palsson, 2007, "Global Reconstruction of the Human Metabolic Network Based on

Genomic and Bibliomic Data", *Proceedings of the National Academy of Sciences*, Vol. 104, No. 6, pp. 1777–1782.

Dunkl, V., C. Cleff, G. Stoffels, N. Judov, S. Sarikaya-Seiwert, I. Law, L. Bøgeskov, K. Nysom, S. B. Andersen, H. J. Steiger, G. R. Fink, G. Reifenberger, N. J. Shah, H. H. Coenen, K. J. Langen and N. Galldiks, 2015. "The Usefulness of Dynamic *O* -(2- ^{18} F-Fluoroethyl)-l-Tyrosine PET in the Clinical Evaluation of Brain Tumors in Children and Adolescents", *Journal of Nuclear Medicine*, Vol. 56, No. 1, pp. 88–92.

Edgar, R., 2002, "Gene Expression Omnibus: NCBI Gene Expression and Hybridization Array Data Repository", *Nucleic Acids Research*, Vol. 30, No. 1, pp. 207–210.

Eguchi, K., D. Mikami, H. Sun, T. Tsumita, K. Takahashi, K. Mukai, K. Yuyama and Y. Igarashi, 2020, "Blood-brain Barrier Permeability Analysis of Plant Ceramides", *PLoS ONE*, Vol. 15, No. 11, p. 241640.

Ellis, C. E., E. J. Murphy, D. C. Mitchell, M. Y. Golovko, F. Scaglia, G. C. Barcelo-Coblijn and R. L. Nussbaum, 2005, "Mitochondrial Lipid Abnormality and Electron Transport Chain Impairment in Mice Lacking Synuclein", *Mol. Cell. Biol.*, Vol. 25, No. 12.

Ermini, L., E. Morganti, A. Post, B. Yeganeh, I. Caniggia, M. Leadley, C. C. Faria, J. T. Rutka and M. Post, 2017, "Imaging Mass Spectrometry Identifies Prognostic Ganglioside Species in Rodent Intracranial Transplants of Glioma and Medulloblastoma", *PLoS One*, Vol. 12, No. 5, p. 176254.

Feltrin, S., F. Ravera, N. Traversone, L. Ferrando, D. Bedognetti, A. Ballestrero and G. Zoppoli, 2020, "Sterol Synthesis Pathway Inhibition as A Target for Cancer Treatment", *Cancer Letters*, Vol. 493, pp. 19–30.

Fleischmann, R. D., M. D.Adams, O. White, R. A. Clayton, E. F. Kirkness, A. R. Kerlavage, C. J. Bult, J. F. Tomb, B. A. Dougherty, J. M. Merrick, K. McKenney, G. Sutton, W. FitzHugh, C. Fields, J. D. Gocyne, J. Scott, R. Shirley, L. I. Liu, A. Glodek and T. R.

Utterback, 1995, "Whole-Genome Random Sequencing and Assembly of Haemophilus Influenzae Rd", *Science, New Series,* Vol. 269, No. 5223, pp. 507-512.

Folger, O., L. Jerby, C. Frezza, E. Gottlieb, E. Ruppin and T. Shlomi, 2011, "Predicting Selective Drug Targets in Cancer through Metabolic Networks", *Molecular Systems Biology*, Vol. 7, No. 1, p. 501.

Fredman, P., 1994, "Gangliosides Associated with Primary Brain Tumors and Their Expression in Cell Lines Established from These Tumors", *In Progress in Brain Research,* Vol. 101, pp. 225–240.

Fujimoto, Y., S. Izumoto, T. Suzuki, M. Kinoshita, N. Kagawa, K. Wada, N. Hashimoto, M. Maruno, Y. Nakatsuji and T. Yoshimine, 2005, "Ganglioside GM3 Inhibits Proliferation and Invasion of Glioma", *Journal of Neuro-Oncology*, Vol. 71, No. 2, pp. 99–106.

Gershon, T. R., A. J. Crowther, A. Tikunov, I. Garcia, R. Annis, H. Yuan, C. R. Miller, J. Macdonald, J. Olson and M. Deshmukh, 2013, "Hexokinase-2-Mediated Aerobic Glycolysis is Integral to Cerebellar Neurogenesis and Pathogenesis of Medulloblastoma", *Cancer Metabolism*, Vol. 1, No. 1, p. 2.

Girardi, F., C. Allemani and M. P. Coleman, 2019, "Worldwide Trends in Survival from Common Childhood Brain Tumors: A Systematic Review", *Journal of Global Oncology*, Vol. 5, pp. 1–25.

Girgert, R., Y. Vogt, D. Becke, G. Bruchelt and P. Schweizer, 1999, "Growth Inhibition of Neuroblastoma Cells by Lovastatin and l-Ascorbic Acid is Based on Different Mechanisms", *Cancer Letters*, Vol. 137, No. 2, pp. 167–172.

Gunes, F., 2013, "Medical Use of Squalene as a Natural Antioxidant", *Journal of Marmara University Institute of Health Sciences,* Vol. 1.

Gottfries, J., J. E. Mansson, P. Fredman, C. J. Wikstrand, H. S. Friedman, D. D. Bigner and L. Svennerholm, 1989, "Ganglioside Mapping of a Human Medulloblastoma Xenograft", *Acta Neuropathologica*, Vol. 77, No. 3, pp. 283–288.

Gross, M. E., D. B. Agus, T. B. Dorff, J. K. Pinski, D. I. Quinn, O. Castellanos, P. Gilmore and J. C. Shih, 2021, "Phase 2 Trial of Monoamine Oxidase Inhibitor Phenelzine in Biochemical Recurrent Prostate Cancer", *Prostate Cancer and Prostatic Diseases*, Vol. 24, No. 1.

Grube, S., P. Dünisch, D. Freitag, M. Klausnitzer, Y. Sakr, J. Walter, R. Kalff and C. Ewald, 2014, "Overexpression of Fatty Acid Synthase in Human Gliomas Correlates with the WHO Tumor Grade and Inhibition with Orlistat Reduces Cell Viability and Triggers Apoptosis", *Journal of Neuro-Oncology*, Vol. 118, No. 2, pp. 277–287.

Gu, Y., J. Zhang, W. Mi, J. Yang, F. Han, F. Lu and X. Yu, 2008, "Silencing of GM3 Synthase Suppresses Lung Metastasis of Murine Breast Cancer Cells", *Breast Cancer Research*, Vol. 10, No. 1.

Gururangan, S., E. Hwang, J. E. Herndon, H. Fuchs, T. George and R. E. Coleman, 2004, "[18F] Fluorodeoxyglucose-Positron Emission Tomography in Patients with Medulloblastoma", *Neurosurgery*, Vol. 55, No. 6, pp. 1280–1289.

Ha, S. H., J. M. Lee, K. M. Kwon, C. H. Kwak, F. Abekura, J. Y. Park, S. H. Cho, K. Lee, Y. C. Chang, Y. C. Lee, H. J. Choi, T. W. Chung, K. T. Ha, H. W. Chang and C. H. Kim, 2016, "Exogenous and Endogeneous Disialosyl Ganglioside GD1b Induces Apoptosis of MCF-7 Human Breast Cancer Cells", *International Journal of Molecular Sciences*, Vol. 17, No. 5, p. 652.

Habib, N. A., C. B. Wood, K. Apostolov, W. Barker, M. J. Hershman, D. Heinemann, B. Fermor, R. C. N. Williamson and M. J. Embleton, 1987, "Stearic Acid and Carcinogenesis", *Br J Cancer*, Vol. 56, No. 4, pp. 455-8.

Haggart, C. R., J. A. Bartell, J. J. Saucerman and J. A. Papin, 2011, "Whole-Genome Metabolic Network Reconstruction and Constraint-Based Modeling", In *Methods in Enzymology*, Vol. 500, pp. 411–433.

Hamamura, K. and K. Furukawa, 2017, "Glycosylation Is Involved in Malignant Properties of Cancer Cells", *Cancer Translational Medicine*, Vol. 3, No. 6, p. 209.

Hanna, V. S. and E. A. A. Hafez, 2018, "Synopsis of Arachidonic Acid Metabolism: A Review", *Journal of Advanced Research*, Vol. 11, pp. 23–32.

Hatzivassiliou, G., F. Zhao, D. E. Bauer, C. Andreadis, A. N. Shaw, D. Dhanak, S. R. Hingorani, D. A. Tuveson and C. B. Thompson, 2005, "ATP Citrate Lyase Inhibition Can Suppress Tumor Cell Growth", *Cancer Cell*, Vol. 8, No. 4, pp. 311–321.

Hawkins, C. C., T. Ali, S. Ramanadham and A. B. Hjelmeland, 2020, "Sphingolipid Metabolism in Glioblastoma and Metastatic Brain Tumors: A Review of Sphingomyelinases and Sphingosine-1-Phosphate", *Biomolecules*, Vol. 10, No. 10, p. 1357.

Hekmatyar, S. K., M. Wilson, N. Jerome, R. M. Salek, J. L. Griffin, A. Peet and R. A. Kauppinen, 2010, "1H Nuclear Magnetic Resonance Spectroscopy Characterisation of Metabolic Phenotypes in the Medulloblastoma of the SMO Transgenic Mice", *British Journal of Cancer*, Vol. 103, No. 8, pp. 1297–1304.

Herrmann, H. A., B. C. Dyson, L. Vass, G. N. Johnson and J. M. Schwartz, 2019, "Flux Sampling is a Powerful Tool to Study Metabolism under Changing Environmental Conditions", *Npj Systems Biology and Applications*, Vol. 5, No. 1, p. 32.

Hindler, K., C. S. Cleeland, E. Rivera and C. D. Collard, 2006, "The Role of Statins in Cancer Therapy", *The Oncologist*, Vol. 11, No. 3, pp. 306–315.

Holthoff, V. A., K. Herholz, F. Berthold, B. Widemann, R. Schröder, I. Neubauer and W. D. Heiss, 1993, "In Vivo Metabolism of Childhood Posterior Fossa Tumors and

Primitive Neuroectodermal Tumors before and after Treatment", *Cancer*, Vol. 72, No. 4, pp. 1394–1403.

Hooper, C. M., S. M. Hawes, U. R. Kees, N. G. Gottardo and P. B. Dallas, 2014, "Gene Expression Analyses of the Spatio-Temporal Relationships of Human Medulloblastoma Subgroups during Early Human Neurogenesis", *PLoS ONE*, Vol. 9, No. 11, p. 112909.

Hovestadt, V., K. S. Smith, L. Bihannic, M. G. Filbin, M. L. Shaw, A. Baumgartner, J. C. DeWitt, A. Groves, L. Mayr, H. R. Weisman, A. R. Richman, M. E. Shore, L. Goumnerova, C. Rosencrance, R. A. Carter, T. N. Phoenix, J. L. Hadley, Y. Tong, J. Houston and P. A. Northcott, 2019, "Resolving Medulloblastoma Cellular Architecture by Single-Cell Genomics", *Nature*, Vol. 572, No. 7767, pp. 74–79.

Hrelia, S., A. Bordoni, P. Biagi, C. A. Rossi, L. Bernardi, D. F. Horrobin and A. Pession, 1996, "G-Linolenic Acid Supplementation Can Affect Cancer Cell Proliferation via Modification of Fatty Acid Composition", *Biochemical and Biophysical Research Communications*, Vol. 225, No. 2, p. 7.

Huang, H. J., H. W. Yu, C. Y. Chen, C. H. Hsu, H. Y. Chen, K. J. Lee, F. J. Tsai and C. Y. C. Chen, 2010, "Current Developments of Computer-Aided Drug Design", *Journal of the Taiwan Institute of Chemical Engineers*, Vol. 41, No. 6, pp. 623–635.

Hung, T. Y., H. Y. I. Huang, S. N. Wu and C. W. Huang, 2021, "Depressive Effectiveness of Vigabatrin (γ-vinyl-GABA), An Antiepileptic Drug, in Intermediate-Conductance Calcium-Activated Potassium Channels in Human Glioma Cells", *BMC Pharmacology and Toxicology*, Vol. 22, No. 1, p. 6.

Ichikawa, S. and Y. Hirabayashi, 1998, "Glucosylceramide Synthase and Glycosphingolipid Synthesis", *Trends in Cell Biology*, Vol. 8, No. 5, pp. 198–202.

Ideker, T., T. Galitski and L. Hood, 2001, "A New Approach to Decoding Life: Systems Biology", *Annual Review of Genomics and Human Genetics*, Vol. *2*, No. 1, pp. 343–372.

Jensen, P. A. and J. A. Papin, 2011, "Functional Integration of a Metabolic Network Model and Expression Data without Arbitrary Thresholding", *Bioinformatics*, Vol. 27, No. 4, pp. 541–547.

Jiang, H., C. Hu and M. Chen, 2021, "The Advantages of Connectivity Map Applied in Traditional Chinese Medicine", *Frontiers in Pharmacology*, Vol. 12, No. 474267.

Jiang, P., R. Mukthavaram, Y. Chao, N. Nomura, I. S. Bharati, V. Fogal, S. Pastorino, D. Teng, X. Cong, S. C. Pingle, S. Kapoor, K. Shetty, A. Aggrawal, S. Vali, T. Abbasi, S. Chien and S. Kesari, 2014, "In Vitro and in Vivo Anticancer Effects of Mevalonate Pathway Modulation on Human Cancer Cells", *British Journal of Cancer*, Vol. 111, No. 8, pp. 1562–1571.

Jiang, S. and W. Yan, 2017, "Succinate in the Cancer–Immune Cycle", *Cancer Letters*, Vol. 390, pp. 45–47.

Joo, J. H. and A. M. Jetten, 2010, "Molecular Mechanisms Involved in Farnesol-Induced Apoptosis", *Cancer Letters*, Vol. 287, No. 2, pp. 123–135.

Kahn, S. A., X. Wang, R. T. Nitta, S. Gholamin, J. Theruvath, G. Hutter, T. D. Azad, L. Wadi, S. Bolin, V. Ramaswamy, R. Esparza, K. W. Liu, M. Edwards, F. J. Swartling, D. Sahoo, G. Li, R. J. Wechsler-Reya, J. Reimand, Y. J. Cho and S. H. Cheshier, 2018, "Notch1 Regulates the Initiation of Metastasis and Self-Renewal of Group 3 Medulloblastoma", *Nature Communications*, Vol. 9, No. 1, p. 4121.

Kanda, N., K. Nakai and S. Watanabe, 2001, "Gangliosides GD1b, GT1b, and GQ1b Suppress the Growth of Human Melanoma by Inhibiting Interleukin-8 Production: The Inhibition of Adenylate Cyclase11 the Nomenclature for Gangliosides Used in This Paper Follows the System of Svennerholm 1963", *Journal of Investigative Dermatology*, Vol. 117, No. 2, pp. 284–293.

Kanehisa, M., M. Furumichi, Y. Sato, M. Ishiguro-Watanabe and M. Tanabe, 2021, "KEGG: Integrating Viruses and Cellular Organisms", *Nucleic Acids Research*, Vol. 49, No. D1, pp. 545–551.

Kang, H. M., H. S. Son, Y. H. Cui, B. Youn, B. Son, N. K. Kaushik, N. Uddin, J. S. Lee, J. Y. Song, N. Kaushik and S. J. Lee, 2017, "Phytosphingosine Exhibits An Anti-Epithelial–Mesenchymal Transition Function by the Inhibition of EGFR Signaling in Human Breast Cancer Cells", *Oncotarget*, Vol. 8, No. 44, pp. 77794–77808.

Kang, J. S., 2020, "Dietary Restriction of Amino Acids for Cancer Therapy", *Nutrition Metabolism*, Vol. 17, No. 1, p. 20.

Kauffman, K. J., P. Prakash and J. S. Edwards, 2003, "Advances in Flux Balance Analysis", *Current Opinion in Biotechnology*, Vol. 14, No. 5, pp. 491–496.

Kenny, F. S., S. E. Pinder, I. O. Ellis, J. M. W. Gee, R. I. Nicholson, R. P. Bryce and J. F. R. Robertson, 2000, "Gamma Linolenic Acid with Tamoxifen as Primary Therapy in Breast Cancer", *International Journal of Cancer*, Vol. 85, No. 5, pp. 643–648.

Kim, H. U., S. B. Sohn and S. Y. Lee, 2012, "Metabolic Network Modeling and Simulation for Drug Targeting and Discovery", *Biotechnology Journal*, Vol. 7, No. 3, pp. 330–342.

Kim, S., J. Chen, T. Cheng, A. Gindulyte, J. He, S. He, Q. Li, B. A. Shoemaker, P. A. Thiessen, B. Yu, L. Zaslavsky, J. Zhang and E. E. Bolton, 2021, "PubChem in 2021: New Data Content and Improved Web Interfaces", *Nucleic Acids Research*, Vol. 49, No. D1, pp. 1388–1395.

Kim, W. S., M. M. Kim, H. J. Choi, S. S. Yoon, M. H. Lee, K. Park, C. H. Park and W. K. Kang, 2001, "Phase II Study of High-Dose Lovastatin in Patients with Advanced Gastric Adenocarcinoma", *Invest New Drugs*, Vol. 19, No. 1, pp. 81-83.

Kohe, S. E., C. D. Bennett, S. K. Gill, M. Wilson, C. McConville and A. C. Peet, 2018, "Metabolic Profiling of the Three Neural Derived Embryonal Pediatric Tumors Retinoblastoma, Neuroblastoma and Medulloblastoma, Identifies Distinct Metabolic Profiles", *Oncotarget*, Vol. 9, No. 13, pp. 11336–11351.

Kominsky, S. L., P. S. Subramaniam, H. M. Johnson and B. A. Torres, 2000, "Inhibitory Effects of IFN-γ and Acyclovir on the Glioblastoma Cell Cycle", *Journal of Interferon Cytokine Research*, Vol. 20, No. 5, pp. 463–469.

Kool, M., J. Koster, J. Bunt, N. E. Hasselt, A. Lakeman, P. van Sluis, D. Troost, N. S. Meeteren, H. N. Caron, J. Cloos, A. Mršić, B. Ylstra, W. Grajkowska, W. Hartmann, T. Pietsch, D. Ellison, S. C. Clifford and R. Versteeg, 2008, "Integrated Genomics Identifies Five Medulloblastoma Subtypes with Distinct Genetic Profiles, Pathway Signatures and Clinicopathological Features", *Plos One*, Vol. 3, No. 8, p. 3088.

Krengel, U. and P. A. Bousquet, 2014, "Molecular Recognition of Gangliosides and Their Potential for Cancer Immunotherapies", *Frontiers in Immunology*, Vol. 5.

Kridel, S. J., F. Axelrod, N. Rozenkrantz and J. W. Smith, 2004, "Orlistat Is a Novel Inhibitor of Fatty Acid Synthase with Antitumor Activity", *Cancer Research*, Vol. 64, No. 6, pp. 2070–2075.

Kuhajda, F. P., K. Jenner, F. D. Wood, R. A. Hennigar, B. Lisa Jacobs, J. D. Dick and G. R. Pasternack, 1994, "Fatty Acid Synthesis: A Potential Selective Target for Antineoplastic Therapy", *Proceedings of the National Academy of Sciences of the United States of America*, Vol. 91, No. 14, pp. 6379–6383.

Kumar, B., C. Andreatta, W. T. Koustas, W. C. Cole, J. Edwards-Prasad and K. N. Prasad, 2002, "Mevastatin Induces Degeneration and Decreases Viability of cAMP-Induced Differentiated Neuroblastoma Cells in Culture by Inhibiting Proteasome Activity, and Mevalonic Acid Lactone Prevents These Effects", *Journal of Neuroscience Research*, Vol. 68, No. 5, pp. 627–635.

Kumar, V., V. Kumar, T. McGuire, D. W. Coulter, J. G. Sharp and R. I. Mahato, 2017, "Challenges and Recent Advances in Medulloblastoma Therapy", *Trends in Pharmacological Sciences*, Vol. 38, No. 12, pp. 1061–1084.

Jimsheleishvili, S. and M. Dididze, 2019, "Neuroanatomy, Cerebellum", In *StatPearls*.

Lahiri, S. and A. H. Futerman, 2007, "The Metabolism and Function of Sphingolipids and Glycosphingolipids. *Cellular and Molecular Life Sciences*, Vol. 64, No. 17, pp. 2270–2284.

Larner, J., J. Jane and E. Laws, 1998, "A Phase I-II Trial of Lovastatin for Anaplastic Astrocytoma and Glioblastoma Multiforme. *Am J Clin Oncol*, Vol. 21, pp. 579-583.

Larsson, I., M. Uhlén, C. Zhang and A. Mardinoglu, 2020, "Genome-Scale Metabolic Modeling of Glioblastoma Reveals Promising Targets for Drug Development. *Frontiers in Genetics*, Vol. 11, p. 381.

Le, A., A. N. Lane, M. Hamaker, S. Bose, A. Gouw, J. Barbi, T. Tsukamoto, C. J. Rojas, B. S. Slusher, H. Zhang, L. J. Zimmerman, D. C. Liebler, R. J. C. Slebos, P. K. Lorkiewicz, R. M. Higashi, T. W. M. Fan and C. V. Dang, 2012, "Glucose-Independent Glutamine Metabolism via TCA Cycling for Proliferation and Survival in B Cells. *Cell Metabolism*, Vol. 15, No. 1, pp. 110–121.

Le, N. Q. K. and Y. Y. Ou, 2016, "Prediction of FAD Binding Sites in Electron Transport Proteins According to Efficient Radial Basis Function Networks and Significant Amino Acid Pairs. *BMC Bioinformatics*, Vol. 17, No. 1, p. 298.

Lewis, N. E., G. Schramm, A. Bordbar, J. Schellenberger, M. P. Andersen, J. K. Cheng, N. Patel, A. Yee, R. A. Lewis, R. Eils, R. König and B. Ø. Palsson, 2010, "Large-Scale in Silico Modeling of Metabolic Interactions Between Cell Types in The Human Brain. *Nature Biotechnology*, Vol. 28, No. 12, pp. 1279–1285.

Li, S., T. Zhou, C. Li, Z. Dai, D. Che, Y. Yao, L. Li, J. Ma, X. Yang and G. Gao, 2014, "High Metastaticgastric and Breast Cancer Cells Consume Oleic Acid in an AMPK Dependent Manner. *PLoS ONE*, Vol. 9, No. 5, p. 97330.

Liang, W., S. Ouyang, N. Shaw, A. Joachimiak, R. Zhang and Z. Liu, 2011, "Conversion of D -Ribulose 5-Phosphate to D -Xylulose 5-Phosphate: New Insights from Structural and Biochemical Studies on Human RPE. *The FASEB Journal*, Vol. 25, No. 2, pp. 497–504.

Lieu, E. L., T. Nguyen, S. Rhyne and J. Kim, 2020, "Amino Acids in Cancer. *Experimental Molecular Medicine*, Vol. 52, No. 1, pp. 15–30.

Liou, G. Y. and P. Storz, 2010, "Reactive Oxygen Species in Cancer. *Free Radical Research*, Vol. 44, No. 5, pp. 479–496.

Longee, D. C., C. J. Wikstrand, J. E. Mansson, X. He, G. N. Fuller, S. H. Bigner, P. Fredman, L. Svennerholm and D. D. Bigner, 1991, "Disialoganglioside GD2 in Human Neuroectodermal Tumor Cell Lines and Gliomas. *Acta Neuropathologica*, Vol. 82, No. 1, pp. 45–54.

López-Valero, I., S. Torres, M. Salazar-Roa, E. García-Taboada, S. Hernández-Tiedra, M. Guzmán, J. M. Sepúlveda, G. Velasco and M. Lorente, 2018, "Optimization of a Preclinical Therapy of Cannabinoids in Combination with Temozolomide against Glioma. *Biochemical Pharmacology*, Vol. 157, pp. 275–284.

Lowe, R., N. Shirley, M. Bleackley, S. Dolan and T. Shafee, 2017, "Transcriptomics Technologies. *PLoS Computational Biology*, Vol. 13, No. 5, p. 1005457.

Lu, J., Z. Xu, H. Duan, H. Ji, Z. Zhen, B. Li, H. Wang, H. Tang, J. Zhou, T. Guo, B. Wu, D. Wang, Y. Liu, Y. Niu and R. Zhang, 2020, "Tumor-Associated Macrophage Interleukin-B Promotes Glycerol-3-Phosphate Dehydrogenase Activation, Glycolysis and Tumorigenesis in Glioma Cells. *Cancer Science*, Vol. 111, No. 6, pp. 1979–1990.

Lu, Y., C. M. Labak, N. Jain, I. J. Purvis, M. R. Guda, S. E. Bach, S. Asuthkar and K. K. Velpula, 2017, "OTX2 Expression Contributes to Proliferation and Progression in Myc-Amplified Medulloblastoma, *Am J Cancer Res*, Vol. 7, No. 3, pp. 647-656.

Lv, Q., D. Wang, Z. Yang, J. Yang, R. Zhang, X. Yang, M. Wang and Y. Wang, 2019, "Repurposing Antitubercular Agent Isoniazid for Treatment of Prostate Cancer. *Biomaterials Science*, Vol. 7, No. 1, pp. 296–306.

Ma, H., A. Sorokin, A. Mazein, A. Selkov, E. Selkov, O. Demin and I. Goryanin, 2007, "The Edinburgh Human Metabolic Network Reconstruction and Its Functional Analysis. *Molecular Systems Biology*, Vol. 3, No. 1, p. 135.

Macaulay, R. J. B., W. Wang, J. Dimitroulakos, L. E. Becker and H. Yeger, 1999, "Lovastatin-Induced Apoptosis of Human Medulloblastoma Cell Lines in Vitro. *Journal of Neuro-Oncology*, Vol. 42, No. 1, pp. 1–11.

Machado, D. and M. Herrgård, 2014, "Systematic Evaluation of Methods for Integration of Transcriptomic Data into Constraint-Based Models of Metabolism. *PLoS Computational Biology*, Vol. 10, No. 4, p. 1003580.

Maddocks, O. D. K., C. R. Berkers, S. M. Mason, L. Zheng, K. Blyth, E. Gottlieb and K. H. Vousden, 2013, "Serine Starvation Induces Stress and p53-Dependent Metabolic Remodelling in Cancer Cells. *Nature*, Vol. 493, No. 7433, pp. 542–546.

Mahmoud, A. M., M. A. M. Aboul-Soud, J. Han, Y. A. Al-Sheikh, A. M. Al-Abd and H. A. El-Shemy, 2016, "Transcriptional Profiling of Breast Cancer Cells in Response to Mevinolin: Evidence of Cell Cycle Arrest, DNA Degradation and Apoptosis. *International Journal of Oncology*, Vol. 48, No. 5, pp. 1886–1894.

Mahoney, C. E., D. Pirman, V. Chubukov, T. Sleger, S. Hayes, Z. P. Fan, E. L. Allen, Y. Chen, L. Huang, M. Liu, Y. Zhang, G. McDonald, R. Narayanaswamy, S. Choe, Y. Chen, S. Gross, G. Cianchetta, A. K. Padyana, S. Murray and G. A. Smolen, 2019, "A Chemical

Biology Screen Identifies a Vulnerability of Neuroendocrine Cancer Cells to SQLE Inhibition. *Nature Communications*, Vol. 10, No. 1, p. 96.

Mardinoglu, A., R. Agren, C. Kampf, A. Asplund, M. Uhlen and J. Nielsen, 2014, "Genome-Scale Metabolic Modelling of Hepatocytes Reveals Serine Deficiency in Patients with Non-Alcoholic Fatty Liver Disease. *Nature Communications*, Vol. 5, No. 1, p. 3083.

Marie, S. K. N. and S. M. O. Shinjo, 2011, "Metabolism and Brain Cancer. *Clinics*, Vol. 66, pp. 33–43.

Martín-Jiménez, C. A., D. Salazar-Barreto, G. E. Barreto and J. González, 2017, "Genome-Scale Reconstruction of the Human Astrocyte Metabolic Network. *Frontiers in Aging Neuroscience*, Vol. 9.

Martirosian, V., K. Deshpande, H. Zhou, K. Shen, K. Smith, P. Northcott, M. Lin, V. Stepanosyan, D. Das, J. Remsik, D. Isakov, A. Boire, H. De Feyter, K. Hurth, S. Li, J. Wiemels, B. Nakamura, L. Shao, C. Danilov and J. Neman, 2021, "Medulloblastoma Uses GABA Transaminase to Survive in the Cerebrospinal Fluid Microenvironment and Promote Leptomeningeal Dissemination. *Cell Reports*, Vol. 35, No. 13, p. 109302.

Maxfield, F. R. and G. van Meer, 2010, "Cholesterol, the Central Lipid of Mammalian Cells. *Current Opinion in Cell Biology*, Vol. 22, No. 4, pp. 422–429.

Medes, G., A. Thomas and S. Weinhouse, 1953, "Metabolism of neoplastic tissue. IV. A Study of Lipid Synthesis in Neoplastic Tissue Slices in Vitro. *Cancer Res*. Vol. 13, pp. 27–29.

Mercadante, A. A. and S. S. Mohiuddin, 2020, "Biochemistry, Replication and Transcription", In *StatPearls*.

Mercadante, A. A. and P. Tadi, 2020, "Neuroanatomy, Gray Matter", In *StatPearls*.

Montgomery, D. C. and G. C. Runger, 2003, *Applied Statistics and Probability for Engineers*, 3rd edition. Wiley.

Moon, B. S., M. T. Park, J. H. Park, S. W. Kim, K. C. Lee, G. I. An, S. D. Yang, D. Y. Chi, G. J. Cheon and S. J. Lee, 2007, "Synthesis of Novel Phytosphingosine Derivatives and Their Preliminary Biological Evaluation for Enhancing Radiation Therapy", *Bioorganic Medicinal Chemistry Letters*, Vol. 17, No. 23, pp. 6643–6646.

Moreno-Sánchez, R., S. Rodríguez-Enríquez, E. Saavedra, A. Marín-Hernández and J. C. Gallardo-Pérez, 2009, "The Bioenergetics of Cancer: Is Glycolysis the Main ATP Supplier in All Tumor Cells?", *BioFactors*, Vol. 35, No. 2, pp. 209–225.

Mukherjee, P., A. C. Faber, L. M. Shelton, R. C. Baek, T. C. Chiles and T. N. Seyfried, 2008, "Thematic Review Series: Sphingolipids. Ganglioside GM3 Suppresses the Proangiogenic Effects of Vascular Endothelial Growth Factor and Ganglioside GD1a", *Journal of Lipid Research*, Vol. 49, No. 5, pp. 929–938.

Mullen, P. J., R. Yu, J. Longo, M. C. Archer and L. Z. Penn, 2016, "The Interplay between Cell Signalling and the Mevalonate Pathway in Cancer", *Nature Reviews Cancer*, Vol. 16, No. 11, pp. 718–731.

Munford, H., 2019, *Investigating Medulloblastoma Metabolism for Better Diagnosis and Treatment*, Ph.D. Dissertation, University of Birmingham.

Nagahara, Y., T. Shinomiya, S. Kuroda, N. Kaneko, R. Nishio and M. Ikekita, 2005, "Phytosphingosine Induced Mitochondria-Involved Apoptosis", *Cancer Science*, Vol. 96, No. 2, pp. 83–92.

Natali, F., L. Siculella, S. Salvati and G. V. Gnoni, 2007, "Oleic Acid Is a Potent Inhibitor of Fatty Acid and Cholesterol Synthesis in C6 Glioma Cells", *Journal of Lipid Research*, Vol. 48, No. 9, pp. 1966–1975.

Nielson, J. R. and J. P. Rutter, 2018, "Lipid-Mediated Signals That Regulate Mitochondrial Biology", *Journal of Biological Chemistry*, Vol. 293, No. 20, pp. 7517–7521.

Niklison-Chirou, M. V., I. Erngren, M. Engskog, J. Haglöf, D. Picard, M. Remke, P. H. R. McPolin, M. Selby, D. Williamson, S. C. Clifford, D. Michod, M. Hadjiandreou, T. Arvidsson, C. Pettersson, G. Melino and S. Marino, 2017, "TAp73 Is a Marker of Glutamine Addiction in Medulloblastoma", *Genes Development*, Vol. 31, No. 17, pp. 1738–1753.

Northcott, P. A., G. W. Robinson, C. P. Kratz, D. J. Mabbott, S. L. Pomeroy, S. C. Clifford, S. Rutkowski, D. W. Ellison, D. Malkin, M. D. Taylor, A. Gajjar and S. M. Pfister, 2019, "Medulloblastoma", *Nature Reviews Disease Primers*, Vol. 5, No. 1, p. 11.

Norton, W. T., T. Abe, S. E. Poduslo and G. H. DeVries, 1975, "The Lipid Composition of Isolated Brain Cells and Axons", *Journal of Neuroscience Research*, Vol. 1, No. 1, pp. 57–75.

Nusinovich, Y., 2008, *Tumor Gangliosides, and Tumor Cell Proliferation and Signaling*. Ph.D. Dissertation. The George Washington University.

Ogretmen, B., 2018, "Sphingolipid Metabolism in Cancer Signalling and Therapy", *Nature Reviews Cancer*, Vol. 18, No. 1, pp. 33–50.

Ohno, T., J. Awaya, T. Kesado, S. Nomura and S. Ōmura, 1974, "Mechanism of Action of CM-55, a Synthetic Analogue of the Antilipogenic Antibiotic Cerulenin", *Antimicrobial Agents and Chemotherapy*, Vol. 6, No. 4, pp. 387–392.

Orth, J. D., I. Thiele and B. Ø. Palsson, 2010, "What Is Flux Balance Analysis?", *Nature Biotechnology*, Vol. 28, No. 3, pp. 245–248.

Oskouian, B. and J. D. Saba, 2010, "Cancer Treatment Strategies Targeting Sphingolipid Metabolism", *Sphingolipids as Signaling and Regulatory Molecules*, Vol. 688, pp. 185–205.

Özcan, E. and T. Çakır, 2016, "Reconstructed Metabolic Network Models Predict Flux-Level Metabolic Reprogramming in Glioblastoma", *Frontiers in Neuroscience*, Vol. 10.

Özdemir, M. D. and D. Göktürk, 2019, "The Concurrent Effect of Acyclovir and Rosemary on Glioblastoma Cell Culture", *Cellular and Molecular Biology*, Vol. 65, No. 3, p. 66.

Palmer, S. L., C. Armstrong, A. Onar-Thomas, S. Wu, D. Wallace, M. J. Bonner, J. Schreiber, M. Swain, L. Chapieski, D. Mabbott, S. Knight, R. Boyle and A. Gajjar, 2013, "Processing Speed, Attention, and Working Memory After Treatment for Medulloblastoma: An International, Prospective, and Longitudinal Study", *Journal of Clinical Oncology*, Vol. 31, No. 28, pp. 3494–3500.

Palsson, B. O., 2015, *Systems Biology Constraint-Based Reconstruction and Analysis*, Cambridge University Press, Cambridge.

Panigrahy, A., M. D. Krieger, I. Gonzalez-Gomez, X. Liu, J. G. McComb, J. L. Finlay, M. D. Nelson, F. H. Gilles and S. Blüml, 2006, "Quantitative Short Echo Time 1H-MR Spectroscopy of Untreated Pediatric Brain Tumors: Preoperative Diagnosis and Characterization", *AJNR Am J Neuroradiol*. Vol. 27, No. 3, pp. 560-72.

Panosyan, E. H., Y. Wang, P. Xia, W. N. P. Lee, Y. Pak, D. R. Laks, H. J. Lin, T. B. Moore, T. F. Cloughesy, H. I. Kornblum and J. L. Lasky, 2014, "Asparagine Depletion Potentiates the Cytotoxic Effect of Chemotherapy against Brain Tumors", *Molecular Cancer Research*, Vol. 12, No. 5, pp. 694–702.

Panwalkar, P., A. Moiyadi, A. Goel, P. Shetty, N. Goel, E. Sridhar and N. Shirsat, 2015, "MiR-206, a Cerebellum Enriched miRNA Is Downregulated in All Medulloblastoma Subgroups and Its Overexpression Is Necessary for Growth Inhibition of Medulloblastoma Cells", *Journal of Molecular Neuroscience*, Vol. 56, No. 3, pp. 673–680.

Park, M. T., J. A. Choi, M. J. Kim, H. D. Um, S. Bae, C. M. Kang, C. K. Cho, S. Kang, H. Y. Chung, Y. S. Lee and S. J. Lee, 2003b, "Suppression of Extracellular Signal-related Kinase and Activation of P38 MAPK Are Two Critical Events Leading to Caspase-8- and Mitochondria-mediated Cell Death in Phytosphingosine-treated Human Cancer Cells", *Journal of Biological Chemistry*, Vol. 278, No. 50, pp. 50624–50634.

Park, M. T., J. A. Kang, J. A. Choi, C. M. Kang, T. H. Kim, S. Bae, S. Kang, S. Kim, W. I. Choi, C. K. Cho, H. Y. Chung, Y. S. Lee and S. J. Lee, 2003a, "Phytosphingosine Induces Apoptotic Cell Death via Caspase 8 Activation and Bax Translocation in Human Cancer Cells", *Cancer Research.*, Vol. 9.

Park, M. T., Y. H. Kang, I. C. Park, C. H. Kim, Y. S. Lee, H. Y. Chung and S. J. Lee, 2007, "Combination Treatment with Arsenic Trioxide and Phytosphingosine Enhances Apoptotic Cell Death in Arsenic Trioxide–Resistant Cancer Cells", *Molecular Cancer Therapeutics*, Vol. 6, No. 1, pp. 82–92.

Park, M. T., M. J. Kim, Y. H. Kang, S. Y. Choi, J. H. Lee, J. A. Choi, C. M. Kang, C. K. Cho, S. Kang, S. Bae, Y. S. Lee, H. Y. Chung and S. J. Lee, 2005, "Phytosphingosine in Combination with Ionizing Radiation Enhances Apoptotic Cell Death in Radiation-Resistant Cancer Cells through ROS-Dependent and -Independent AIF Release", *Blood*, Vol. 105, No. 4, pp. 1724–1733.

Paul, A., R. Anand, S. P. Karmakar, S. Rawat, N. Bairagi and S. Chatterjee, 2021, "Exploring Gene Knockout Strategies to Identify Potential Drug Targets Using Genome-Scale Metabolic Models", *Scientific Reports*, Vol. 11, No. 1, p. 213.

Pearson, G., F. Robinson, T. B. Gibson, B. Xu, M. Karandikar, K. Berman and M. H. Cobb, 2001, "Mitogen-Activated Protein (MAP) Kinase Pathways: Regulation and Physiological Functions", *Endocrine Society*, Vol. 22, No. 2, p. 31.

Peters, G. J., 2014, "Novel Developments in the Use of Antimetabolites", *Nucleosides, Nucleotides and Nucleic Acids*, Vol. 33, No. 4–6, pp. 358–374.

Porras, A. M. G., B. S. Terra, T. C. Braga, T. F. F. Magalhães, C. V. B. Martins, D. L. da Silva, L. M. Baltazar, L. F. Gouveia, G. J. C. de Freitas, D. A. Santos, M. A. Resende-Stoianoff, B. B. Fuchs, E. Mylonakis, R. P. de Freitas and Â. de Fátima, 2018, "Butenafine and Analogues: An Expeditious Synthesis and Cytotoxicity and Antifungal Activities", *Journal of Advanced Research*, Vol. 14, pp. 81–91.

Puchałka, J., M. A. Oberhardt, M. Godinho, A. Bielecka, D. Regenhardt, K. N. Timmis, J. A. Papin and V. A. P. Martins dos Santos, 2008, "Genome-Scale Reconstruction and Analysis of the Pseudomonas Putida KT2440 Metabolic Network Facilitates Applications in Biotechnology", *PLoS Computational Biology*, Vol. 4, No. 10, p. 1000210.

Puniya, B. L., R. Amin, B. Lichter, R. Moore, A. Ciurej, S. J. Bennett, A. R. Shah, M. Barberis and T. Helikar, 2021, "Integrative Computational Approach Identifies Drug Targets in CD4+ T-Cell-Mediated Immune Disorders", *Npj Systems Biology and Applications*, Vol. 7, No. 1, p.4.

Purves, D. (Ed.)., 2004, *Neuroscience*, 3rd edition, Sinauer Associates, Publishers.

Pushpakom, S., F. Iorio, P. A. Eyers, K. J. Escott, S. Hopper, A. Wells, A. Doig, T. Guilliams, J. Latimer, C. McNamee, A. Norris, P. Sanseau, D. Cavalla and M. Pirmohamed, 2019, "Drug Repurposing: Progress, Challenges and Recommendations.", *Nat Rev Drug Discov*. Vol.18, No. 1, pp. 41-58.

Quinville, B. M., N. M. Deschenes, A. E. Ryckman and J. S. Walia, 2021, "A Comprehensive Review: Sphingolipid Metabolism and Implications of Disruption in Sphingolipid Homeostasis", In *International Journal of Molecular Sciences*, Vol. 22, p. 11.

Raabe, E. and C. G. Eberhart, 2013, "Therapeutic Targeting of Developmental Signaling Pathways in Medulloblastoma: Hedgehog, Notch, Wnt and Myc", *Current signal transduction therapy*, Vol. 8, pp. 55-66.

Raman, K. and N. Chandra, 2009, "Flux Balance Analysis of Biological Systems: Applications and Challenges", *Briefings in Bioinformatics*, Vol. 4. pp. 435-449.

Rao, C. V., H. L. Newmark and B. S. Reddy, 1998, "Chemopreventive Effect of Squalene on Colon Cancer", *Carcinogenesis*, Vol. 2, pp. 287–290

Raškevičius, V., V. Mikalayeva, I. Antanavičiūtė, I. Ceslevičienė, V. A. Skeberdis, V. Kairys and S. Bordel, 2018, "Genome Scale Metabolic Models as Tools for Drug Design and Personalized Medicine", *PLoS ONE*, Vol. 13, No. 1, p. 190636.

Reed, J. L., 2017, "Genome-Scale Metabolic Modeling and Its Application to Microbial Communities", *The Chemistry of Microbiomes: Proceedings of a Seminar Series*, p. 24751.

Ren, L., E. S. Hong, A. Mendoza, S. Issaq, C. T. Hoang, M. Lizardo, A. LeBlanc and C. Khanna, 2017, "Metabolomics Uncovers a Link between Inositol Metabolism and Osteosarcoma Metastasis", *Oncotarget*, Vol. 8, No. 24, pp. 38541–38553.

Resendis-Antonio, O., A. Checa and S. Encarnación, 2010, "Modeling Core Metabolism in Cancer Cells: Surveying the Topology Underlying the Warburg Effect", *PLoS ONE*, Vol. 5, No. 8, p. 12383.

Riggs, L., E. Bouffet, S. Laughlin, N. Laperriere, F. Liu, J. Skocic, N. Scantlebury, F. Wang, N. J. Schoenhoff, D. Strother, J. Hukin, C. Fryer, D. McConnell and D. J. Mabbott, 2014, "Changes to Memory Structures in Children Treated for Posterior Fossa Tumors", *Journal of the International Neuropsychological Society*, Vol. 20, No. 2, pp. 168–180.

Rioja, A., A. R. Pizzey, C. M. Marson and N. S. B. Thomas, 2000, "Preferential Induction of Apoptosis of Leukaemic Cells by Farnesol", *FEBS Letters*, Vol. 467, No. 2–3, pp. 291–295.

Ripps, H. and W. Shen, 2012, "Review: Taurine: A "Very Essential" Amino Acid", *Molecular Vision*, p. 14.

Robinson, G., M. Parker, T. A. Kranenburg, C. Lu, X. Chen, L. Ding, T. N. Phoenix, E. Hedlund, L. Wei, X. Zhu, N. Chalhoub, S. J. Baker, R. Huether, R. Kriwacki, N. Curley,

R. Thiruvenkatam, J. Wang, G. Wu, M. Rusch and R. J. Gilbertson, 2012, "Novel Mutations Target Distinct Subgroups of Medulloblastoma", *Nature*, Vol. 488, No. 7409, pp. 43–48.

Röhrig, F. and A. Schulze, 2016, "The Multifaceted Roles of Fatty Acid Synthesis in Cancer", *Nature Reviews Cancer*, Vol. 16, No. 11, pp. 732–749.

Roser, M., D. Josic, M. Kontou, K. Mosetter, P. Maurer and W. Reutter, 2009, "Metabolism of Galactose in the Brain and Liver of Rats and Its Conversion into Glutamate and Other Amino Acids", *Journal of Neural Transmission*, Vol. 116, No. 2, pp. 131–139.

Ruggiero, M., E. Ward, R. Smith, J. J. V. Branca, D. Noakes, G. Morucci, M. Taubmann, L. Thyer and S. Pacini, 2014, "Oleic Acid, Deglycosylated Vitamin D-Binding Protein, Nitric Oxide: A Molecular Triad Made Lethal to Cancer", *Anticancer Research*, p. 10.

Russo, D., L. Capolupo, J. S. Loomba, L. Sticco and G. D'Angelo, 2018, "Glycosphingolipid Metabolism in Cell Fate Specification", *Journal of Cell Science*, Vol. 131, No. 24, p. 219204.

Ryland, L. K., T. E. Fox, X. Liu, T. P. Loughran and M. Kester, 2011, "Dysregulation of Sphingolipid Metabolism in Cancer", *Cancer Biology Therapy*, Vol. 11, No. 2, pp. 138–149.

Scandroglio, F., J. K. Venkata, N. Loberto, S. Prioni, E. H. Schuchman, V. Chigorno, A. Prinetti and S. Sonnino, 2008, "Lipid Content of Brain, Brain Membrane Lipid Domains, and Neurons from Acid Sphingomyelinase Deficient Mice: Lipid Content and ASM Deficient Mice", *Journal of Neurochemistry*, Vol. 107, No. 2, pp. 329–338.

Schmahmann, J. D. and D. Caplan, 2006, "Cognition, Emotion and the Cerebellum", In *Brain: A Journal of Neurology*, Vol. 129, p. 2.

Schmeel, L. C., F. C. Schmeel, S. Blaum-Feder and I. G. H. Schmidt-Wolf, 2015, "In Vitro Efficacy of Naftifine against Lymphoma and Multiple Myeloma", *Anticancer Research*, p. 6.

Schnepp, P. M., D. D. Lee, I. H. Guldner, T. K. O'Tighearnaigh, E. N. Howe, B. Palakurthi, K. E. Eckert, T. A. Toni, B. L. Ashfeld and S. Zhang, 2017, "GAD1 Upregulation Programs Aggressive Features of Cancer Cell Metabolism in the Brain Metastatic Microenvironment", *Cancer Research*, Vol. 77, No. 11, pp. 2844–2856.

Schömel, N., G. Geisslinger and M. S. Wegner, 2020, "Influence of Glycosphingolipids on Cancer Cell Energy Metabolism", *Progress in Lipid Research*, Vol. 79, No. 101050.

Schuller-Levis, G. B. and E. Park, 2003, "Taurine: New Implications for an Old Amino Acid", *FEMS Microbiology Letters*, Vol. 226, No. 2, pp. 195–202.

Segre, D., D. Vitkup and G. M. Church, 2002, "Analysis of Optimality in Natural and Perturbed Metabolic Networks", *Proceedings of the National Academy of Sciences*, Vol. 99, No. 23, pp. 15112–15117.

Selzner, M., A. Bielawska, M. A. Morse and P. A. Clavien, 2001, "Induction of Apoptotic Cell Death and Prevention of Tumor Growth by Ceramide Analogues in Metastatic Human Colon Cancer", *Cancer research*, Vol. 61, pp. 1233–1240.

Sertbaş, M., K. Ülgen and T. Çakir, 2014, "Systematic Analysis of Transcription-Level Effects of Neurodegenerative Diseases on Human Brain Metabolism by a Newly Reconstructed Brain-Specific Metabolic Network", *FEBS Open Bio*, Vol. 4, pp. 542–553.

Seyfried, T. N. and P. Mukherjee, 2010, "Ganglioside GM3 Is Antiangiogenic in Malignant Brain Cancer", *Journal of Oncology*, pp. 1–8.

Seyfried, T. N., T. M. Sanderson, M. M. El-Abbadi, R. McGowan and P. Mukherjee, 2003, "Role of Glucose and Ketone Bodies in the Metabolic Control of Experimental Brain Cancer", *British Journal of Cancer*, Vol. 89, No. 7, pp. 1375–1382.

Sheikholeslami, K., A. Ali Sher, S. Lockman, D. Kroft, M. Ganjibakhsh, K. Nejati-Koshki, S. Shojaei, S. Ghavami and M. Rastegar, 2019, "Simvastatin Induces Apoptosis in Medulloblastoma Brain Tumor Cells via Mevalonate Cascade Prenylation Substrates", *Cancers*, Vol. 11, No. 7, p. 994.

Shellman, Y. G., D. Ribble, L. Miller, J. Gendall, K. VanBuskirk, D. Kelly, D. A. Norris and R. P. Dellavalle, 2005, "Lovastatin-Induced Apoptosis in Human Melanoma Cell Lines", *Melanoma Research*, Vol. 15, No. 2, pp. 83–89.

Shlomi, T., T. Benyamini, E. Gottlieb, R. Sharan and E. Ruppin, 2011, "Genome-Scale Metabolic Modeling Elucidates the Role of Proliferative Adaptation in Causing the Warburg Effect", *PLoS Computational Biology*, Vol. 7, No. 3, p. 1002018.

Shlomi, T., M. N. Cabili, M. J. Herrgård, B. Ø. Palsson and E. Ruppin, 2008, "Network-Based Prediction of Human Tissue-Specific Metabolism", *Nature Biotechnology*, Vol. 26, No. 9, pp. 1003–1010.

Singh, G., 2014, "Mitochondrial FAD-Linked Glycerol-3-Phosphate Dehydrogenase: A Target for Cancer Therapeutics", *Pharmaceuticals*, Vol. 7, No. 2, pp. 192–206.

Singh, V., 2014, *Textbook of Anatomy Head, Neck and Brain*, Volume III, In Reed Elsevier India Private Limited.

Slade, R. F., D. A. Hunt, M. M. Pochet, V. J. Venema and R .A. Hennigar, 2003, "Characterization and Inhibition of Fatty Acid Synthase in Pediatric Tumor Cell Lines", *Anticancer Res*, Vol. 23, No. 2B, pp. 1235-43.

Sławińska-Brych, A., B. Zdzisińska and M. Kandefer-Szerszeń, 2014, "Fluvastatin Inhibits Growth and Alters the Malignant Phenotype of the C6 Glioma Cell Line", *Pharmacological Reports*, Vol. 66, No. 1, pp. 121–129.

Smith, A. L., 1997, *Oxford Dictionary of Biochemistry and Molecular Biology*. Oxford [Oxfordshire]: Oxford University Press.

Song, H. H. G., K. M. Park and S. Gerecht, 2014, "Hydrogels to Model 3D in vitro Microenvironment of Tumor Vascularization", *Advanced Drug Delivery Reviews*, Vol. 79, No. 80, pp. 19–29.

Stelzer, G., N. Rosen, I. Plaschkes, S. Zimmerman, M. Twik, S. Fishilevich, T. I. Stein, R. Nudel, I. Lieder, Y. Mazor, S. Kaplan, D. Dahary, D. Warshawsky, Y. Guan-Golan, A. Kohn, N. Rappaport, M. Safran and D. Lancet, 2016, "The GeneCards Suite: From Gene Data Mining to Disease Genome Sequence Analyses", *Current Protocols in Bioinformatics*, Vol. 54, No. 1.

Stewart B, B. W. Stewart and C. Wild, 2014, "International Agency for Research on Cancer, World Health Organization. 2014", *World cancer report 2014*.

Stincone, A., A. Prigione, T. Cramer, M. M. C. Wamelink, K. Campbell, E. Cheung, V. Olin-Sandoval, N. Grüning, A. Krüger, M. Tauqeer Alam, M. A. Keller, M. Breitenbach, K. M. Brindle, J. D. Rabinowitz and M. Ralser, 2015, "The Return of Metabolism: Biochemistry and Physiology of the Pentose Phosphate Pathway", *Biological Reviews*, Vol. 90, No. 3, pp. 927–963.

Subramanian, A., R. Narayan, S. M. Corsello, D. D. Peck, T. E. Natoli, X. Lu, J. Gould, J. F. Davis, A. A. Tubelli, J. K. Asiedu, D. L. Lahr, J. E. Hirschman, Z. Liu, M. Donahue, B. Julian, M. Khan, D. Wadden, I. C. Smith, D. Lam and T. R. Golub, 2017, "A Next Generation Connectivity Map: L1000 Platform and the First 1,000,000 Profiles", *Cell*, Vol. 171, No. 6, pp. 1437-1452.

Sultan, F., 2002, "Brain Evolution: Analysis of Mammalian Brain Architecture", *Nature,* Vol. 415, No. 6868.

Sun, J., B. Sayyar, J. E. Butler, P. Pharkya, T. R. Fahland, I. Famili, C. H. Schilling, D. R. Lovley and R. Mahadevan, 2009, "Genome-Scale Constraint-Based Modeling of Geobacter Metallireducens", *BMC Systems Biology*, Vol. 3, No. 1, p. 15.

Tao, Y. H., Z. Yuan, X. Q. Tang, H. B. Xu and X. L. Yang, 2006, "Inhibition of GABA Shunt Enzymes' Activity by 4-Hydroxybenzaldehyde Derivatives", *Bioorganic Medicinal Chemistry Letters*, Vol. 16, No. 3, pp. 592–595.

Tavassoly, I., J. Goldfarb and R. Iyengar, 2018, "Systems Biology Primer: The Basic Methods and Approaches", *Essays in Biochemistry*, Vol. 62, No. 4, pp. 487–500.

Tech, K., M. Deshmukh and T. R. Gershon, 2015, "Adaptations of Energy Metabolism during Cerebellar Neurogenesis Are Co-Opted in Medulloblastoma", *Cancer Letters*, Vol. 356, No. 2, pp. 268–272.

Tech, K. and T. R. Gershon, 2015, "Energy Metabolism in Neurodevelopment and Medulloblastoma", *Translational Pediatrics*, Vol. 4, No. 1, p. 8.

Ternes, P., T. Wobbe, M. Schwarz, S. Albrecht, K. Feussner, I. Riezman, J. M. Cregg, E. Heinz, H. Riezman, I. Feussner and D. Warnecke, 2011, "Two Pathways of Sphingolipid Biosynthesis Are Separated in the Yeast Pichia Pastoris", *Journal of Biological Chemistry*, Vol. 286, No. 13, pp. 11401–11414.

Thiele, I., N. Swainston, R. M. T. Fleming, A. Hoppe, S. Sahoo, M. K. Aurich, H. Haraldsdottir, M. L. Mo, O. Rolfsson, M. D. Stobbe, S. G. Thorleifsson, R. Agren, C. Bölling, S. Bordel, A. K. Chavali, P. Dobson, W. B. Dunn, L. Endler, D. Hala and B. Ø. Palsson, 2013, "A Community-Driven Global Reconstruction of Human Metabolism", *Nature Biotechnology*, Vol. 31, No. 5, pp. 419–425.

Töpfer, N., S. Jozefczuk and Z. Nikoloski, 2012, "Integration of Time-Resolved Transcriptomics Data with Flux-Based Methods Reveals Stress-Induced Metabolic Adaptation in Escherichia Coli", *BMC Systems Biology*, Vol. 6, No. 1, p. 148.

Valvona, C. J., 2016, *LDHA as a Potential Therapeutic Target for Medulloblastoma*. Ph.D. Dissertation, University of Portsmouth.

Van Berlo, R. J. P., D. De Ridder, J. M. Daran, P. A. S. Daran-Lapujade, B. Teusink and M. J. T. Reinders, 2011, "Predicting Metabolic Fluxes Using Gene Expression Differences as Constraints", *IEEE/ACM Transactions on Computational Biology and Bioinformatics*, Vol. 8, No. 1, pp. 206–216.

Vazquez, A., 2011, "Molecular Crowding Defines a Common Origin for the Warburg Effect in Proliferating Cells and the Lactate Threshold in Muscle Physiology", *Nature Precedings*.

Vazquez Rodriguez, G., A. Abrahamsson, M. V. Turkina and C. Dabrosin, 2020, "Lysine in Combination with Estradiol Promote Dissemination of Estrogen Receptor Positive Breast Cancer via Upregulation of U2AF1 and RPN2 Proteins", *Frontiers in Oncology*, Vol. 10, No. 598684.

Venneti, S. and C. B. Thompson, 2017, "Metabolic Reprogramming in Brain Tumors. *Annual Review of Pathology: Mechanisms of Disease*", Vol. 12, No. 1, pp. 515–545.

Ventura, R., K. Mordec, J. Waszczuk, Z. Wang, J. Lai, M. Fridlib, D. Buckley, G. Kemble and T. S. Heuer, 2015, "Inhibition of de novo Palmitate Synthesis by Fatty Acid Synthase Induces Apoptosis in Tumor Cells by Remodeling Cell Membranes, Inhibiting Signaling Pathways, and Reprogramming Gene Expression", *EBioMedicine*, Vol. 2, No. 8, pp. 808–824.

Villa, E., E. Ali, U. Sahu and I. Ben-Sahra, 2019, "Cancer Cells Tune the Signaling Pathways to Empower de Novo Synthesis of Nucleotides", *Cancers*, Vol. 11, No. 5, p. 688.

Volpe, J. J. and P. R. Vagelos, 1976, "Mechanisms and Regulation of Biosynthesis of Saturated Fatty Acids", *Physiological Reviews. American Physiological Society*, Vol. 56, No. 2, pp. 339–417.

von Bartheld, C. S., J. Bahney and S. Herculano-Houzel, 2016, "The Search for True Numbers of Neurons and Glial Cells in the Human Brain: A Review of 150 Years of Cell Counting: Quantifying Neurons and Glia in Human Brain", *Journal of Comparative Neurology*, Vol. 524, No. 18, pp. 3865–3895.

Vrionis, F. D., C. J. Wikstrand, P. Fredman and J. E. Mã, 1989, "Five New Epitope-Defined Monoclonal Antibodies Reactive with GM2 and Human Glioma and Medulloblastoma Cell Lines", *Cancer research*, Vol. 49, pp. 6645-6651.

Vucenik, I., 2019, "Anticancer Properties of Inositol Hexaphosphate and Inositol: An Overview", *Journal of Nutritional Science and Vitaminology*, Vol. 65, pp. 18–22.

Wang, D., Q. Chen, B. Liu, Y. Li, Y. Tan and B. Yang, 2016, "Ellagic Acid Inhibits Proliferation and Induces Apoptosis in Human Glioblastoma Cells", *Acta Cirurgica Brasileira*, Vol. 31, No. 2, pp. 143–149.

Wang, D., Q. Chen, Y. Tan, B. Liu and C. Liu, 2017, "Ellagic Acid Inhibits Human Glioblastoma Growth in vitro and in vivo", *Oncology Reports*, Vol. 37, No. 2, pp. 1084–1092.

Wang, J., A. Garancher, V. Ramaswamy and R. J. Wechsler-Reya, 2018, "Medulloblastoma: From Molecular Subgroups to Molecular Targeted Therapies", *Annual Review of Neuroscience*, Vol. 41, No. 1, pp. 207–232.

Wang, Y., J. A. Eddy and N. D. Price, 2012, "Reconstruction of Genome-Scale Metabolic Models for 126 Human Tissues Using mCADRE", *BMC Systems Biology*, Vol. 6, No. 1, p. 153.

Warburg, O., 1925, “The Metabolism of Carcinoma Cells”, *The Journal of Cancer Research*, Vol. 9, No. 1, pp. 148–163.

Wasserman, D. H., 2009, “Four Grams of Glucose”, In *American Journal of Physiology - Endocrinology and Metabolism*.

Wei, Z., X. Liu, C. Cheng, W. Yu and P. Yi, 2021, “Metabolism of Amino Acids in Cancer”, *Frontiers in Cell and Developmental Biology*, Vol. 8, p. 603837.

West, N. J., S. K. Clark, R. K. S. Phillips, J. M. Hutchinson, R. J. Leicester, A. Belluzzi and M. A. Hull, 2010, “Eicosapentaenoic Acid Reduces Rectal Polyp Number and Size in Familial Adenomatous Polyposis”, *Gut*, Vol. 59, No. 7, pp. 918–925.

Wishart, D. S., 2006, “DrugBank: A Comprehensive Resource for in Silico Drug Discovery and Exploration”, *Nucleic Acids Research*, Vol. 34, No. 90001, pp. 668–672.

Wolf, U., M. J. Rapoport and T. A. Schweizer, 2009, “Evaluating the Affective Component of the Cerebellar Cognitive Affective Syndrome”, *Journal of Neuropsychiatry and Clinical Neurosciences*, Vol. 21, No. 3.

Wortham, M., G. Jin, J. L. Sun, D. D. Bigner, Y. He and H. Yan, 2012, “Aberrant Otx2 Expression Enhances Migration and Induces Ectopic Proliferation of Hindbrain Neuronal Progenitor Cells”, *PLoS ONE*, Vol. 7, No. 4, p. 36211.

Xin, Y., X. Yue, H. Li, Z. Li, H. Cai, A. K. Choudhary, S. Zhang, D. C. Chugani and S. A. Langhans, 2020, “PET Imaging of Medulloblastoma with an 18F-Labeled Tryptophan Analogue in a Transgenic Mouse Model”, *Scientific Reports*, Vol. 10, No. 1, p. 3800.

Yang, M. and K. H. Vousden, 2016, “Serine and One-Carbon Metabolism in Cancer”, *Nature Reviews Cancer*, Vol. 16, No. 10, pp. 650–662.

Yazlovitskaya, E. M. and G. Melnykovych, 1995, "Selective Farnesol Toxicity and Translocation of Protein Kinase C in Neoplastic HeLa-S3K and Nonneoplastic CF-3 Cells", *Cancer Lett.,* Vol. 88, pp. 179–183.

Yizhak, K., B. Chaneton, E. Gottlieb and E. Ruppin, 2015, "Modeling Cancer Metabolism on a Genome Scale", *Molecular Systems Biology*, Vol. 11, No. 6, p. 817.

Yizhak, K., S. E. Le Dévédec, V. M. Rogkoti, F. Baenke, V. C. Boer, C. Frezza, A. Schulze, B. Water and E. Ruppin, 2014, "A Computational Study of the Warburg Effect Identifies Metabolic Targets Inhibiting Cancer Migration", *Molecular Systems Biology*, Vol. 10, No. 8, p. 744.

Yu, R. K., Y. T. Tsai, T. Ariga and M. Yanagisawa, 2011, "Structures, Biosynthesis, and Functions of Gangliosides-an Overview", *Journal of Oleo Science*, Vol. 60, No. 10, pp. 537–544.

Yu, W. and A. D. MacKerell, 2017, "Computer-Aided Drug Design Methods", *Antibiotics*, Vol. 1520, pp. 85–106.

Zhou, S. F. and W. Z. Zhong, 2017, "Drug Design and Discovery: Principles and Applications", *Molecules*, Vol. 22, No. 2, p. 279.

Zhu, Y., S. Schwarz, B. Ahlemeyer, S. Grzeschik, S. Klumpp and J. Krieglstein, 2005, "Oleic Acid Causes Apoptosis and Dephosphorylates Bad", *Neurochemistry International*, Vol. 46, No. 2, pp. 127–135.

Zhuo, D., X. Li and F. Guan, 2018, "Biological Roles of Aberrantly Expressed Glycosphingolipids and Related Enzymes in Human Cancer Development and Progression", *Frontiers in Physiology*, Vol. 9, p. 466.

APPENDIX A: THE LIST OF REACTIONS

The content is given in CD.

APPENDIX B: INTEGRATION OF GIMME

The content is given in CD.

APPENDIX C: THE LIST OF METABOLITE ANTIMETABOLITE PAIRS

The content is given in CD.

APPENDIX D: THE LIST OF P VALUES

The content is given in CD.

APPENDIX E: THE LIST OF COMMON ESSENTIAL GENES

The content is given in CD.